Diplomarbeit

Proteomic and Redox Metabolomic Investigation of Pathological Mechanisms of the Failing Heart

Ausgeführt am

Institut für Chemische Technologien und Analytik

an der

Technischen Universität Wien

unter der Anleitung von

Univ. Prof. Priv.-Doz. Dipl.-Ing. Dr. techn. Ruth Birner-Grünberger

Tamara Tomin, PhD

durch

Dominik Hofreither, BSc

01501395

Wien, _____ _____

Dominik Hofreither

Abstract

Oxidative stress plays a significant role in the development and progression of various pathologies. In heart failure, a leading cause of death worldwide, oxidative stress is associated with multiple risk factors, such as diabetes and metabolic syndrome. Heart disease in various stages can be linked to disrupted and abnormal metabolism in cardiac cells.

In order to address the crosstalk of aberrant metabolism and alterations of the myocardial redox state correlated with oxidative stress and heart failure, differentially treated hSC-derived cardiac organoids (cardioids) were subjected to parallel mass spectrometry-based redox metabolomic and quantitative proteomic analyses. The impact of glucose availability and oxygen levels on the redox environment was within homeostatic range based on the adaptive abundance of antioxidative enzymes specific to increased glycolytic flux or mitochondrial activity. Cardioids displayed distinct changes in the expression of proteins involved in collagen synthesis and modification, stress-mediated extracellular matrix remodelling, lipid metabolism and ion transport, as previously observed in preliminary data in the tissue of failing hearts. Additionally, metabolic alterations in response to hypoxic signalling further illustrate the impact of local oxygen concentrations on cellular activity.

Results further disclosed the embryonic metabolic phenotype of the cardioid model. With glycolysis appearing to be the preferred catabolic pathway compared to fatty acid oxidation and high glucose levels being very well tolerated, further *in vitro* models for investigating nutrient-driven redox signalling were explored. In efforts to improve the translational ability of AC16 proliferating human cardiomyocytes, a collection of differentiation media was designed and evaluated. RT-qPCR analysis of AC16 cells cultured in a defined, serum-free bovine serum albumin/lipid concentrate medium revealed an improved phenotype as per increased gene expression of multiple cardiomyocyte-specific markers (ACTN2, TNNT2, TNNI3). Additionally, results indicate changes in gene expression as early as after 48 h of treatment. A maturation protocol building on these results has since been implemented.

Further elucidation of the intricate pathomolecular events in heart failure will require patient-derived samples and utilization of cardiac *in vitro* models appropriate to their respective translational ability to drive the discovery and validation of novel strategies in diagnosis and treatment.

Kurzfassung

Oxidativer Stress spielt eine wichtige Rolle bei der Entstehung und dem Fortschreiten verschiedener Krankheiten. Bei Herzinsuffizienz, einer der häufigsten Todesursachen weltweit, wird oxidativer Stress mit mehreren Risikofaktoren wie Diabetes und metabolischem Syndrom in Verbindung gebracht. Herzkrankheiten in verschiedenen Stadien können weiter mit einem gestörten Stoffwechsel in den Herzzellen in Verbindung gebracht werden.

Um die Wechselwirkung zwischen anormalem Stoffwechsel und Veränderungen des Redoxzustands des Herzmuskels zu untersuchen, wurden unterschiedlich behandelte hSC-Herzorganoide (Kardioide) massenspektrometrischen Redoxmetabolom- und quantitativen Proteomanalysen unterzogen. Die Auswirkungen des Sauerstoffgehalts und der Verfügbarkeit von Glukose auf das Redoxmilieu lagen im homöostatischen Bereich, basierend auf der adaptiven Häufigkeit antioxidativer Enzyme, die jeweils spezifisch für einen erhöhten glykolytischen Fluss oder mitochondriale Aktivität sind. Kardioide wiesen deutliche Veränderungen in der Expression von Proteinen auf, die an der Kollagensynthese, dem stressvermittelten Umbau der extrazellulären Matrix, dem Lipidstoffwechsel und dem Ionentransport beteiligt sind, wie dies bereits in früheren Untersuchungen beobachtet wurde. Darüber hinaus verdeutlichen Adaptionen des Stoffwechsels in Reaktion auf hypoxische Signale die Konsequenzen lokaler Sauerstoffkonzentrationen.

Die Ergebnisse zeigten weiter den embryonalen Stoffwechselphänotyp des Kardioidmodells auf. Da die Glykolyse im Vergleich zur Fettsäureoxidation metabolisch präferiert wird und hohe Glukosespiegel toleriert werden, wurde nach alternativen *in vitro* Modellen zur Untersuchung der nährstoffabhängigen Redox-Signalübertragung gesucht. In dem Bemühen, die Translationsfähigkeit von AC16 menschlichen Kardiomyozyten zu verbessern, wurden eine Reihe von Differenzierungsmedien evaluiert. RT-qPCR-Analysen von AC16-Zellen, die in einem definierten, serumfreien Rinderserumalbumin/Lipidkonzentrat-Medium kultiviert wurden, ergaben einen differenzierteren Phänotyp entsprechend einer erhöhten Genexpression mehrerer kardiomyozytenspezifischer Marker (ACTN2, TNNT2, TNNI3). Darüber hinaus konnten Adaptionen bereits nach 48 Stunden identifiziert werden. Resultate wurde inzwischen implementiert. Weitere Aufklärung der komplexen pathomolekularen Vorgänge bei Herzinsuffizienz werden geeigneten *in vitro* Herzmodellen erfordern.

Acknowledgements

I would like to take this opportunity to thank all those who supported me throughout the process of my thesis and my studies. First and foremost, I want to thank Univ. Prof. Ruth Birner-Grünberger for giving me the opportunity to join her team and be part of fascinating research. Ruth has fueled my passion for bioanalytics as well as medical research and has always provided me with support and advice.

Working on the *Proteomic Pirates* team has only been a pleasure and has provided me with countless unforgettable memories. I would like to express my gratitude to each and every person who has made me feel part of a supportive, enthusiastic, and welcoming work environment. I would like to extend my thanks to anyone who has provided me with laughter and snacks during those long hours in the lab.

I owe special thanks to my supervisor Tamara Tomin, PhD. Her mentorship has been invaluable and has made me a better scientist.

Furthermore, I would like to thank Assistant Prof. Matthias Schittmayer-Schantl and Maximilian Schinagl, MSc, for providing their extensive knowledge of analytical chemistry and molecular biology.

I would like to express my appreciation to all the people who have provided me with priceless inspiration and learning opportunities in the academic environment.

Above all, I would like to show my gratitude to my family for always supporting me in my endeavours. I especially want to thank Dipl. Ing. Florian Klapal for our friendship and show my appreciation for our scientific and “not very scientific” discussions. Additionally, I would like to thank all my friends for making life that much more interesting.

Last but not least, I want to express my deepest gratitude to my girlfriend for her tireless kindness and mutual support.

Abbreviations

3R	replacement, reduction, and refinement
AA	ammonium acetate
ABC	ammonium bicarbonate
AC	adult ventricular cardiomyocyte
ACN	acetonitrile
ADP	adenosine diphosphate
AGEs	advanced glycation end products
AMP	adenosine monophosphate
AMPK	AMP-activated protein kinase
AR	aldose reductase
ara-C	Cytosine arabinoside
ARVC	arrhythmogenic right ventricular cardiomyopathy
ATP	adenosine triphosphate
ATRA	all-trans retinoic acid
AV	atrioventricular
BCA	bicinchoninic acid
BCAA	branched-chain amino acids
BDIX	Berlin-Druckrey IX
BMC	bone marrow cell
BMP	bone morphogenic protein
BSA	bovine serum albumin
cardioid	cardiac organoid
CCS	copper chaperone for superoxide dismutase 1
CE	collision energy
CID	collision-induced dissociation
CoQ	coenzyme Q
CSC	cardiac stem cell
Ct	cycle threshold
CVD	cardiovascular disease

Cyt	cytochrome
d5-NEM	N-ethylmaleimide-d_5
DCM	dilatative cardiomyopathy
DDA	data-dependent acquisition
DHTKD1	dehydrogenase E1 and transketolase domain-containing 1
DIA	data-independent acquisition
DMEM	Dulbecco's Modified Eagle's Medium
DMSO	dimethyl sulfoxide
ECAR	extracellular acidification rate
ECG	electrocardiogram
ECM	extracellular matrix
ESI	electrospray ionization
ETC	electron transport chain
F12	Ham’s F-12 Nutrient Mixture
F12K	Ham's F-12K (Kaighn's) Medium
F6P	fructose 6-phosphate
FA	fatty acids
FAD	oxidised flavin adenine dinucleotide
$FADH_2$	reduced flavin adenine dinucleotide
FAO	fatty acid oxidation
FBS	fetal bovine serum
FDR	false discovery rate
FFA	free fatty acids
FMN	flavin mononucleotide
G6P	glucose 6-phosphate
G6PD	glucose 6-phosphate dehydrogenase
GC	guanine-cytosine content
Glc	glucose
GLUT	glucose transporter protein
GOBP	Gene Ontology Biological Process

GOCC	Gene Ontology Cellular Component
GOMF	Gene Ontology Molecular Function
GPI	glycosylphosphatidylinositol
GPx	glutathione peroxidase
GR	glutathione reductase
GSH	reduced glutathione
GSSG	oxidised glutathione (glutathione disulfide)
HBP	hexosamine biosynthetic pathway
HCM	hypertrophic cardiomyopathy
hESC	human embryonic stem cells
HF	heart failure
HFpEF	heart failure with preserved ejection fraction
HFrEF	heart failure with reduced ejection fraction
HIF-1α	hypoxia-inducible factor 1-alpha
hiPSC	human induced pluripotent stem cells
F6P	fructose 6-phosphate
HPLC	high-performance liquid chromatography
HS	horse serum
hSC	human stem cells
HIF-PH2	hypoxia-inducible factor prolyl hydroxylase 2
I/R	ischemia/reperfusion
ICM	ischemic cardiomyopathy
IMDM	Iscove's Modified Dulbecco's Medium
IS	internal standard
LC	liquid chromatography
LCFA	long-chain fatty acids
LDHA	lactate dehydrogenase A
LFQ	label-free quantification
LVEF	left ventricular ejection fraction
LVNC	left ventricular noncompaction cardiomyopathy

m/z	mass-to-charge ratio
MCL	Markov Cluster algorithm
MeOH	methanol
MI	myocardial infarction
MPI	mannose-6 phosphate isomerase
MRM	multiple reaction monitoring
MS	mass spectrometry
MS/MS	tandem mass spectrometry
NAD	oxidised nicotinamide adenine dinucleotide
NADH	reduced nicotinamide adenine dinucleotide
NADPH	reduced nicotinamide adenine dinucleotide phosphate
nano-ESI	nano-electrospray ionization
nanoLC	nano-liquid chromatography
NEM	N-ethylmaleimide
NPC	no-primer control
NTC	no-template control
OCR	oxygen consumption rate
OMM	outer mitochondrial membrane
OXPHOS	oxidative phosphorylation
PASEF	parallel accumulation-serial fragmentation
PBS	phosphate-buffered saline
PCA	principal component analysis
PCr	phosphocreatine
PDH	pyruvate dehydrogenase
PEDF	pigment-epithelium-derived factor
PEP	phosphoenolpyruvate
PFK	phosphofructokinase
P_i	inorganic phosphate
PKM	pyruvate kinase isozymes M1/M2
PPP	pentose phosphate pathway

PRM	parallel reaction monitoring
PSM	peptide spectrum matches
PTM	post-translational modification
QQQ	triple quadrupole
qTOF	quadrupole time-of-flight
R5P	ribulose 5-phosphate
RCM	restrictive cardiomyopathy
RONS	reactive oxygen and nitrogen species
ROS	reactive oxygen species
RPLC	reverse-phase liquid chromatography
RT-qPCR	real-time quantitative polymerase chain reaction
SAM	S-adenosyl methionine
SDB-RPS	(poly)styrene divinylbenzene-reverse phase sulfonate
SEM	standard error of the mean
SLC2A	solute carrier family 2, facilitated glucose transporter member
SOD	manganese superoxide dismutase
SRM	selective reaction monitoring
stage	stop and go extraction
SV40	simian vacuolating virus 40
TCA	tricarboxylic acid cycle
TCEP	tris(2-carboxyethyl)phosphine
TFA	trifluoroacetic acid
TFE	trifluoroethanol
TIC	total ion chromatogram
TIMS	trapped ion mobility spectrometry
Tm	melting temperature
TOF	time-of-flight
UCP	uncoupling protein
UDP-GlcNAc	uridine diphosphate N-acetylglucosamine
UHPLC	ultrahigh-performance liquid chromatography

UPR	unfolded protein response
VAD	ventricular assist device
WHO	World Health Organisation

Table of Content

1 Introduction

1.1 Heart Disease and The Molecular Aspects of the Failing Heart

Chronic heart disease and cardiac events are of most concern for modern medical sciences and represent an enormous global burden on public health. They possess great complexity and variety in underlying causes, pathology and accompanying symptoms.[1]

The great intricacy of the human heart can be illustrated by the current understanding of at least 400 genes involved in regulating heart cell development. Key regulators of gene expression, such as the transcription factors Nkx2.5, GATA, Mef2C and Tbx5, seem to be at the core of controlling both cardiac development as well as homeostasis in the adult and ageing organ. The mammalian heart is dynamic, and adaptive processes such as cardiac hypertrophy happen during heart development and in response to physiological and pathological stimuli.[2, 3]

In health and under normal physiological conditions, the heart is able to respond to stress by short-term adaptations in gene regulation of heart cell function to restore homeostasis. Compensation may be impossible if the stressor is too potent or persistent. Cellular responses might be insufficient or improper, especially if an already compromised or predisposed organ is put under additional strain.[2, 4]

Diseases of the heart affecting children are primarily of congenital origin. Heart diseases in adults can briefly be categorised into cardiovascular diseases (CVD), degenerative dilated heart diseases, and cardiac arrhythmias. Adult pathologies can be acquired (e.g., lifestyle factors) or caused by genetic defects. In the majority of cases, the causes are neither of purely genetic nor lifestyle origin but constitute diverse, and most often multiple, underlying pathophysiological mechanisms.[5, 6]

Impaired heart function is the leading cause of death globally, representing 32% of all deaths in 2019, according to the World Health Organization (WHO) reports. Possible underlying conditions include coronary heart diseases, e.g., atherosclerosis of the coronary arteries or, most acutely, myocardial infarction (MI). Additional causes are hypertension (persistent high blood pressure), heart valve damage, conditions affecting the heart muscle (cardiomyopathies) and arrhythmias (e.g., atrial fibrillation), among others.[6, 7]

The different forms of congenital heart disease can manifest in, e.g. arrhythmias and anatomic abnormalities of the heart, and are thought to only constitute 1% of all heart disease cases. Genetic predisposition, however, plays a significant but varying role in the development of all forms of heart disease. The primary risk factors originate from comorbidities and lifestyle (see Figure 1). Those include obesity (dyslipidaemia and inflammation), alcoholism, smoking, hyperthyroidism, pulmonary hypertension, (untreated) diabetes mellitus, autoimmune diseases, infections (bacterial or viral endocarditis) and anaemia.[6–8]

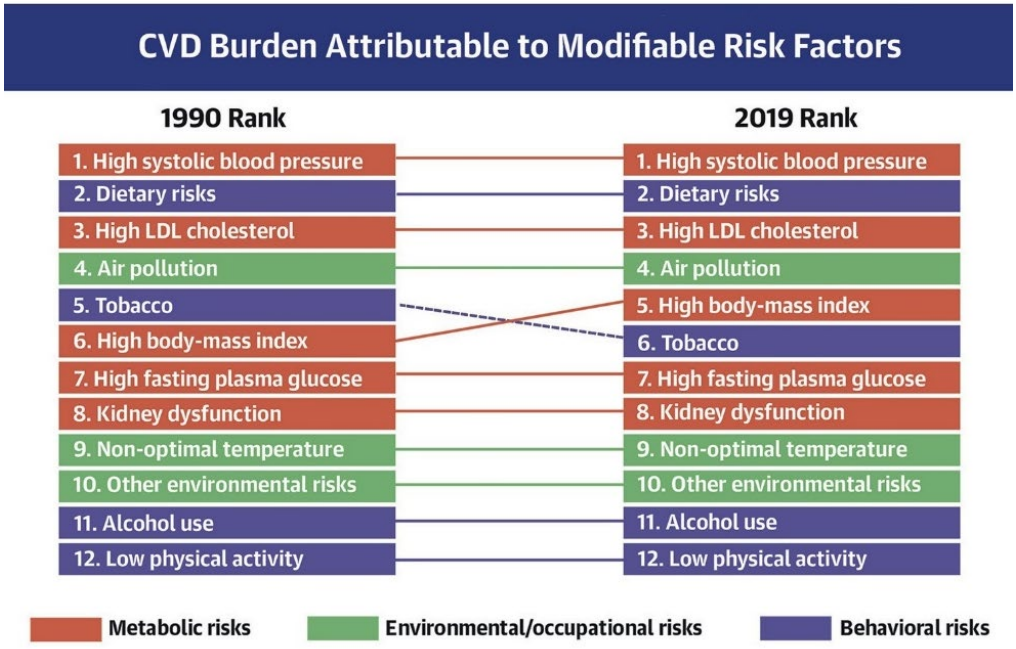

Figure 1. Listed above is the global comparison of the rankings of modifiable (i.e., lifestyle) risk factors attributable to CVD (cardiovascular disease) in 1990 (left) and 2019 (right). The impact of the individual risk factors further varies based on location and other demographics (e.g., age, income, ethnicity, and education). The diverse underlying mechanisms of CVD and heart disease are tightly connected and typically result from the synergistic effect of multiple risk factors driving the pathogenesis and progression of the disease. Illustration by Roth, G.A. et al. used with permission by Elsevier B.V.[6]

Heart failure (HF) happens once the organ fails to sufficiently pump blood through the circulatory system. The main pathophysiology of HF can be described as a reduction in the efficiency of the cardiac muscle through overloading or damage. Once heart disease has developed, its progression and acute cardiac events will result in the remodelling of the heart over time. A cardiac infarction can cause a significant loss of the myocardium (heart muscle) due to oxygen starvation and compensatory overgrowth of fibroblasts. Associated increases in ectopic calcification, and the resulting stiffness of coronary arteries and heart valves, further reduce cardiac blood flow and pump function of the weakened organ.[7, 9]

Other causes of HF affect cardiac output and the total workload of the heart muscle as well. Conditions such as cardiac amyloidosis result in additional stiffness due to the deposition of misfolded proteins in the heart muscle. Hypertension, on the other hand, increases the force of contraction needed to pump blood and asserts additional ventricular wall stress. As the strained cardiac muscle becomes over-stretched and stiff, contractions become less efficient due to a reduced ability of actin and myosin filaments to cross-link. The organ must work harder to meet the regular metabolic demand, and the amount of potential cardiac output in situations of increased oxygen demand (i.e., exercise) is reduced. This intolerance to exercise and overall exhaustion is commonly observed in patients with HF.[4, 5, 10]

Reduced ventricular ejection fraction can most often (but not invariably) be observed in heart failure. Left ventricular ejection fraction (LVEF) is a common descriptor as it indicates the effectiveness of pumping blood into systemic circulation. LVEF is generally between 55 and 70% in healthy individuals and worsens as the disease progresses. Life-threatening conditions are described with LVEF below 40%, with acute MI causing a LVEF of well below 35%.[7, 11]

Most heart diseases are progressive, and heart failure is a long-term condition that gradually worsens over time. Heart failure will ultimately lead to cardiac arrest. The condition can develop quickly (acute heart failure) or gradually over weeks to months (chronic heart failure). While heart failure can occur at any time, it is most common among older people. Medical attention does not allow for a cure, but the progression can be stunted, and the symptoms can be managed for years or even decades. Treatment options depend on the individual and include the modulation of associated risk factors by lifestyle changes to slow disease progression and prevent the reoccurrence of cardiac events. Additionally, pharmacological intervention, bypass operation and the implantation of a pacemaker or a ventricular assist device (VAD) are commonly practised.[5, 12]

Patients generally require lifelong medical care, and currently, the only way to fend off the endpoint of the disease, death, is heart transplantation. Novel and formerly promising interventions like regenerative stem cell therapy have not been proven beneficial so far. The human heart indeed constitutes a small number of cardiac stem cells and adult cardiomyocytes can re-enter the cell cycle (0.5 to 1% per year).[12–14]

However, heart cells are not capable of asserting regenerative effects to repair defects by proliferation. Adult stem cells have also not been shown to participate in cardiomyocyte generation. Novel developments suggest that stem cell therapy may assert a small, positive paracrine effect that aids in the recovery of LVEF. Despite multiple small animal models revealing mechanisms for successful heart regeneration, no therapeutically introduced cell type was shown to significantly increase the patient's quality of life after acute MI or in the course of dilatative cardiomyopathies (DCM). Cardiac stem cells (CSCs) have not been shown to be superior to supportive bone marrow cell (BMC) therapy in large animal models or human studies. Hence alternative strategies should be evaluated. Advancing the current understanding of pathomolecular mechanisms is of most importance to increase the pool of viable diagnostic and treatment options.[14–17]

1.1.1 Cardiac Remodelling Alters Cellular Function

As already stated, physiological and pathological compensation strategies of the human heart occur to preserve homeostasis and contractile function (Figure 2). Physiological adaptation may, at first, include cell growth and increases in angiogenesis, energy efficiency, protein synthesis and quality control, autophagy, and antioxidant generation. Depending on the stimuli, and as the responses transpire to be insufficient, disease onset and progression will follow. This adaptive process will transition to HF through pathological remodelling. The distinct maladaptation in cardiac cells may result in fibrosis, altered sarcomere structure, impaired Ca^{2+} handling, induction of fetal gene programming, mitochondrial dysfunction, disbalance in reactive oxygen and nitrogen species (RONS; see 1.1.2), metabolic reprogramming (see 1.1.1.1) and cell death.[18, 19]

While there are many specific components to cardiac remodelling in the various forms of heart disease, the further focus will be on characteristic functional and structural adaptions in patients of heart failure with underlying cardiomyopathy. Cardiomyopathy describes a heterogeneous group of diseases affecting the heart muscle.[5, 20]

Cardiomyopathies caused by genetic mutations are grouped into the morphological subtypes DCM, hypertrophic cardiomyopathy (HCM), restrictive cardiomyopathy (RCM), left ventricular noncompaction cardiomyopathy (LVNC) and arrhythmogenic right ventricular cardiomyopathy (ARVC; characteristic myocardial substitution by fibrofatty tissue). HCM (prevalence of 1:500), ARVC and LVNC are considered

dominantly congenital, while DCM (prevalence of 1:2500) and RCM are thought to have genetic and acquired components in pathogenesis. DCM, the leading indication for heart transplantation, is characterised by the heart becoming enlarged and unable to effectively pump blood. Beside genetic origin, causes include complications during pregnancy, toxins, substance abuse and certain infectious diseases. Hypertension and coronary artery disease may play a role but do not primarily drive pathogenesis.[20, 21]

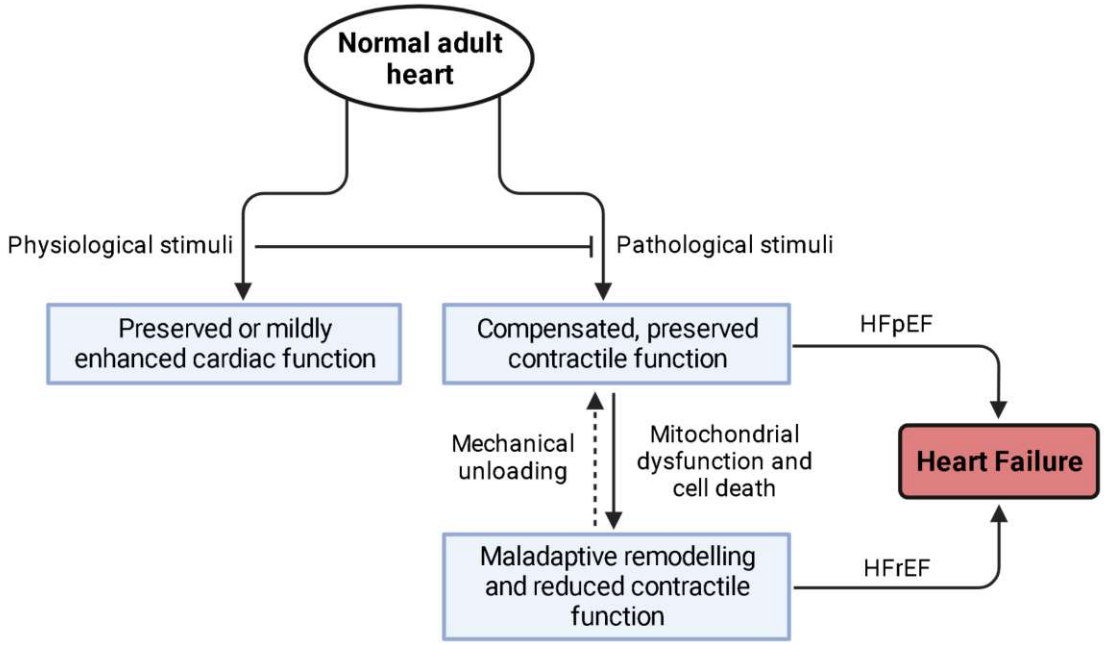

Figure 2. Overview of physiological (i.e., during endurance training and pregnancy) and pathological adaptations of the heart trying to preserve homeostasis and contractile function. Physiological signalling pathways in homeostasis may assert an antagonizing effect to pathological cardiac remodelling and dysfunction. In the example of cardiac hypertrophy in endurance athletes (left), the heart can return to its original dimensions after relief from the stimulus (not shown). In pathology (right), e.g., after MI, a reduction in left ventricular chamber dimension and cardiac output is compensated by increased wall thickness. Progression in disease will result in further maladaptation in cardiac cells and ultimately in heart failure with preserved or reduced ejection fraction (HFpEF and HFrEF, respectively). Acute and long-term clinical strategies to achieve left ventricular unloading (e.g., by mechanical circulatory support) are possible and might reverse some aspects of remodelling.[22] Illustration adapted from Nakamura, M. et al. used with permission by Springer Nature Limited.[18]

Acquired forms of cardiomyopathy include conditions caused by significant physical (Takotsubo syndrome) or emotional stress (broken heart syndrome), or myocarditis (inflammation and injury of the heart tissue in part due to infiltration by different types of leukocytes). Ischemic cardiomyopathy (ICM) is formally not included in these classifications as it is a direct consequence of another cardiac pathology. This leading cause of sudden cardiac death predominantly occurs in patients with a history of acute MI or coronary artery disease. As indicated by the nomenclature, the disease is accompanied by local anaemia and oxygen deprivation due to obstruction of the blood supply. Ischemia drives myocardial remodelling, tissue damage and cell death.[20]

1.1.1.1 Metabolism in Cardiac Health and Disease

The heart is constantly consuming a variety of energy substrates for ATP (adenosine triphosphate) production to fuel life-long contractions and deliver oxygen and blood to the rest of the body.[23]

Cellular uptake of glucose from the bloodstream by cardiomyocytes is mainly mediated by the class I glucose transporters GLUT1 (solute carrier family 2, facilitated glucose transporter member 1; SLC2A1) and GLUT4 (SLC2A4). Whereas GLUT1 is widely distributed in fetal tissues and erythrocytes, it is also responsible for insulin-independent basal glucose uptake in most cell types. Cellular glucose levels inversely regulate the number of transporters in the cell membrane. GLUT1 upregulation is characteristic in many forms of cancer. GLUT4 is primarily expressed in adipose and striated muscle tissue, including skeletal and cardiac muscles. GLUT4 is responsible for insulin-regulated glucose uptake and storage. As insulin binds the insulin receptor and activates the signal transduction pathway, cellular translocation of GLUT4 proteins (stored in transport vesicles inside the cell) to the plasma membrane is facilitated. While basal glucose uptake and GLUT1 are especially important in the cardiac muscle, GLUT4 is still believed to be the primary transporter.[19, 24]

The fate of glucose inside the cardiomyocyte after uptake can be seen in Figure 3. It depends on multiple layers of crosstalk among metabolic pathways and cellular state of energy, and substrate availability. While glycolysis is the most important route for cellular glucose metabolism, it (and glucose metabolism overall) only contributes little to the overall ATP production in the healthy heart. Still, pyruvate, NADH (reduced form of nicotinamide adenine dinucleotide) and ATP are substantial yields from this pathway. Glycolysis-derived ATP is tightly coupled with maintaining contractile function. Pyruvate can be used to form alanine or be reduced to lactate. In the case of regular glucose oxidation, pyruvate will ultimately form acetyl-CoA by pyruvate dehydrogenase (PDH), fuelling the tricarboxylic acid cycle (TCA) and oxidative phosphorylation (OXPHOS) inside mitochondria.[25, 26]

Glycolysis is governed by the key enzymes hexokinase (HK), phosphofructokinase (PFK) and pyruvate kinase isozymes M1/M2 (PKM), all catalysing irreversible reactions. Further regulation is asserted by substrate concentrations, hormones and oxygen availability.[19]

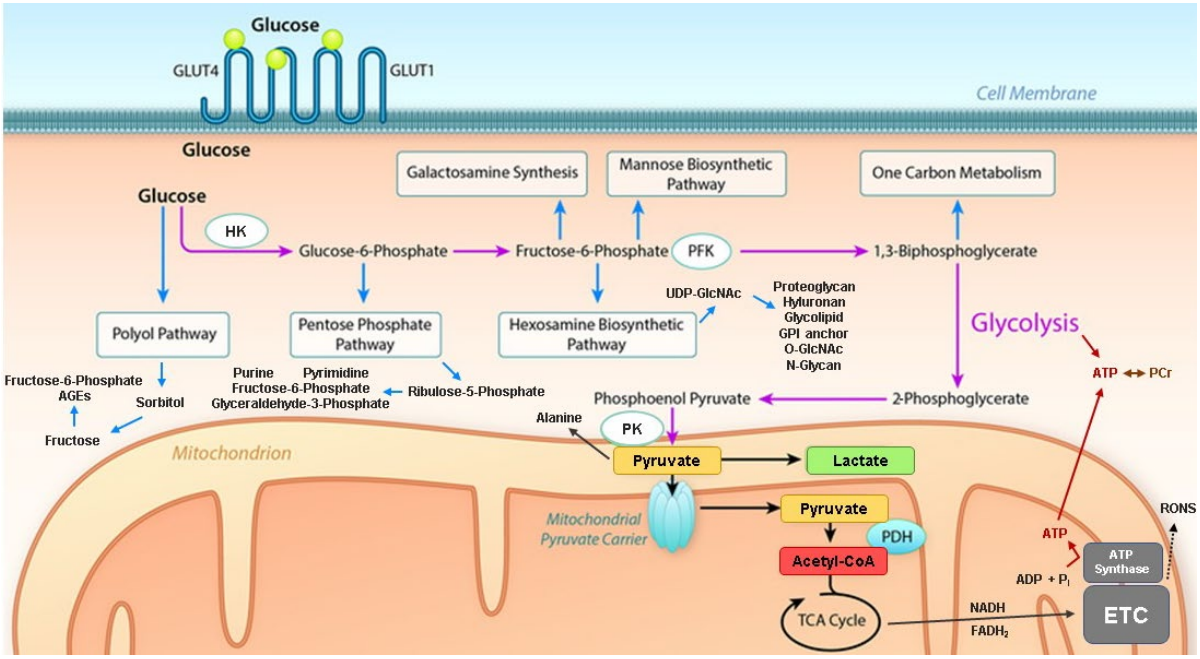

Figure 3. The fate of cellular glucose after uptake involves multiple metabolic pathways inside the cytosol and mitochondria. Glucose may be phosphorylated to glucose 6-phosphate (G6P) via hexokinase (HK) activity or be converted to sorbitol in the polyol pathway (see 1.1.2). Glucose 6-phosphate may enter glycolysis, the pentose phosphate pathway (PPP; see 1.1.2) or the hexosamine biosynthetic pathway (HBP). Glucose will either be utilized as a substrate for ATP production or a building block. ATP and the phosphocreatine system fuel contraction. AGEs indicate advanced glycation end products. ETC indicates the electron transport chain. GPI indicates glycosylphosphatidylinositol. PCr indicates the phosphocreatine system. PDH indicates pyruvate dehydrogenase. P_i indicates inorganic phosphate. Illustration adapted from Lopaschuk, G.D et al. with permission by Wolters Kluwer Health, Inc.[19, 25]

Heart disease in various stages can be linked to disrupted and abnormal metabolism in cardiac cells. While healthy mature cardiomyocytes primarily rely on fatty acids (FA) as an energy substrate, with beta-oxidation and mitochondrial activity tightly synchronised, impaired cardiomyocytes during pathological remodelling may show reduced fatty acid oxidation (FAO) and instead rely on glucose as fuel (see Figure 4). The increasing glycolytic phenotype in the onset of heart disease is proposed as a protective response against further cardiac injury. Increases in glycolysis may be the consequence of elevated intracellular free AMP (adenosine monophosphate) levels associated with pressure overload. Subsequent signal transduction by AMP-activated protein kinase (AMPK) leads to upregulated synthesis of fructose 2,6-bisphosphate by PFK2 activation by phosphorylation, downstream activation of PFK1 and glucose transporter (GLUT4) migration to the membrane. Further activation is asserted by ADP (adenosine diphosphate), whereas ATP, NADH and citrate (TCA overflow) exert an inhibitory effect. Failure to increase glycolysis in this way has been shown to elevate disease progression and fibrosis in transgenic animal models.[19, 27–29]

However, prolonged activation of the glycolytic phenotype may result in decompensation, induction of pathological hypertrophy, and progression of HF. The adaptive increase in glycolysis may not be matched in glucose oxidation and lead to an uncoupling between substrate uptake and oxidation. Preservation of or increases in FAO have also been observed in cardiac hypertrophy. The rate of glycolysis may be modulated by elevated FAO through the inhibition of PFK1 and the development of insulin resistance. GLUT4 translocation is reduced in the insulin-resistant heart, and metabolic flexibility is subsequently impaired. FA utilization may consequently be upregulated in the case of diabetic cardiomyopathy. Dysregulated energy metabolism can lead to impaired ATP synthesis and thereby advance the development of heart failure.[30–32]

Alterations in glycolysis and glucose, lactate, long-chain fatty acid (LCFA), ketone, and amino acid (including branched-chain amino acids; BCAA) utilization differ between physiological stimuli and disease state. E.g., exercise-induced acute suppression of PFK activity and glycolysis are followed by increased glycolytic activity in the recovery stage. Regular exercise may therefore be essential for maintaining metabolic flexibility and compensatory adaptions in physiological ranges.[30, 33]

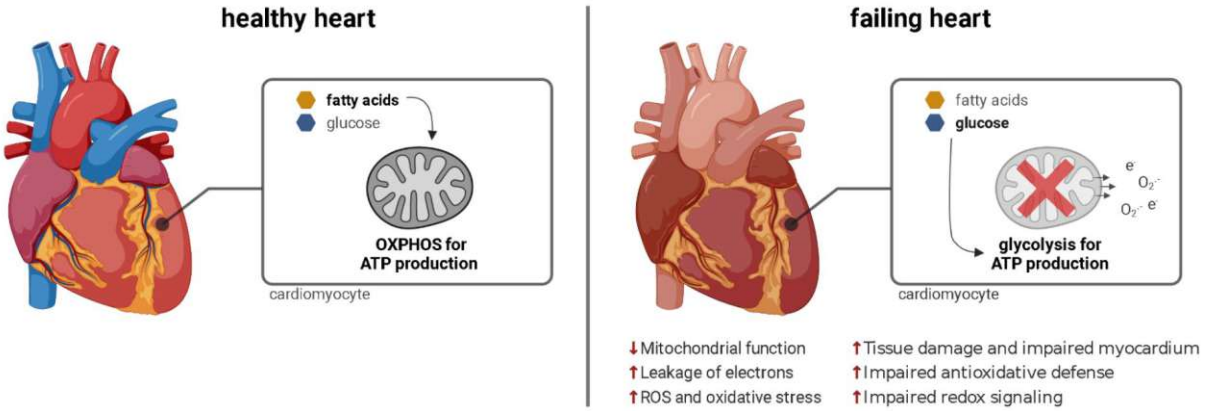

Figure 4. Illustration of the central hypothesis of energy metabolism in the healthy (left) and failing (right) heart. Listed as well are the downstream effects of aberrant metabolism and oxidative damage. However, specific time points and events in the progression of heart disease may show distinct alterations in glucose and fatty acid utilization in both ways.[19, 34]

Cardiac ischemia leads to inadequate oxygen supply and improper metabolic waste removal. Insufficient oxygen reduces the capacity for FAO, leading to increased dependency on glycolysis and glucose uptake. Upregulated glycolytic efflux has been shown in mild ischemia, whereas severe obstruction of coronary blood flow ultimately decreases glucose uptake. Increased glycolysis in severe ischemia could disturb ionic

homeostasis, affecting contractile function. In addition, elevated lactate levels would further contribute to the uncoupling of glucose oxidation and myocardial injury. Restoring blood flow (reperfusion) is the most promising approach for mitigating cardiac damage. However, reperfusion injury may occur due to increased glycolytic efflux without the ability to adequately increase glucose oxidation. Analogously, an overload in intracellular Ca^{2+} and Na^{+} could further impair contractility. Reperfusion increases FAO, further downregulating glucose oxidation and promoting the uncoupling to glycolysis. Temporary suppression of FAO may be viable in countering reperfusion injury and preserving homeostasis in myocardial energy metabolism.[25, 35]

The uncoupling of glycolysis and glucose oxidation has been indicated to play a significant role in the early pathogenesis of HFpEF. Restoration of the coupling may therefore provide novel treatment options. Reduction in FAO has only been shown in the later stages of disease and not in the onset of HFpEF. The currently available data suggest that reduced FA utilization plays a significant role in the later and end stages of HF. Modulation of metabolic pathway use by inhibiting FAO and thereby promoting glucose oxidation is proposed as a therapeutic option in treating (earlier stage) HF and ischemia/reperfusion (I/R) injury.[19, 36]

Different approaches have been explored, including inhibiting FA uptake into mitochondria by modulation of carnitine palmitoyltransferase 1. Suppression of FAO can also be achieved by the inhibition of 3-ketoacyl-CoA thiolase, the last enzyme in β-oxidation. Furthermore, infusion of glucose-insulin-potassium (GIK) reduces circulating levels of FA, promotes glycolysis and helps to electrically stabilize the myocardial cell membrane. While initial promising results have been achieved, clinical consistency and safe usage remain to be validated.[26, 36, 37]

While studied significantly less, additional pathways of glucose metabolism have also been linked to cardiac pathology. HBP and O-GlcNAcylation may assist the unfolded protein response (UPR) in accommodating metabolic fluctuations in heart disease and I/R injury. Additionally, cardiac glycogenesis and glycogenolysis support steady energy production and may play a critical role in managing glucose efflux and calcium homeostasis.[38–40]

In conclusion, HF can be associated with profound metabolic remodelling, affecting contractility not only by changes in substrate utilization but also protein quality control, ionic balance, autophagy and redox homeostasis. Increased utilization of one

particular fuel may not be harmful if the metabolic shift is balanced and the ATP demand of the cardiac muscle is met. Restoring metabolic flexibility and substrate oxidation may be essential in preventing disease progression and treating acute cardiac events.[30]

1.1.2 Oxidative Stress and Mitochondrial Dysfunction

Oxidative stress plays a major role in various pathologies. In heart disease it is linked not only to disease progression but also to underlying risk factors for pathogenesis, such as diabetes, obesity, metabolic syndrome and ageing. While free radicals occur naturally in cellular processes, a disturbance of the tightly regulated homeostasis between oxidative species and antioxidants can result in oxidative damage.[41, 42]

As already mentioned with FAO, mitochondrial activity in cardiac cells is most important for fuelling contractions. An overview of mitochondrial metabolism and the electron transport chain (ETC) is illustrated in Figure 33 in the appendix. OXPHOS, utilizing the generated redox equivalents from the metabolization of various energy substrates, is responsible for 95% of ATP production in healthy cardiomyocytes. Thus, high mitochondrial activity and an extensive number of organelles require non-enzymatic and enzymatic (e.g., superoxide dismutases, peroxiredoxins, thioredoxin and glutathione systems) attenuation of generated RONS (e.g., peroxides, free radicals, lipid peroxides). Involved antioxidants include N-acetylcysteine, glutathione, carnosine, ascorbic acid and tocopherol. These molecules either act as radical scavengers or reducing agents or synergize in replenishing antioxidants. Under physiological conditions, RONS assert essential signalling functions for regulating mitochondrial activity and cellular adaptions to stressors, e.g. mitochondrial biogenesis and the modulation of the immune response following exercise.[26, 43, 44]

Prolonged exposure to oxidative stress contributes to the impairment of the antioxidative defense, dysregulation of redox signalling and damage to biomolecules (e.g., lipids, proteins, nucleic acids), advancing the functional decline of the myocardium (see Figure 4). Damage to proteins includes oxidation of the amino acid side chains and post-translational modifications (PTMs), which are reported to arise early into the decline of the myocardium and may trigger protein degradation pathways.[42, 43, 45]

Previous studies have reported impairment of the mitochondrial ETC and disturbance in redox homeostasis in HFpEF and HFrEF. Lowered ATP production, electron

leakage and dysregulated Ca^{2+} signalling can be the consequence of ischemia. Furthermore, the switch away from mitochondrial activity and towards glycolysis is considered a possible compensatory mechanism to reduce the adverse effects of dysfunctional mitochondrial organelles. This may indeed reduce the load of RONS at first. However, this increased glucose uptake leads to high cellular concentrations of this by itself oxidative molecule. Further problems arise from decoupling glycolysis and subsequent glucose oxidation and OXPHOS. Metabolic frontloading by high glucose concentrations beyond metabolic capacity results in increased oxidative stress and mentioned adverse downstream complications.[26, 45, 46]

Disturbed redox environments may also occur in acute events. Increased oxidative stress is an important pathological mechanism in reperfusion injury following myocardial ischemia. The already weakened heart, dysfunctional mitochondria and impaired antioxidative defense are unable to attenuate the influx of substrates, oxygen and the subsequent increase in RNOS. Studies report severe inflammation, accelerated cardiac remodelling, and increased apoptosis.[43, 47]

As mentioned, mitochondrial dysfunction and increased redox stress have been reported in diabetic heart disease. The altered metabolism of the insulin-resistant heart may result in fatty acid-induced lipotoxicity and the uncoupling of OXPHOS. Accumulating FA intermediates (e.g., long-chain acylcarnitines) inhibits pyruvate and lactate metabolism and OXPHOS, thus disturbing the mitochondrial membrane structure and respiratory complexes. Additionally, induction of uncoupling proteins (UCP2; UCP3) and activation of ADP/ATP carriers by FA have also been proposed to be responsible for increased leak respiration.[48, 49]

Aspects of glucose metabolism not mentioned so far have substantial implications in redox homeostasis. The polyol pathway involves the conversion of glucose to sorbitol by aldose reductase (AR) and subsequent oxidation to fructose. Implications for HF are not fully illuminated. While the polyol pathway may be increased in hyperglycaemia and aid in preserving osmotic balance, AR should assert significant antioxidative activity. However, studies have shown mixed participation in protecting against or contributing to cardiac damage. Furthermore, increased conversion of glucose to fructose may reduce FA utilization. AR may also impair mitochondrial membrane function in I/R injury and reduce the antioxidant activity of manganese superoxide dismutase (SOD). A limited number of studies suggest cardioprotective effects of AR

inhibition due to increased glycolysis and ATP generation rates. Additionally, AR inhibition may allocate NADPH (reduced form of nicotinamide adenine dinucleotide phosphate) for the glutathione reductase pathway. The role of polyol pathway-driven generation of ROS by a reduction in NADPH and subsequent glutathione availability has been discussed in diabetes mellitus.[25, 50]

While the oxidative phase of PPP generates ribulose 5-phosphate (R5P) and NADPH, the non-oxidative phase delivers multiple substrates for glycolysis and the synthesis of nucleotides. The PPP can be classified as having more of an anabolic character than catabolic nature and is a significant source of NADPH for maintaining cytosolic glutathione levels. Implications for cardiac redox status and contractility have been observed. Acute induction of glucose 6-phosphate dehydrogenase (G6PD), the first enzyme of the PPP, improves cardiomyocyte protection against oxidative injury. Depletion of G6PD was shown to adversely affect preserved contraction. However, prolonged and exaggerated PPP activation may be associated with increased oxidative stress and contributes to the progression of cardiomyopathies and HF. This adds to the two-sided nature of cardiac metabolism and redox homeostasis.[19, 51]

The serine biosynthetic pathway utilizes glyceraldehyde 3-phosphate to synthesize serine, which can be further used to create glycine and cysteine. Furthermore, serine provides the carbon unit to the 1-carbon metabolism. The folate cycle, methionine cycle and trans-sulfuration pathway generate purines, pyrimidines, S-adenosyl methionine (SAM; cellular methyl donor) and glutathione. Activating the serine biosynthetic pathway and 1-carbon metabolism may increase ATP synthesis and total glutathione levels, subsequently asserting cardioprotective effects against oxidative injury.[52]

1.1.2.1 Glutathione Status as Cellular Biomarker of Oxidative Stress

Glutathione (GSH) is an essential and abundant antioxidant inside the cytosol and organelles. There it aids directly (and indirectly) in neutralising free radicals and RONS, such as peroxides, and serves as a thiol-protecting agent. Under normal cellular conditions, the GSH form, as shown in Figure 5, is highly abundant and tightly regulated in homeostasis. The ratio of reduced to oxidised glutathione (GSSG) is disturbed in acute responses to cellular stressors and in various pathologies. A lower GSH/GSSG ratio can therefore serve as a marker for increased oxidative stress and has been proposed as a biomarker for disease progression. Decreased glutathione ratio has been observed in the tissue of failing hearts.[45, 53]

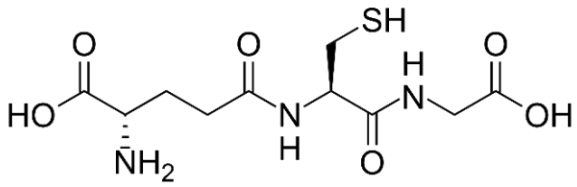

Figure 5. Glutathione (γ-L-Glutamyl-L-cysteinylglycine; GSH) is an abundant and vital cellular antioxidant. This active, reduced, monomeric form of glutathione (GSH) gets oxidised by glutathione peroxidase (GPx) while acting against ROS (e.g., hydrogen peroxide, lipid peroxides) and forms the GSSG dimer (disulfide bond between the cysteines). The cysteinyl residue's thiol group may act directly as a reducing equivalent. Recovery of GSSG to GSH is catalysed by glutathione reductase (GR). In addition to the antioxidant activity, glutathione is also used for conjugation to lipophilic xenobiotics to facilitate their metabolism and excretion.[53]

1.2 Hypothesis and Research Aim

Based on preliminary data in the tissue of failing hearts, the aim was to conduct a follow-up experiment further focusing on cellular changes *in vitro* to address the crosstalk of aberrant metabolism and oxidative stress in cardiac cells in the context of heart disease.[45]

It is still unknown if the occurring redox stress during the progression of HF can be clearly or partially annotated as causative or just a by-product resulting from cardiac remodelling. As heart disease is a multifaceted and complex research topic, further and novel mechanistic insights into its development and progression are yet to be gained. Exploration of these intricate molecular events might further allow the identification of a target of early disease onset for prospects in diagnostics as well as possible treatment options.

Therefore, the design and evaluation of an appropriate *in vitro* experimental setup in the context of this thesis were deemed detrimental to advancing this project. To replicate environments reflecting different stages in the pathological progression of HF and acute myocardial events, the cardiac cell model was to be exposed to variations in oxygen and glucose availability.

Using modern high throughput, high sensitivity mass spectrometry analysis of the cellular proteome and redox status, valuable insight into pathophysiological adaption can be gained. Furthermore, the translational ability of the deployed *in vitro* model compared to previously observed changes in cardiac tissue was to be inspected.

1.3 Translational Aspects of the Experimental Design

CVD and HF are challenging to examine as these conditions arise from multiple underlying factors and exhibit multi-systemic pathology. Cardiac biopsies of patients

(and potential controls) are limited to the endomyocardial region, and catheterization is a highly invasive procedure. As tissue of non-failing and failing hearts of diseased specimens is of very limited availability and subject to elaborate and robust clinical study design, research depends on animal models and *in vitro* experiments based on human and non-human cell cultures. Additionally, *in silico* approaches have become widely applied as computational power and bioinformatical tools advance.[54, 55]

Animal models can provide valuable *in vivo* and *ex vivo* insight into disease mechanisms on tissue, organ, systemic and organismal levels. Various species have been established in routine research practice. Zebrafish and *Drosophila* are heavily used model organisms in developmental biology research. Mammalian i*n vivo* models include rodents and larger animals (e.g., pigs and dogs). The advancement in molecular biological techniques of the last decades further allowed the creation of disease-specific animal models, such as diabetic pig models and rabbits overexpressing mutant proteins identified in patients of congenital cardiomyopathy. While research in animals, especially rodents, allows for relatively elaborate experimental throughput, it is often difficult to translate to humans. Additionally, research practice should include laboratory animal use replacement, reduction, and refinement (3R).[54, 55]

In vitro models can complement and (partially) replace animal-based and patient-derived research. Cardiac cell culture allows for precise control of experimental conditions. It is widely applied in the initial identification of pathological mechanisms and drug target, compound and toxicology screening.[54]

1.3.1 Anatomy of the Human Heart

The complex composition and developmental mechanisms of the organ drive the difficulty of representing the heart in research models. The human heart's anatomy and description of cardiac blood flow can be found in Figure 6 as well as in Figure 34 in the appendix. Contractions require a complex interplay of multiple cell types and the cardiac conduction system. It is controlled by the sympathetic and parasympathetic, and autonomous nervous systems.[56]

Above 80 genes are expressed in the various conductive cardiomyocytes responsible for contraction (e.g., pacemaker cells in the atrioventricular and sinoatrial node or Purkinje fibres). The electrocardiogram (ECG) is the sum of the individual action

potentials of all contracting cells. Nutrient and oxygen delivery is autonomous as the coronary arteries supply the heart with blood. Severe obstruction results in MI.[57]

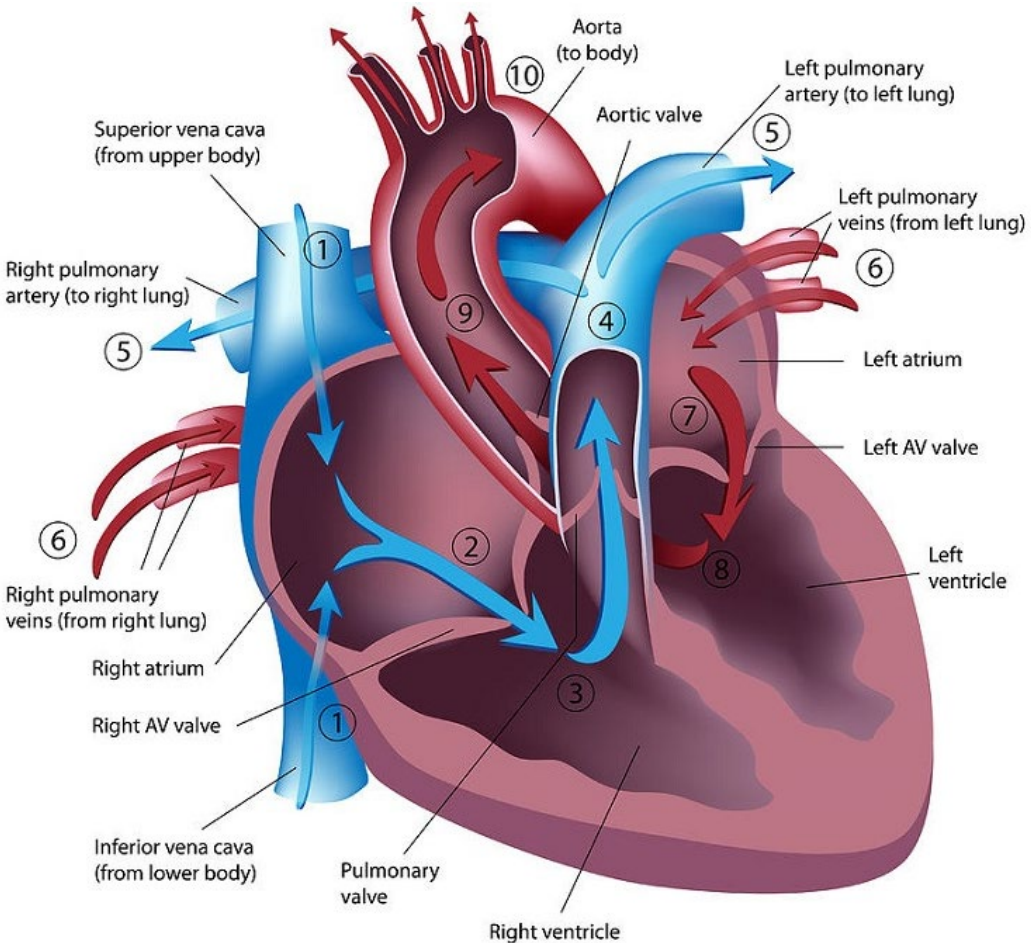

Figure 6. The pathway of blood flow through the anatomically healthy heart. Deoxygenated blood from the body returns through the superior and inferior vena cava (1) to the right atrium (2). It then enters the right ventricle (3) through the right atrioventricular (AV) valve and is pumped further through the pulmonary valve into the pulmonary arteries (4,5). Delivery to the lungs allows reoxygenation before returning through the pulmonary veins (6) into the left atrium (7). After entering the left ventricle (8) through the left AV valve, it is distributed to the body via the aortic valve and aorta (9,10). Illustration by Harrison, T.M. et al. used with permission by John Wiley and Sons.[58]

At least 20 different cell types constitute the heart, all contributing to mechanical, structural, biochemical, and electrical functions. Above half of all cardiac cells are fibroblasts of, e.g., the epicardium and coronary vasculature. Ventricular and atrial cardiomyocytes build the myocardium, filling a majority of tissue space at relatively low numbers. The interior lining of cardiac valves and blood vessels (endocardium) is formed by endothelial cells. Further types include smooth muscle cells of the coronary arteries and cardiac vasculature, immune cells and a small number of CSCs.[56]

1.3.2 Cardiac *in vitro* Models In Heart Disease Research

Recent literature on currently applied *in vitro* models of human and animal origin has shown their specific limitations in medical research. Primary cells derived from the cardiac tissue of clinical patients are of limited availability, and not every research facility has or wants access to a laboratory animal facility. Still, neonatal cardiomyocytes, isolated from newborn rats, are commonly used. Isolation requires a high number of animals and experienced operators. As neonatal cell cultures contain mixed cell populations and are hardly reproducible and fragile, immortalisation has allowed new possibilities in cardiac cell attainability and larger-scale studies. H9C2 myoblasts originate from female embryonic BDIX (Berlin-Druckrey IX) rat ventricular tissue. HL-1 cells are simian vacuolating virus 40 (SV40) transformed mouse atrial tumour-derived cardiomyocytes. The limited commercial options for human cell lines include cardiomyocytes by PromoCell GmbH among others (see 1.3.2.2 below). Drawbacks of immortalised and adapted cell lines include dedifferentiation and elaborate maintenance protocols. Commercial cell lines may further be associated with dependency on proprietary materials or lack of information on origin and creation.[55, 59]

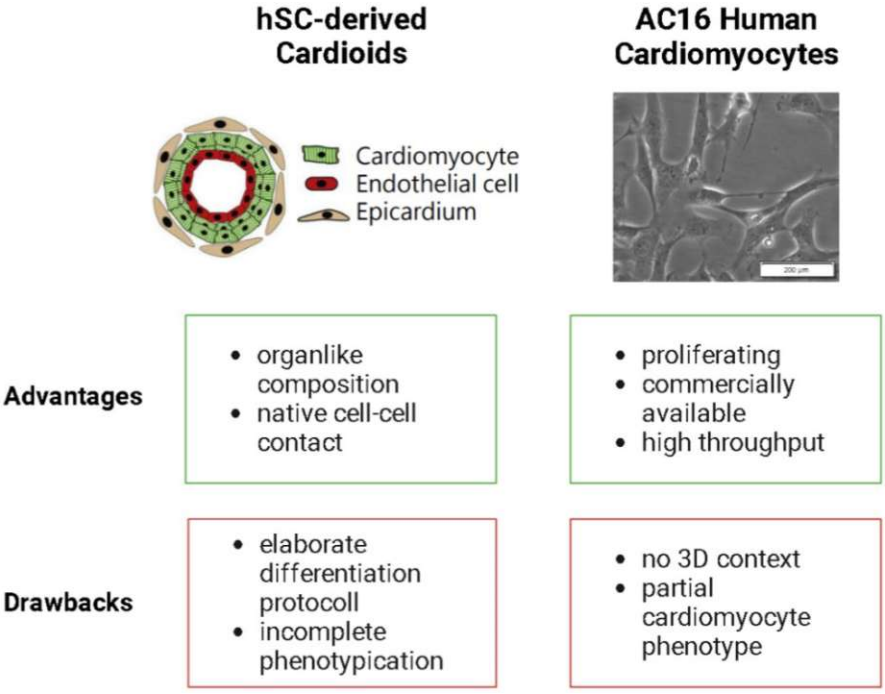

Figure 7. Illustrated above is the comparison of the cardiac cell models used in the context of this thesis. As pictured, both the human stem cell (hSC)-derived cardiac organoid (cardioid) model and the immortalised, adult ventricular cardiomyocyte (AC16) model exhibit advantages and drawbacks, which were further examined. The illustration includes a microscopic picture of AC16 cells taken during the experimental part (right). The incorporated illustration of the cardioid composition (left) has been adapted from Hofbauer, P. et al. with permission by Elsevier B.V.[60, 61]

In the last decade, human embryonic and induced pluripotent stem cells (hESC and hiPSC, respectively) have allowed new *in vitro* approaches to modelling cardiac cellular systems. This includes the possibility of cardiac precision medicine as somatic progenitor cells can be obtained from patients without cardio-invasive procedures. However, (novel) disease models must be thoroughly inspected and characterised to identify appropriate research applications. The *in vitro* models subsequently utilized in the context of this thesis are listed in Figure 7 and further elaborated below.[55, 62]

1.3.2.1 Human Stem Cell-Derived Cardiac Specific Self-Organizing Organoids

Many potent models for high throughput screening in 2D culture lack the native structure and spatial cell-to-cell contact needed for pathomolecular research with significant translational ability. High throughput differentiation of hiPSC and hESC establishes the self-organisation of cardiac chamber-like organoids. Wnt-BMP signalling (Wnt signalling cascade involving bone morphogenic protein) can instruct cardiomyocyte/endothelial layer separation and direct cavity formation (see Figure 7). Therefore, the cardioid model exhibits additional 3D context and *in vivo* character, showing promising potential in research of congenital heart defects, regeneration and HF. Past 3D systems were based on spherical aggregation or tissue engineering of cardiomyocytes and other cardiac cell types. Limitations in reflecting clinically relevant aspects of cardiomyopathies and HF are yet to be examined. Incomplete phenotyping and possible fetal characteristics may pose challenges.[59, 60]

1.3.2.2 AC16 Human Proliferating Cardiomyocytes

The AC16 cell line, as pictured in Figure 7, are immortalised adult primary human ventricular cardiomyocytes. Fusion with uridine auxotroph, SV40 transformed human fibroblasts devoid of mitochondrial DNA allowed for the establishment of a proliferating *in vitro* model. While multiple myogenic markers and characteristics of cardiac metabolism are reported for this cell line, translational ability has been questioned in the literature. Difficulties with differentiation, dedifferentiation and predominant fibroblast phenotype restrict the applicability in HF research. *In vitro* or *in vivo* models always differ from native pathology in the patient's cells. However, the question should be how much this deviation constitutes and how limitations can be mitigated to allow appropriate utilization in research with increased translational ability. High throughput cell lines such as AC16 may be improved in their weaknesses to add on to their strengths.[59, 61]

1.4 Analytical Strategies for the Investigation of Pathological Mechanisms

1.4.1 Quantitative Proteomics

Mass spectrometry (MS)-based collective characterization and quantification of class-specific biological molecules (omics) has gained popularity in recent years. Especially proteomics has asserted incredible usefulness in providing access to changes in metabolism and biomarker discovery in pathological research. As an essential addition to genomics and transcriptomics, analysis of the proteome (the entirety of cellular proteins inside a specific biological system) allows for the identification and quantification of those biomolecules that carry out most of the cellular functions. Unlike nucleic acids, proteins exhibit dynamic and heterogenous attributes (e.g., hydrophobicity, structure, size, modifications).[45, 63]

Proteomic analysis begins with the extraction of proteins from the sample, often utilizing reagents (e.g., detergents, salts, buffers) to support cell lysis. Additional mechanical disruption to improve recovery can include ultrasonication unto others. Sample preparation aims for the complete isolation of the biomolecule(s) of interest while reducing the complexity of the sample matrix. One widely applied method is the precipitation of proteins using organic solvents such as acetone. Whereas top-down proteomics includes the analysis of intact proteins, bottom-up (shotgun) strategies rely on enzymatic digestion to drive subsequent chromatographic separation and MS analysis on the peptide level. Sequence-specific cleavage of the isolated proteins generates a mixture of peptides of much greater complexity. The original proteins can be identified by identification of their constituent peptides. Enzymatic digestion results in peptides of average size 700 to 2500 Da, which matches ionization and MS analytical range. Trypsin, a highly specific serine hydrolase, characteristically cuts at the carboxyl side of lysine and arginine (except when followed by proline). This most commonly applied protease generates C-terminally charged peptides. Protein digestion is possible in-solution, in-gel and on-bead. Further purification and desalting prior to LC-MS analysis to improve sensitivity can be achieved by the binding of peptides to hydrophobic material, washing and subsequent elution using an organic solvent.[63, 64]

1.4.1.1 High-Performance Liquid Chromatography

The rapid improvement in chromatographic separation techniques, mass spectrometers, software and methodology, and quality of public databases has driven advancement in the MS-based analysis of proteins and metabolites. Ultrahigh-performance liquid chromatography (UHPLC) is an essential technique of peptide separation. Reverse-phase liquid chromatography (RPLC) reduces the eluting sample complexity before hitting the mass spectrometer, improving identification and quantification. Analytes inside the mobile phase interact with alkyl chains of defined length (e.g., C_4, C_6, C_{18};), immobilized on the column surface as the stationary phase. This hydrophobic interaction results in the faster elution of more hydrophilic peptides compared to more hydrophobic peptides. Mobile phase composition typically involves an acidic gradient of water and organic solvents (e.g., acetonitrile; ACN). The popularity of RPLC is based on the compatibility of mobile phases with ionization methods as well as high peak capacities. Modern instrumentalization capitalizes on the smaller dimension of nanoLC (nano-liquid chromatography) columns. Lower flow rates and reduced amounts of mobile phase increase peak height, ionization efficiency and sensitivity. This further improves the detection of low abundant proteins despite facing the enormous dynamic range (up to 10^{12}) of biological samples.[63, 65]

1.4.1.2 Mass Spectrometry

The most frequently applied “soft ionization” technique for ion generation of peptides eluting from the LC column is electrospray ionization (ESI). It produces an aerosol with intact ions from macromolecules with high ionization efficiency by leading the sample liquid through a needle with applied high voltage. The electrical field applied to the solution exiting the tip of the needle leads to the formation of a Taylor cone, emitting charged droplets that subsequently evaporate. The coulomb repulsion rises with increasing charge density until smaller droplets form from Coulomb explosions. This process repeats until the remaining solvent can no longer hold the ions. ESI may produce multiple-charged gas-phase ions and does not lead to fragmentation, unlike “hard ionization”. Subsequent fragmentation for the gain of structural information, in addition to the molecular parent ion, can be achieved by coupling ESI to tandem mass spectrometry (MS/MS).[63]

Determining the *m/z* of intact peptide ions (precursor ions; MS1 level) after entering the gas phase can be achieved using e.g., time-of-flight (TOF) measurement. An

electrical field of specified strength accelerates ions with the same energy into a field-free region. The velocity of ions that exhibit an identical charge is only determined by their respective mass. The time it takes for a heavier ion to reach a detector at a specified distance is longer than for a lighter ion (of the same charge). Measurement of travel time, therefore, allows for the determination of the *m/z* of accelerated ions. Identification of proteins based on the mass-to-charge ratio (*m/z*) of eluting peptides is practically impossible in complex mixtures. High transmission efficiency, measurement range and speed, and sensitivity make TOF suitable for the analysis of intact molecule ions as well as for MS/MS. In a second MS measurement (MS2), ions of specific m/z (from MS1) are selected. E.g., a quadrupole mass analyser can select a precursor ion based on the stability of their respective trajectories in the oscillating electrical fields applied to the quadrupole rods. The precursor ion is then accelerated into a collision cell containing inert gas by applying an electric potential. Peptide ions collide with inert gas atoms (or molecules in the case of N_2) to generate fragments in the process of collision-induced dissociation (CID). Fragmentation along the peptide backbone yields C- and N-terminally shortened product ions. TOF measurement of the product ions (MS2) generates sequence-specific MS/MS spectra.[63, 66]

In data-dependent acquisition (DDA) experiments, a subset of precursor ions based on intensity is selected for isolation, fragmentation and MS2 measurement. Stochastic selection of the most abundant precursor ions may result in low reproducibility and loss of information on low abundant peptides. However, the simplicity in setup and data analysis still drives the particular, remaining popularity of DDA compared to the fragmentation of all peptides within a defined *m/z* window (data-independent acquisition; DIA). DIA requires highly reproducible sample preparation and more elaborate data analysis tools to deal with highly complex MS/MS spectra but provides more complete coverage of peptides across multiple samples (fewer missing values). Regardless of precursor selection, identification of peptides and, subsequently, proteins can be achieved by matching peptide fragment ion spectra to theoretical spectra generated *in silico* from protein databases reflective of the enzymatic digestion prior. The experimentally determined masses are then compared to the predicted peptide masses. Relative quantification is based on the intensities of identified proteins as the sum of respective peptide intensities (label-free quantification; LFQ). Modern algorithms such as MaxLFQ allow for the normalisation of slight deviations in fractionation and injection amounts across measurement runs.[63, 67]

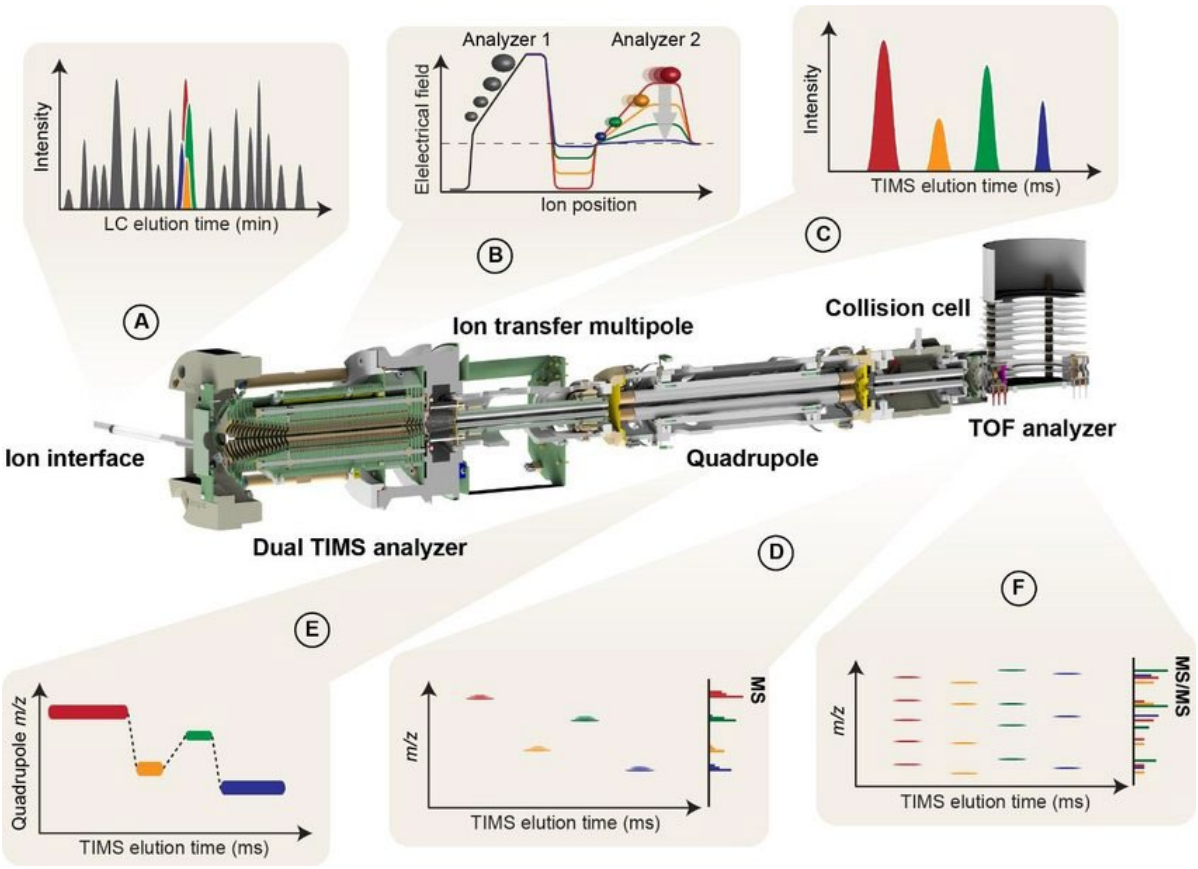

Figure 8. Principle and ion path of a timsTOF Pro (Bruker Daltonics – Bremen, Germany) mass spectrometer. Peptides elute from the chromatographic column and are transferred to the mass spectrometer by nano-electrospray ionization (nano-ESI) through a glass capillary (A). An orthogonal ion path into the dual TIMS analyser limits the number of debris entering the instrument. Ion packets are trapped and stored in the first section and resolved by mobility in the second analyser (B). Separated ions are released sequentially from the dual analyser unit as a function of decreasing electrical field strength and yield mobility-resolved mass spectra (C, D). In online parallel accumulation-serial fragmentation (PASEF) MS/MS scans, the subsequent quadrupole and TIMS analyser are synchronized. The quadrupole isolation window switches within ms between mobility-resolved precursor ions of different *m/z* (E). Accumulation of ions in the TIMS analyser may result in increased sensitivity. Multiple trapped precursor ion species are used for fragmentation inside the multipole collision cell, yielding multiple ion mobility-resolved MS/MS spectra from a single TIMS scan. (F). Spectra without ion mobility separation are projected onto the right axes in (D) and (F) to illustrate potency. Illustration by Meier, F. et al. with permission by Elsevier B.V.[66]

Peptides in bottom-up proteomics are separated by LC with peak widths in the range of seconds. Since mass spectra in TOF instruments are acquired in approximately 100 µs, ion mobility can be added as the third dimension of separation. As a gas flow moves ions, an electrical field prevents each respective ion from moving beyond a position in the TIMS (trapped ion mobility spectrometer) tunnel defined by the ion's collisional cross section. The force of the field is matched by the push the ion experiences from the gas flow (based on charge, size and shape). The concept has been implemented in modern MS/MS qTOF (quadrupole time-of-flight) instruments utilizing the "parallel accumulation-serial fragmentation" (PASEF) scan mode to significantly improve sequencing speed without losses in sensitivity (Figure 8).[66, 68]

1.4.2 Targeted Redox-Metabolomics

Whereas the proteome can illustrate what is happening inside a cell, the metabolome gives additional context to what has happened and what the consequences have been. While peptides in proteomics incorporate various possible modifications (PTMs), they are polymers based on only 21 proteinogenic amino acids (including selenocysteine). Problems typically include measuring rare and difficult-to-extract proteins. Additional challenges arise in MS-based metabolomics as metabolites are chemically diverse and highly heterogeneous. Global or targeted metabolome analyses require a more extensive toolbox of extraction and separation methods. Further challenges in identification are due to metabolites no longer displaying collinearity to genome sequences (i.e., dogma of molecular biology). Utilizing isotope-labelled metabolomes (e.g., ^{13}C, ^{15}N and ^{34}S labelled *E. coli* extracts) or internal standards enables reliable annotation by measuring identical compounds with specific mass shifts.[63]

As redox balance is highly dynamic, rapid and reproducible determination is of utter importance. Addressing the glutathione redox status of harvested cells and other samples (e.g., biofluids) can be carried out using acute and preservative two-step alkylation with N-ethylmaleimide isotopologues. The method is illustrated and further elaborated in Figure 9 below.[69]

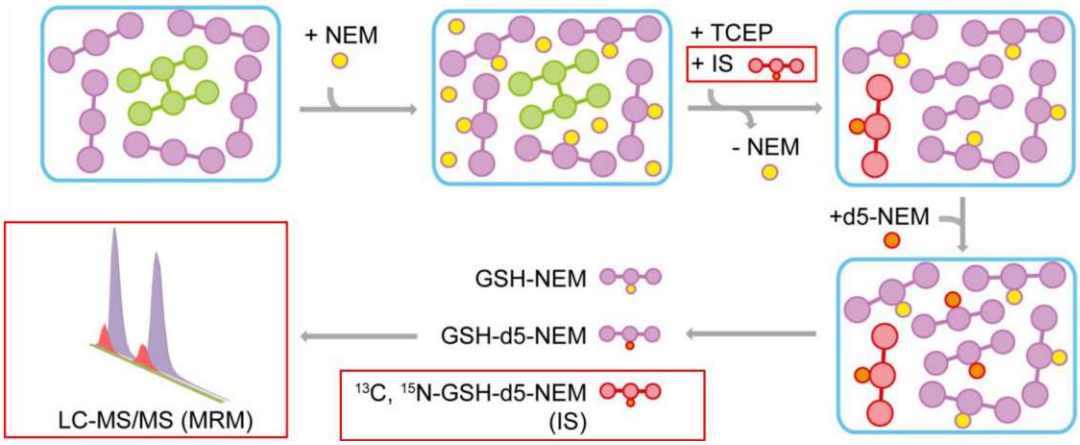

Figure 9. Analysis of cellular glutathione status is achieved by the preservation of susceptible GSH (pink), as previously reported by Tomin, T. et al.. Derivatization with the alkylating reagent N-ethylmaleimide; (NEM; yellow) is carried out parallel to polar metabolite extraction (methanol; MeOH) during harvesting or other forms of sampling. The distinction of initially oxidised glutathione (GSSG; green) is possible by subsequent reduction with tris(2-carboxyethyl)phosphine (TCEP) and re-alkylation with deuterated NEM (d5-NEM; N-ethylmaleimide-d_5). An alkylated heavy glutathione internal standard (IS; red) enables increased analytic validity and compensated deviations in sample preparation. Derivatisation allows for highly sensitive analysis by liquid chromatography (LC) coupled to triple quadrupole (QQQ) mass spectrometry using multiple reaction monitoring (MRM). Illustration by Tomin, T. et al. used with permission by MDPI.[69]

1.4.2.1 Multiple Reaction Monitoring

Multiple reaction monitoring (MRM) is a highly sensitive and specific method of tandem MS for the selective quantification of compounds in complex matrixes. In contrast to single reaction monitoring (also referred to as selected reaction monitoring; SRM), MRM targets multiple ions. Variants of MRM such as parallel reaction monitoring (PRM; quadrupole-Orbitrap or qTOF) are distinguished by instrumentation and mode of operation (i.e., parallel detection of all target product ions).[63, 70, 71]

In the case of triple quadrupole (QQQ) instrumentation, two quadrupole mass analysers are used for the ion selection and analysis at the stages MS1 (Q1) and MS2 (Q3). An additional non-mass resolving (radio frequency- only) quadrupole (q2) is placed between them as collision-induced dissociation (CID) cell for fragmentation of precursor ions (see Figure 10). Instrumentation typically involves a further "assisting" quadrupole placed in front to focus the generated ions of the sample coming from the interface. Precursor ions are selected at Q1 and fragmented at q2. Q3 does not scan for production ion selection over the whole range of *m/z* but instead selectively scans *m/z*-values of one or multiple known fragmentations. SRM allows for the highest sensitivity as only one fragmentation is scanned for. However, errors in identification are improved at scanning multiple fragmentations. In MRM, Q1 alternates through multiple, small m/z ranges, whereas Q3 filters for known fragmentations of the respective *m/z* of the targeted molecule.[63]

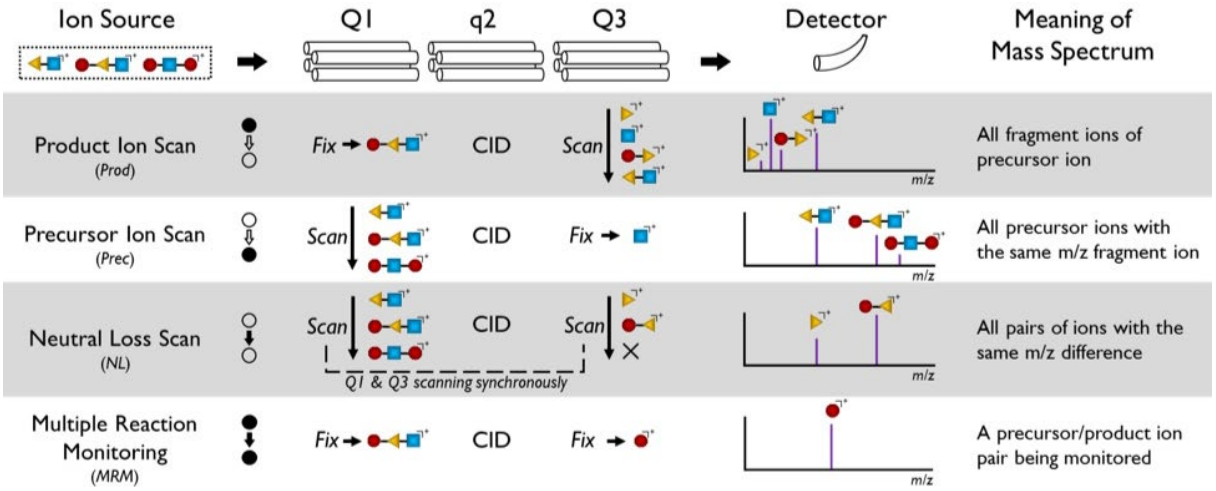

Figure 10. The operation mode of a triple quadrupole mass spectrometer (QQQ-MS) utilized for multiple reaction monitoring (MRM; bottom)). Variations of QQQ mass spectrometry always include fragmentation at q2, but Q1 and Q3 quadrupole mass filters are either set to fixed (Fix) *m/z* or operate in scanning mode (Scan). CID indicates collision-induced dissociation. Illustration by Cooks, R.G. et al. with permission by the Aston Labs.[72]

2 Materials and Methods

2.1 Chemicals and Preparation of Applied Solutions

If not stated otherwise, all chemicals were purchased from Sigma-Aldrich (St. Louis, MO, USA). The following solutions were prepared fresh for subsequent usage. For convenience, all used treatments are summarized below.

Bovine serum albumin (BSA) in Iscove's Modified Dulbecco's Medium (IMDM)

1.2508 g of BSA were dissolved in 5 mL IMDM medium (21980; Thermo Fisher Scientific - Waltham, MA, USA) for a final concentration of 0.25 g/mL.

BSA in glucose-free Dulbecco's Modified Eagle's Medium (DMEM)

0.2505 g of BSA were dissolved in 5 mL glucose-free, phenol red-free, glutamine-free DMEM medium (A1443001; Thermo Fisher Scientific - Waltham, MA, USA) for a final concentration of 0.25 g/mL.

Transferrin in IMDM

101 mg of transferrin were dissolved in 3.33 mL IMDM medium for a final concentration of 30 mg/mL.

Transferrin in glucose-free DMEM

100 mg of transferrin were dissolved in 3.33 mL glucose-free, phenol red-free, glutamine-free DMEM medium for a final concentration of 30 mg/mL.

Insulin in IMDM

11.3 mg of insulin were dissolved in 1.13 mL IMDM medium for a final concentration of 10 mg/mL.

Insulin in glucose-free DMEM

11.3 mg of insulin were dissolved in 1.13 mL glucose-free, phenol red-free, glutamine-free DMEM medium for a final concentration of 10 mg/mL.

Glucose in glucose-free DMEM

0.8101 g glucose were dissolved in 50 mL glucose-free, phenol red-free, glutamine-free DMEM medium for a final concentration of 0.30 mg/mL.

Cardioid maintenance medium

23.74 mL of IMDM medium were mixed with 0.5 mL chemically defined lipid concentrate (1% v/v final concentration; 11905031; Thermo Fisher Scientific - Waltham, MA, USA), 24.74 mL Ham's F-12 Nutrient Mixture (F12; 31765027; Thermo

Fisher Scientific - Waltham, MA, USA), 25 µL transferrin (30 mg/mL in IMDM; 15 µg/mL final concentration), 50 µL insulin (10 mg/mL in IMDM; 10 µg/mL final concentration) and 1 mL BSA (0.25 g/mL in IMDM; 5 mg/mL final concentration). The final glucose concentration was 17 mM based on the applied IMDM medium and Ham's F-12 Nutrient Mixture.

Cardioid physiological glucose medium

45.78 mL of glucose-free, phenol-red free, glutamine-free DMEM medium were mixed with 0.5 mL L-glutamine (100x stock solution; 2 mM final concentration), 0.5 mL chemically defined lipid concentrate (1% v/v final concentration), 2.69 mL glucose stock (16.2 mg/mL in glucose-free, phenol red-free, glutamine-free DMEM; 5 mM final concentration), 25 µL transferrin (30 mg/mL in glucose-free, phenol red-free, glutamine-free DMEM; 15 µg/mL final concentration), 50 µL insulin (10 mg/mL in glucose-free, phenol red-free, glutamine-free DMEM; 10 µg/mL final concentration) and 1 mL BSA (0.25 g/mL in glucose-free, phenol red-free, glutamine-free DMEM; 5 mg/mL final concentration).

Cardioid high glucose medium

32.31 mL of glucose-free, phenol-red free, glutamine-free DMEM medium were mixed with 0.5 mL L-glutamine (100x stock solution; 2 mM final concentration), 0.5 mL chemically defined lipid concentrate (1% v/v final concentration), 16.16 mL glucose stock (16.2 mg/mL in glucose-free, phenol red-free, glutamine-free DMEM; 30 mM final concentration), 25 µL transferrin (30 mg/mL in glucose-free, phenol red-free, glutamine-free DMEM; 15 µg/mL final concentration), 50 µL insulin (10 mg/mL in glucose-free, phenol red-free, glutamine-free DMEM; 10 µg/mL final concentration) and 1 mL BSA (0.25 g/mL in glucose-free, phenol red-free, glutamine-free DMEM; 5 mg/mL final concentration).

100 mM N-ethylmaleimide (NEM)

29.84 mg NEM were dissolved in 2385 µL ddH_2O.

100 mM d5-NEM

10 mg d5-NEM were dissolved in 768 µL ddH_2O.

50 mM tris(2-carboxyethyl)phosphine (TCEP) in 50 mM ammonium acetate (AA)

29.62 mg TCEP were dissolved in 2067 µL 50 mM AA (in ddH_2O), and the pH was set to 7.1 by the addition of NH_4OH.

Heavy glutathione (GSH) internal standard: $^{13}C_2$, ^{15}N-GSH-d5-NEM (IS)

10 µL 50 mM TCEP (in 50 mM AA) were mixed with 20 µL $^{13}C_2$, ^{15}N-GSH and incubated at 37 °C for 30 min. Afterwards, 50 µL 100 mM d5-NEM and 20 µL 50 mM AA (in ddH_2O) were added, and the solution was incubated at room temperature for 20 min. The organic extraction of excess NEM was carried out by adding 300 µL dichloromethane, vortexing and centrifuging at 13000 x g and 4 °C for 5 min. As much as possible liquid was collected from the upper phase of this separation.

Harvesting solution (80% methanol, 2.5 mM NEM, 0.2% IS)

20 mL methanol were mixed with 50 µL IS, 626 µL 100 mM NEM and 4324 µL ddH_2O. The mixture was stored at -20 °C until further use.

50% TFE (trifluoroethanol) in 50 mM ABC (ammonium bicarbonate)

3 mL 100 mM ABC (in ddH_2O) were mixed with 3 mL TFE.

Insulin in DMEM/F12K

11.3 mg of insulin were dissolved in 1.13 mL phenol red-free, glutamine-free DMEM/F12K (1:1) medium (D6434) for a final concentration of 10 mg/mL, representing a 1000x stock solution. The solution was sterile filtrated prior to use.

Transferrin in DMEM/F12K

100 mg of transferrin were dissolved in 3.33 mL phenol red-free, glutamine-free DMEM/F12K medium for a final concentration of 30 mg/mL. The solution was sterile filtrated prior to use.

AC16 fetal bovine serum (FBS) proliferation medium

427.5 mL of phenol-red free, glutamine-free DMEM/F12K medium were mixed with 5 mL L-glutamine (100x stock solution; 2 mM final concentration), 62.5 mL FBS (12.5% v/v final concentration) and 5 mL penicillin-streptomycin (100x stock solution; 100 U penicillin, 100 µg/mL streptomycin final concentration).

AC16 horse serum (HS) differentiation medium

14.378 mL of phenol-red free, glutamine-free DMEM/F12K medium were mixed with 0.15 mL L-glutamine (100x stock solution; 2 mM final concentration), 0.3 mL HS (2% v/v final concentration), 0.15 mL penicillin-streptomycin (100x stock solution; 100 U penicillin, 100 µg/mL streptomycin final concentration), 7.5 µL transferrin (30 mg/mL in phenol red-free, glutamine-free DMEM/F12K; 15 µg/mL final concentration) and 15 µL

insulin (1000x stock solution in phenol-red free, glutamine-free DMEM/F12K; 10 µg/mL final concentration).

BSA in DMEM/F12K

0.2505 g of BSA were dissolved in 5 mL phenol red-free, glutamine-free DMEM/F12K medium for a final concentration of 0.25 g/mL. The solution was sterile filtrated prior to use.

AC16 BSA differentiation medium

14.235 mL of phenol-red free, glutamine-free DMEM/F12K medium were mixed with 0.15 mL L-glutamine (100x stock solution; 2 mM final concentration), 0.15 mL chemically defined lipid concentrate (1% v/v final concentration), 0.15 mL penicillin-streptomycin (100x stock solution; 100 U penicillin, 100 µg/mL streptomycin final concentration),15 µL insulin (10 mg/mL in phenol red-free, glutamine-free DMEM/F12K; 10 µg/mL final concentration) and 0.3 mL BSA (0.25 g/mL in phenol red-free, glutamine-free DMEM/F12K; 5 mg/mL final concentration).

All-trans retinoic acid (ATRA) stocks

50 mg ATRA were dissolved in 1 mL dimethyl sulfoxide (DMSO) and subsequently diluted in phenol red-free, glutamine-free DMEM/F12K for a final concentration of 66.5 and 1.3 µM. The final concentration of DMSO in the applied media was < 0.1% v/v.

5-Azacytidine stock

1.7 mg 5-azacytidine were dissolved in 1.7 mL DMSO and subsequently diluted in phenol red-free, glutamine-free DMEM/F12K for a final concentration of 81.9 µM. The final concentration of DMSO in the applied media was < 0.1% v/v.

Cytosine arabinoside (ara-C) stock

20.88 mg ara-C were dissolved in 1.044 mL DMSO and diluted in phenol red-free, glutamine-free DMEM/F12K for a final concentration of 0.82 mM. The final concentration of DMSO in the applied media was < 0.1% v/v.

AC16 low FBS differentiation medium

14.4 mL of phenol-red free, glutamine-free DMEM/F12K medium were mixed with 0.15 mL L-glutamine (100x stock solution; 2 mM final concentration), 0.3 mL FBS (2% v/v final concentration) and 0.15 mL penicillin-streptomycin (100x stock solution; 100 U penicillin, 100 µg/mL streptomycin final concentration).

AC16 low ATRA differentiation medium

19.02 mL of phenol-red free, glutamine-free DMEM/F12K medium were mixed with 0.2 mL L-glutamine (100x stock solution; 2 mM final concentration), 0.4 mL FBS (2% v/v final concentration), 0.2 mL penicillin-streptomycin (100x stock solution; 100 U penicillin, 100 µg/mL streptomycin final concentration), 20 µL insulin (10 mg/mL in phenol red-free, glutamine-free DMEM/F12K; 10 µg/mL final concentration), 10 µL transferrin (30 mg/mL in phenol red-free, glutamine-free DMEM/F12K; 15 µg/mL final concentration) and 0.15 mL ATRA (1.3 µM in phenol red-free, glutamine-free DMEM/F12K; 10 nM final concentration).

AC16 high ATRA differentiation medium

18.87 mL of phenol-red free, glutamine-free DMEM/F12K medium were mixed with 0.2 mL L-glutamine (100x stock solution; 2 mM final concentration), 0.4 mL FBS (2% v/v final concentration), 0.2 mL penicillin-streptomycin (100x stock solution; 100 U penicillin, 100 µg/mL streptomycin final concentration), 20 µL insulin (10 mg/mL in phenol red-free, glutamine-free DMEM/F12K; 10 µg/mL final concentration), 10 µL transferrin (30 mg/mL in phenol red-free, glutamine-free DMEM/F12K; 15 µg/mL final concentration) and 0.3 mL ATRA (66.5 µM in phenol red-free, glutamine-free DMEM/F12K; 1 µM final concentration).

AC16 nucleoside derivatives differentiation medium I

8.975 mL of phenol-red free, glutamine-free DMEM/F12K medium were mixed with 0.1 mL L-glutamine (100x stock solution; 2 mM final concentration), 0.2 mL HS (2% v/v final concentration), 0.1 mL penicillin-streptomycin (100x stock solution; 100 U penicillin, 100 µg/mL streptomycin final concentration), 5 µL transferrin (30 mg/mL in phenol red-free, glutamine-free DMEM/F12K; 15 µg/mL final concentration), 10 µL insulin (1000x stock solution in phenol-red free, glutamine-free DMEM/F12K; 10 µg/mL final concentration) and 0.611 mL 5-azacytidine (81.9 µM in phenol red-free, glutamine-free DMEM/F12K; 5 µM final concentration).

29 µL of ara-C (0.82 mM in phenol red-free, glutamine-free DMEM/F12K) were carefully added directly to the wells at the respective time point for a final concentration of 23 µM.

AC16 nucleoside derivatives differentiation medium II

13.042 mL of phenol-red free, glutamine-free DMEM/F12K medium were mixed with 0.15 mL L-glutamine (100x stock solution; 2 mM final concentration), 0.3 mL HS (2%

v/v final concentration), 0.15 mL penicillin-streptomycin (100x stock solution; 100 U penicillin, 100 µg/mL streptomycin final concentration), 7.5 µL transferrin (30 mg/mL in phenol red-free, glutamine-free DMEM/F12K; 15 µg/mL final concentration), 15 µL insulin (1000x stock solution in phenol-red free, glutamine-free DMEM/F12K; 10 µg/mL final concentration), 0.916 mL 5-azacytidine (81.9 µM in phenol red-free, glutamine-free DMEM/F12K; 5 µM final concentration) and 420 µL of ara-C (0.82 mM in phenol red-free, glutamine-free DMEM/F12K; 23 µM final concentration).

2.2 Proteomic and Redox Metabolomic Analysis of Differentially Treated Cardiac Organoids

2.2.1 Cell Culture

2.2.1.1 Initial Culturing

Human stem cell-derived cardiac organoids were kindly supplied by the team of Sasha Mendjan, PhD (Institute of Molecular Biotechnology, Vienna, Austria) and transported to the laboratory site using heat packs within 30 min(96-well plate; one organoid in 200 µL of maintenance medium). The organoids were inspected for viability under the optical microscope and exhibited a mean rate of 3 contractions per min. The acclimatisation involved 24 h of incubation as obtained. If not stated otherwise, incubation was carried out at 5% CO_2, 37 °C, in normoxia (20% O_2) and appropriate humidity. After 24 h, the cardioids were inspected for recovery and now exhibited an increased mean rate of 14 contractions per min.

2.2.1.2 Differential Treatments

Precultured cardioids were challenged with different oxygen and nutrient environments, reflecting aspects of heart pathology. Sets of 4 organoids per well were subsequently seeded in 2 mL of respective media in 6-well plates. This included three wells (12 organoids) per condition, and the transfer of organoids was carefully carried out using cut-off pipette tips. The first subset of cardioids was then incubated for 48 h in IMDM maintenance medium in normoxia or physioxia (5% O_2). The second subset of cardioids was incubated for 48 h in normoxia in physiological (5 mM) or high glucose (30 mM) DMEM medium. An overview of the differential treatments can be seen in Figure 11 below.

2.2.1.3 Harvesting for Subsequent Analysis

Organoids were quickly inspected after 48 h of treatment before harvesting. No visible changes or differences in contraction frequency were observed in response to variations in media glucose concentration. Harvesting cardioids cultured in normoxia occurred inside a hypoxia chamber at the respective oxygen level. This was carried out to reflectively assess the oxidative state of the cells as unsought oxidation by exposure to atmospheric oxygen can introduce artefacts. Therefore, an appropriate harvesting environment, quick handling and immediate alkylation of free thiols by NEM are required for quantitative analysis of cellular glutathione status (see 1.4.2).

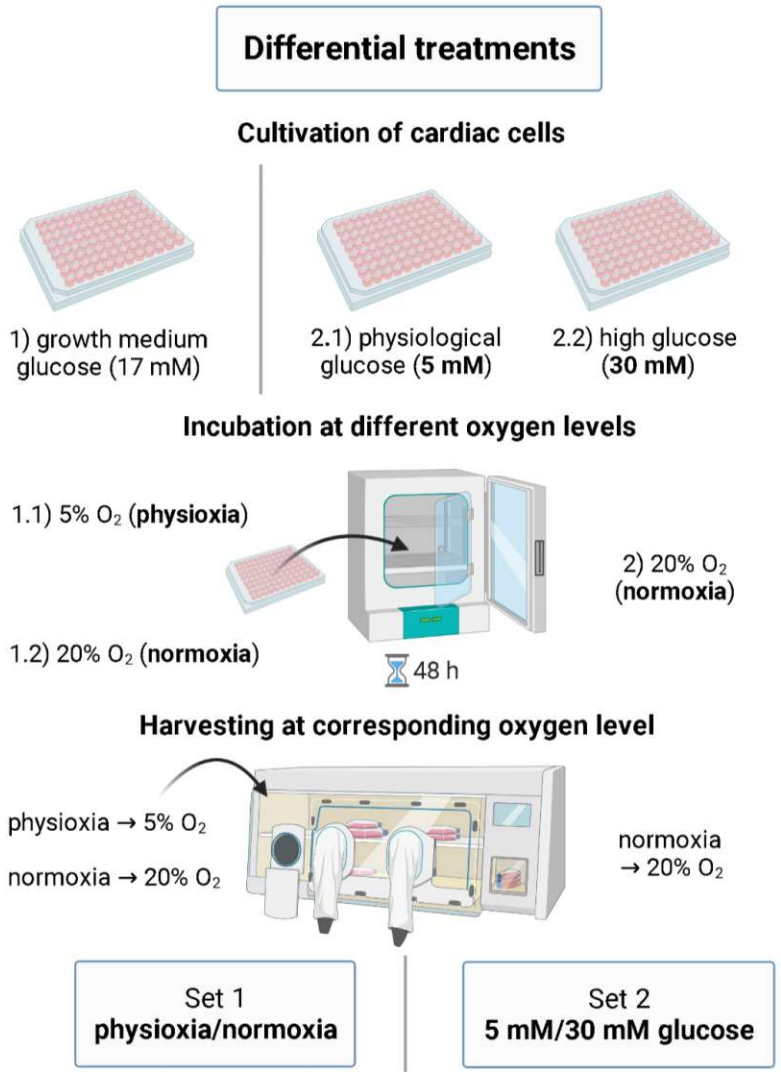

Figure 11. Overview of applied differential treatments of hSC-derived cardiac organoids. Illustrated are the chosen variables reflecting molecular pathological aspects of heart disease, including variations in glucose and oxygen availability. The cardioid maintenance medium reflected typical growth medium glucose concentrations. Cells were harvested after 48 h incubation at corresponding oxygen levels, utilising a hypoxia chamber for physioxia conditions.

For harvesting, sets of two respective cardioids were pooled and subsequently handled as one sample. Cardioids were sequentially transferred to two Eppendorf tubes containing 200 µL PBS (phosphate-buffered saline), reflecting two washing steps. The cardioids were then transferred to an Eppendorf tube containing 200 µL of harvesting solution (80% MeOH, 2.5 mM NEM, 0.2% IS) prior to sonication for sufficient lysis. Samples were stored at -20 °C until further processing.

For protein precipitation and separation of methanolic extract, the samples were centrifuged at 15000 x g at 4 °C for 15 min. The supernatant containing the polar metabolites, including glutathione, was then moved to a fresh Eppendorf tube and dried down at 40 °C for 60 min using a SpeedVac™ vacuum concentrator. Glutathione

samples were then stored at -20 °C until further processing. The remaining protein pellet after centrifugation was air dried for 10 min and resuspended in 100 µL 50% TFE in 50 mM ABC. Complete solubility was achieved by using a sonicator. Proteomic samples were stored at -20 °C until further processing.

2.2.2 Multi-Omics Analysis of the Cellular Proteome and Oxidative Stress

A multi-omics workflow was deployed to analyse the harvested cardiac cell culture samples. This included targeted redox-metabolomics in the context of cellular glutathione status and bottom-up LFQ proteomics. An overview of this parallel workflow can be found illustrated in Figure 12 below.

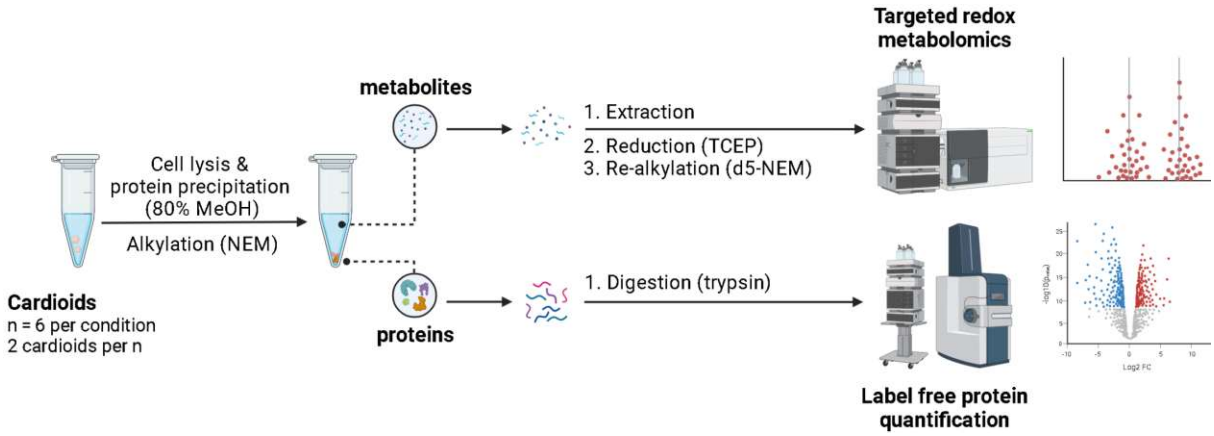

Figure 12. A multi-omics workflow allows for parallel analysis of cellular glutathione status and proteome. The metabolomic workflow utilises methanolic polar extraction, while the proteomic workflow is carried out from the resulting cell pellet. Both workflows utilize high-resolution mass spectrometry, including LC-TIMS-TOF-MS/MS for proteomics and LC-QQQ-MS/MS for glutathione analysis.

2.2.2.1 Targeted Redox-Metabolomics for Analysis of Glutathione Status

The dried metabolomic samples were resuspended in 100 µL 50 mM AA. To remove excess NEM, 300 µL of dichloromethane were added before thorough mixing. The samples were centrifuged for 5 min at 4 °C at 13000 x g. 45 µL of the upper polar phase were moved to a new Eppendorf tube. 2.5 µL 50 mM TCEP (in 50 mM AA) were added to reduce GSSG, and the samples were incubated at 37 °C for 30 min. 2.5 µL of 100 mM d5-NEM were added to the samples before 20 min of incubation at room temperature. 25 µL of the respective sample were diluted in 25 µL 50 mM AA inside a glass vial insert prior to LC-MS/MS measurement.

For analysis of the applied differential treatments, the targeted redox metabolomic method was carried out as previously reported by Tomin, T. et al.[69] with the following adaptions. Namely, 2 µL (instead of 10 µL) of each 1:1 diluted sample were injected into the LCMS-8060 system (Shimadzu - Kyoto, Japan). Chromatography included a

ZORBAX Eclipse Plus Rapid Resolution HT HPLC C18 column (50 mm x 2.1 mm x 1.8 µm; Agilent Technologies). Flow rate was set to 0.2 mL/min with the following gradient of solvent A (A; 0.1% formic acid in ddH_2O) and solvent B (B; 0.1% formic acid in ACN): 0-10 min: 1-16% B, 10.01-15.00 min: 1% B. MS was operating in positive mode, with gas flow of 2.5, 10 and 10 L/min for nebulizing, drying and heating gas, respectively. Desolvation line temperature was set to 250 °C and heat block temperature to 400 °C. The respective transition parameters for the analytes can be found in Table 4 in the appendix. Peak integration was carried out in Shimadzu Postrun Analysis.

Calibration was carried out by measurement of a dilution series before and after the samples had run on the MS. The calibration curve consisted of a 10 mM GSH-NEM standard solution (in ddH_2O) diluted in 50 mM AA (blank) to 0.01, 0.1, 1, 10 and 25 µM. As for all the glutathione isotopologues measured (GSH-NEM, GSH-d5-NEM, IS), both isomeric forms (chromatographically separated) were summed in their peak area before log10 treatment and data analysis. The resulting calibration curve can be found in Figure 35 in the appendix.

The GSH/GSSG ratio was calculated by determining the concentration of GSH-NEM, GSH-d5-NEM and IS of the samples using the calibration curve. Concentrations were further accounted for dilution and normalised on IS content. GSSG concentration has to further account for two glutathione monomers forming the dimer. The resulting mean ratios of GSH (GSH-NEM) to GSSG (GSH-d5-NEM/2) for differentially treated samples can be found in 3.1. Additionally, the concentrations of GSH and GSSG were normalised based on the protein content of the respective cell lysate (see 2.2.1.3 and 2.2.2.2).

2.2.2.2 Label-Free Quantification Proteomics

The following workflow included steps for parallel analysis of cysteine protein residues (redox proteomics), analogue to the analysis of glutathione status listed above. While the measurement and subsequent data analysis have been carried out, the results will not be discussed as this was outside this thesis's scope.

Measurement of protein content of the samples was based on the bicinchoninic acid (BCA) assay (see 0). Analysis utilizing the Pierce BCA Protein Assay Kit (Thermo Fisher Scientific - Waltham, MA, USA) was carried out according to the manufacturer's instructions. The calibration series was prepared by serial dilution of an albumin (BSA)

standard solution (2 mg/mL) in a 1:5 dilution of 50% TFE (in 50 mM ABC) in ddH_2O as dilutant. The dilution scheme can be found in Figure 36 in the appendix.

Samples were diluted 1:5 by mixing 12 µL of the sample with 48 µL of ddH_2O. Measurement was carried out in technical duplicates. 25 µL of the respective sample or standard were combined with 200 µL of the final Pierce colour solution (consisting of 25 mL BCA reagent A and 0.5 mL BCA reagent B) inside a 96-well plate. The well plate was then incubated at 37 °C and 300 rpm for 30 min in the plate spectrometer before measurement at 580 nm.

Protein concentration was calculated using the linear calibration curve, which can be found in Figure 37 in the appendix. The samples were then normalised to 21.85 µg protein. According to the BCA assay results, the respective sample volume was filled up to a total volume of 87.5 µL with 50 mM ABC.

2.5 µL TCEP (200 mM in 50 mM ABC; frozen stocks have been made available) were added to the samples for a final concentration of 5 mM TCEP. The samples were then incubated at 37 °C for 30 min at 300 rpm. Afterwards, 10 µL of 100 mM d5-NEM were added, and the samples were further incubated for 30 min at room temperature. Samples were diluted 1:5 by the addition of 400 µL 25 mM ABC (pH 8.5) prior to digestion. 1 µg of trypsin (4 µL of 0.25 µg/µL in 25 mM ABC) was added for overnight digestion at 37 °C at 300 rpm.

4 µg were subsequently desalted for proteomic LC-MS/MS measurement. 92.3 µL of the digested sample were mixed with 107.7 µL 1% trifluoroacetic acid (TFA; in ddH_2O). The mixture was loaded onto a pipette tip packed with two layers of (poly)styrene divinylbenzene-reverse phase sulfonate (SDB-RPS). This stage (stop and go extraction) tip was then placed onto a 2 mL Eppendorf tube using an adapter and centrifuged at 1500 x g for 10 min at room temperature. No liquid remained in the tip, and the flowthrough was discarded. The tip was loaded with 100 µL 0.2% TFA (in ddH_2O) for washing and centrifuged at room temperature at 1500 x g for 10 min. For elution of the peptides into a fresh 2 mL Eppendorf tube with a glass vial insert, 100 µL 5% NH_4OH in 80% ACN (aqueous solution) were added to the tip prior to centrifugation at 1500 x g for 10 min at room temperature. The vials were dried for 90 min at 30 °C using a SpeedVac™ vacuum concentrator. Samples were redissolved in 20 µL HPLC running buffer A (2% ACN, 0.1% formic acid in ddH_2O) and sonicated for subsequent LC-MS/MS measurement.

Chromatography for proteomics was carried out on an Ultimate 3000 RCS Nano Dionex system equipped with an Aurora Series UHPLC C18 column (250 mm x 75 µm x 1.6 µm; Ionopticks). Solvent A (A) was 0.1% formic acid in ddH_2O and solvent B (B) was 0.1% formic acid in ACN.

Total run time amounted to 86.5 min per sample using the following gradient: 0-5.5 min: 2% B; 5.5-25.5 min: 2-10% B; 25.5-45.5 min: 10-25% B, 45.5-55.5 min: 25-37% B, 55.5-85.5 min: 37-80% B; 65.5-75.5 min: 80% B; 75.5-76.5 min: 80-2% B; 76.5-86.5: 2% B. The flow rate was set to 400 nl/min and the column oven temperature to 40 °C.

The coupled timsTOF Pro mass spectrometer (Bruker Daltonics - Bremen, Germany) was operated in positive mode with enabled TIMS at 100% duty cycle (100 ms ramp and accumulation time). Source capillary voltage was set to 1400 V and dry gas flow to 3 L/min at 180 °C. Scan mode was set to PASEF for the range of 100-1700 m/z. Precursor selection was based on their intensity (DDA) and the precursors were allowed to accumulate for a total of four ramps per PASEF cycle, bringing the total cycle time to 0.53 s.

Subsequent raw data analysis was carried out using MaxQuant (v1.6.17.0) Andromeda search of the human database, including common contaminants (20067 entries; FASTA file downloaded on 14.02.2022) using a threshold of 1% PSM (peptide spectrum matches) and protein FDR (false discovery rate) for identification (matched between runs). This included NEMylation and d5-NEMylation on cysteine residues as well as oxidation on methionine residues and acetylation on protein N-terminus as variable modifications. The minimum peptide length was set to 7 amino acids and a minimum of 2 ratios of unique and razor peptides for label-free quantification. LFQ was normalised against the TIC (total ion chromatogram).

Intensity values were log2 transformed and categorically annotated to the respective treatment set inside Perseus (v2.0.3.0) after import of the resulting protein list (including their measured intensities). In total, 5587 proteins over all groups were initially identified and quantified. Prior to further statistical analysis, filtering for sole identification by site modification (212), reverse sequences (53) and potential contaminants (58) was carried out. Protein identifications ranged from 4066 to 4169 for individual samples.

Additionally, the matrix was filtered to only include proteins with reported valid values in at least 80% of samples in at least one group. Missing values were then imputed from a normal distribution with a width of 0.3 and a downshift of 1.8.

Further analysis inside Perseus for the comparison of two conditions included principal component analysis (PCA) and scatterplots. The respective datasets were visualised for subsequent interpretation using either a volcano plot or regular scatterplot. The corresponding two-sample *t*-tests (two-sided) corrected for multi-testing for volcano plotting were performed between the groups at 0.05 FDR and a S0 of 0.1. In some cases, non-FDR corrected *t*-tests were additionally carried out (*p*-value of 0.05 as significance cut-off).

Proteins reduced for *t*-test significance (*p*-value < 0.05) were submitted to STRING (protein-protein interaction networks) functional enrichment analysis with value-based ranking (fold-change based). The FDR stringency for enrichment was set to 5%. Active interactions were mapped based on the software's native sources of experiments, databases, co-expression, neighbourhood, gene fusion and co-occurrence. The minimum required interaction score was set to 0.4. The clustering of the network by MCL (Markov Cluster algorithm) inflation parameter set to 3 as well as differential expression analysis (fold-change based) was carried out inside Cytoscape (v3.9.1). Further annotation based on GOCC (Gene Ontology Cellular Component) and GOMF Gene Ontology Molecular Function) was carried out inside Perseus and further visualised in the respective scatter plots. Visualisation based on STRING functional enrichment analysis of *t*-test significant proteins GOBP (Gene Ontology Biological Process) was carried out inside RStudio (v2022.07.2; R v4.1.3).

2.3 Differentiation of AC16 Cardiomyocytes

As preliminary data and recent reviews on commonly utilized cardiac *in vitro* models have shown apparent limitations in mature cardiomyocyte phenotype, media composition for further differentiation of AC16 cells was to be explored and subsequently evaluated.[54]

2.3.1 Design of Maturation Media

The design of differentiation media was derived from the available literature on improving the phenotype and translational ability of cardiac cell lines (incl. AC16). Suitable candidates for media composition (see 2.1) or acting components were

chosen based on the quality of respective evidence and the frequency of utilization in the published literature.

AC16 FBS proliferating medium, reflecting standard cultivation, was chosen as the control.[54, 61] The most common approach for inducing differentiation is the switch from 12.5% (v/v) medium fetal bovine serum to 2% (v/v) horse serum (AC16 HS differentiation medium).[54, 61] Complete mitogen reduction (sera replacement) was implemented by adapting the cardioid maintenance medium for culturing AC16 cells (AC16 BSA differentiation medium).[60, 61, 73, 74] Furthermore, the induction of gene expression by all-trans retinoic acid at varying concentrations has been reported to improve maturation (AC16 high/low ATRA differentiation media) in combination with the reduction in sera.[54, 75–77] Lastly, the anti-replicative effect of cytosine arabinoside (ara-C) and 5-azacytidine was inspected (AC16 nucleoside derivatives differentiation medium).[61]

2.3.2 First Set of Experiments

2.3.2.1 Initial Culturing

A frozen aliquot of AC16 cardiomyocytes (SCC109; 2nd passage) was quickly thawed at 37 °C, resuspended in 1 mL of AC16 FBS proliferation medium and transferred to a T175 culture flask containing 16 mL of proliferation medium. If not stated otherwise, incubation was carried out at 5% CO_2, 37 °C and appropriate humidity as well as normoxia.

After 21 h of initial incubation, the cells were inspected for viability, and the medium was exchanged. This was repeated after an additional 72 h for further proliferation and recovery. At this point, the cells reached 80% confluency and were split. The medium was removed entirely, and the cells were washed twice with 10 mL PBS. 4 mL trypsin (0.25% v/v with EDTA) were added to the flask, and the cells were incubated for 5 min at 37 °C. The cells were then checked for detachment from the flask surface under the optical microscope. To neutralise the trypsin, 10 mL of proliferation medium were added. The resulting cell suspension was then transferred to a 15 mL Falcon tube. 3 mL of the cell suspension were transferred back into the culture flask and mixed with 10 mL of proliferation medium. The cells were then incubated at 37°C until reaching 80% confluence again an additional 72 h later for subsequent seeding. The remaining cell suspension was then centrifuged, the supernatant discarded, and the cell pellet

resuspended in 2 mL of freezing medium (consisting of 5% DMSO in proliferation medium). Two aliquots of 1 mL each were slowly frozen for storage at -80 °C.

Harvesting the cells with trypsin for seeding was then carried out analogue to the process of cell splitting described above. 10 µL of the resulting cell suspension were mixed with 10 µL trypan blue solution for cell counting using the EVE^{TM} automatic cell counter (AlphaMetrix Biotech). 10 µL of the trypan blue-cell mixture were applied onto the counting slide, and the cell density was measured. The cell count was 772680 cells/mL (viable).

The subsequent culturing for the experiment was carried out in 12-well plates. The well plates were coated with collagen by applying a 0.5 g/L gelatine solution. A seeding density of 80000 cells/well was chosen. By diluting 2.8 mL of the measured cell suspension in 24.2 mL proliferation medium, an 80000 cells/mL solution was prepared, and 1 mL of this solution was applied to each well. Seeding included four wells (four biological replicates) per condition, as discussed below. The cells were then incubated for 24 h before treatment.

The remaining cell suspension was transferred back to the flask and subsequently kept in culture in proliferation medium as the control. The cells were split once they reached 80% confluence.

2.3.2.2 Differential Treatments

Differential treatment included exchanging the medium for the respective differentiation media composition (see 2.1). Cells were washed twice with 1 mL PBS to sufficiently remove leftover mitogens (sera) prior to the addition of fresh medium. The applied treatments for a total incubation time of 8 days are listed in Figure 13 below and included five differentiation medium candidates, as discussed above.

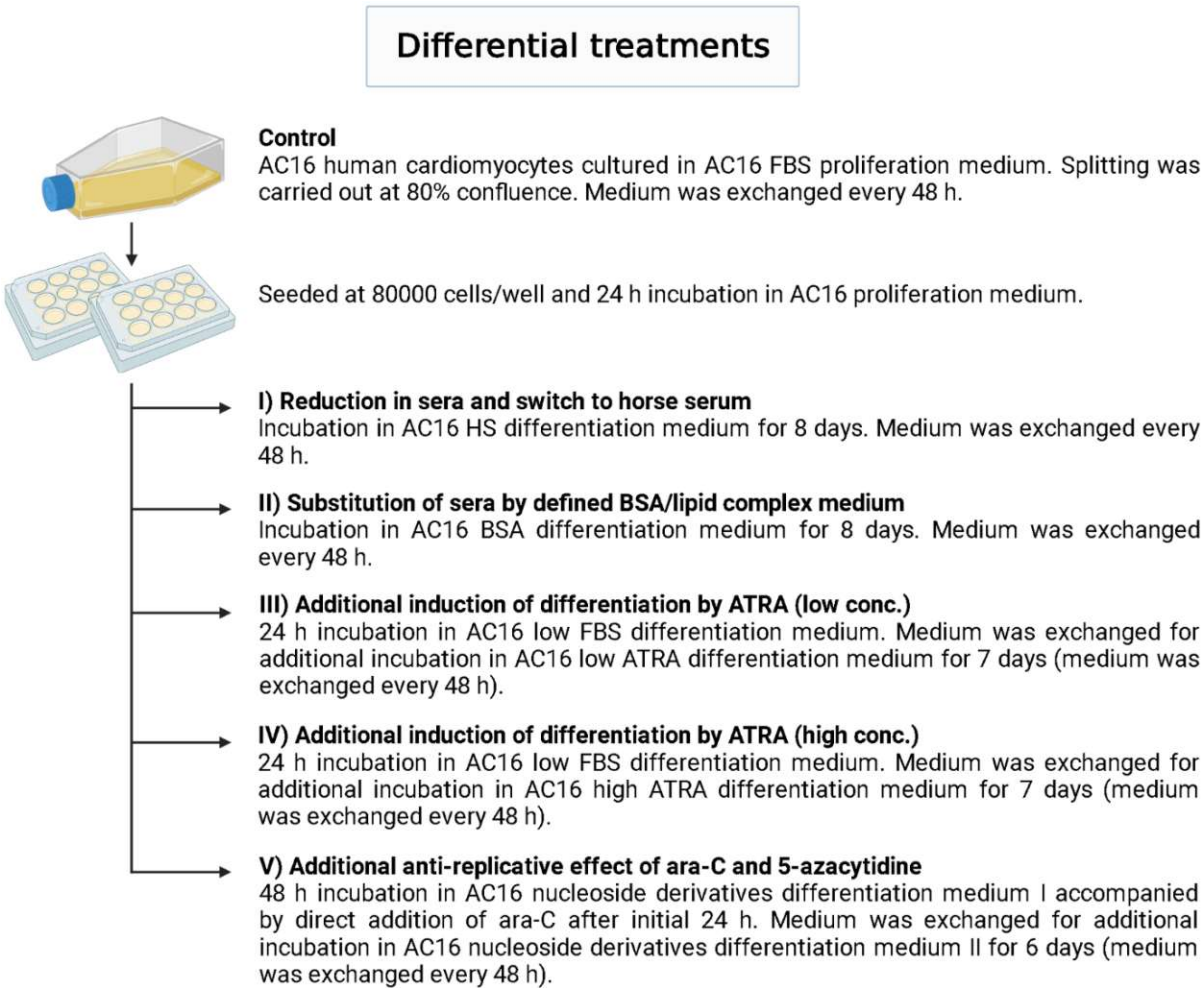

Figure 13. Overview of the applied differential treatments, including the variation in differentiation medium composition. Total treatment time was 8 days before harvesting for subsequent analysis of changes in gene expression of cardiac differentiation markers. Additionally, the proposed mechanism of action for differentiation is listed as the header for the respective medium (I-V; for a total of five different treatments). A (complete) reduction in sera represents a reduction in mitogens and growth factors, commonly cited as cofounding driver of cytostasis and cell differentiation in combination with differentiation factors, high cell density and cell-cell as well as cell-matrix interactions.[78]

2.3.2.3 Harvesting for Subsequent Analysis

After 8 days of incubation in the respective medium, the cells were harvested. The medium was removed, and the cells were washed twice with 1 mL of PBS. 300 µL of TRIzol reagent (guanidium thiocyanate/phenol; Thermo Fisher Scientific - Waltham, MA, USA) were added to each respective well, and the cell lysate was transferred to an Eppendorf tube for storage at -20 °C until further processing. Parallel harvesting of the control inside the T175 flask was carried out using 900 µL of TRIzol reagent. The volumes of applied TRIzol reagent were based on cell mass according to the manufacturer's instructions. Cells incubated in AC16 nucleoside derivatives differentiation medium were not harvested as the cells were not viable (see 3.3.1 for further discussion).

2.3.2.4 Sample Preparation for Gene Expression Analysis

Total RNA isolation from frozen samples, including TRIzol reagent for guanidinium thiocyanate-phenol-chloroform extraction and i-propanol precipitation of RNA, was carried out according to the manufacturer's instructions. The resulting RNA concentration and purity were evaluated spectrophotometrically using a Nanodrop One/One^{C} Microvolume UV-VIS Spectrophotometer (Thermo Fisher Scientific - Waltham, MA, USA). All samples utilized in the subsequent analysis showed a 260/280 nm absorbance ratio above 1.8. RNA isolates were stored at -80 °C until further analysis.

RNA was reverse-transcribed to cDNA with a High-Capacity cDNA Reverse Transcription Kit (Thermo Fisher Scientific - Waltham, MA, USA) according to the manufacturer's instructions. cDNA samples synthesized from 2 µg of total RNA were stored at -20 °C until further processing. 150 ng of cDNA were subjected to RT-qPCR (real-time quantitative polymerase chain reaction) analysis with a Rotor-Gene Q MDx 5plex HRM Real-time PCR cycler and High-Resolution Melt analyser (QIAGEN - Venlo, Netherlands) using a Blue S'Green qPCR Kit (Biozym) according to the manufacturer's instructions. Primer sequences used in the final analysis are listed in Table 5 in the appendix. The data were analysed with the ΔΔCt method, applying RPLP0 as a normalisation control (housekeeping gene). Further information on gene expression analysis is listed below. The results can be found in 3.3.

Common differentiation markers were chosen based on the available literature on cardiac markers.[59, 61, 73, 74, 76, 79–83] Primers were either designed using NCBI tools or adapted from the Harvard primer bank, including an *in silico* review of secondary structure, guanidine-cytosine-content (GC), complementary sites and product length via NCBI Primer-BLAST. The dry primers were diluted to 100 µM final concentration in RNase-free water according to the manufacturer's instructions. The respective forward and reverse primer mix at 10 µM final concentration was prepared by adding 50 µL of 100 µM forward and 50 µL 100 µM reverse primer to 400 µL of RNase-free water.

Prior to gene expression analysis for all samples, the designed primer candidates (including multiple variations of the same target or housekeeping gene) were evaluated in a test run of RT-qPCR on cDNA from cells incubated in AC16 proliferation medium and AC16 BSA differentiation medium. Final primer pairs for subsequent gene expression analysis for evaluation of differentiation were chosen by applicability based

on the resulting amplification and melting curves. The inspected parameters of the respective primer pair included the range of reported Ct (cycle threshold) values, stability (deviation) of Ct values for housekeeping genes across biological replicates and conditions, and observable primer dimerization (no-template controls, NTC). No-primer controls (NPCs) were included in all RT-qPCR runs to inspect possible contaminations.

2.3.3 Second Set of Experiments

Based on the results in 2.3.2, the evaluation of cardiac phenotype was repeated in samples from AC16 cells incubated in AC16 BSA differentiation medium for 2 days. This was done to assess early changes and reflect shorter preculturing periods, as commonly used in experimental setups. Furthermore, additional differentiation markers were included and also applied to stored samples (see 3.3.2).

2.3.3.1 Initial Culturing

Culturing of AC16 cells (frozen aliquots from 2.3.2.1) for the second experiment was carried out as described in 2.3.2.1 with the following adaptations. Namely, seeding for subsequent treatment was carried out inside 6-well plates in 2 mL medium to gain additional cell mass for improved RNA yield. Furthermore, AC16 cells in AC16 proliferation media (control) were seeded in wells, analogue to the applied treatment.

2.3.3.2 Differential Treatments

Incubation of AC16 cells in AC16 BSA differentiation medium was carried out as described in 2.3.2.2 with the following adaptations. Namely, treatments only included AC16 BSA differentiation medium for a shorter period of 48 h. The medium was not exchanged during that time.

2.3.3.3 Harvesting for Subsequent Analysis

Harvesting with 900 µL TRIzol reagent was carried out as described in 2.3.2.3.

2.3.3.4 Sample Preparation for Gene Expression Analysis

Gene expression analysis of harvested samples was carried out as described in 2.3.2.4 with the following adaptions. Namely, the analysis now included an extended list of primers for additional markers of differentiation. The complete set of primers was further applied in the repeated analysis of stored cDNA (-20 °C) of AC16 cells cultured for 8 days in AC16 proliferation medium (control) or AC16 BSA differentiation medium from the first set of experiments (see 2.3.2).

3 Results and Discussion

3.1 Cardiac Organoids Respond to Oxidative Stress with Changes in Cellular Glutathione Status

Preservative two-step alkylation of sulfides allowed the analysis of the abundant endogenous antioxidant glutathione and derivatives in differentially treated cardiac organoids. The results illustrate distinct alterations in the redox environment and provide valuable insights into the cellular response to changes in nutrient availability and atmospheric oxygen levels (Figure 14). A lower GSH/GSSG ratio serves as a marker for increased oxidative stress as GSH is oxidised (forming GSSG) while neutralizing RONS and aiding in the antioxidative defense (see 1.1.2.1).

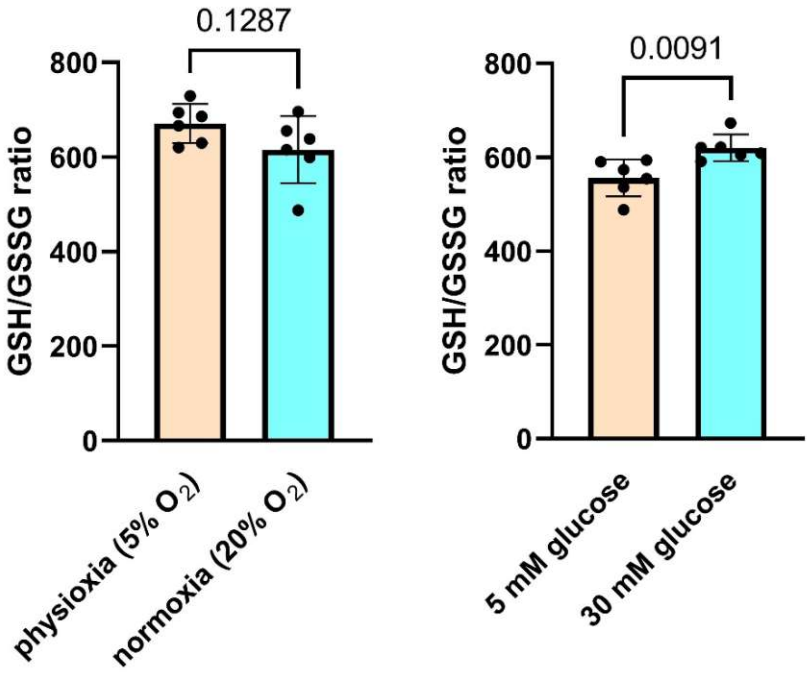

Figure 14. Cardioids cultured in physiological glucose (5 mM) display a significantly reduced GSH/GGSG ratio compared to high glucose (30 mM, right). The GSH/GSSG ratio in cardioids cultured in normoxia is slightly reduced (not significant) compared to physioxia (left). Treatment included 48 h incubation. N = 6 per condition (2 cardioids per N). Variations in oxygen and glucose environment are not illustrated on the same graph to point out that the individual sets were cultured in different media (IMDM/DMEM). Therefore, a direct comparison of glutathione status is only possible with careful consideration of this limitation. Individual values and standard error of the mean (SEM) are listed together with the mean value for the respective condition in all box plots. Additionally, Student *t*-test *p*-values are listed.

The results of glutathione status indicate a slight increase in oxidative stress at increased oxygen levels. This is due to reduced levels of GSH and more abundant GGSG (Figure 15) in normoxic conditions compared to physioxia. As discussed in 1.1.2, the observed GSH/GGSG ratio reduction could be based on the more oxidizing

environment linked to increased oxygen abundance. Based on these results, reduced oxygen availability does not impair metabolic flexibility to the extent of disrupted cellular redox homeostasis in physioxia compared to normoxia. The possibility of reduced mitochondrial activity under physioxia is explored in 3.2. However, this might only represent a trend, and it must be noted that the alteration in glutathione status is not statistically significant (Student *t*-test *p*-value = 0.1287; Figure 14). Nevertheless, these findings match previous reports on reduced GSH values in patients with reperfusion injury (and HF). Higher oxygen environments *in vitro* have now been repeatedly shown to mimic increased oxidative stress.[45, 84, 85] Follow-up experiments representing I/R injury, including culturing cardiac organoids in hypoxia and switching to normoxia before harvesting, may provide additional context.

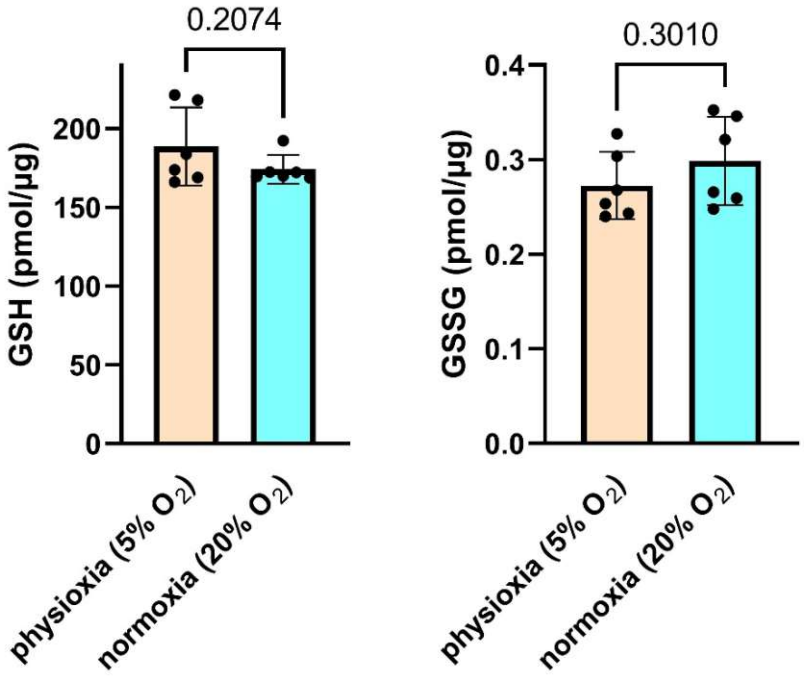

Figure 15. Absolute GSH levels (normalised on protein content) of cardioids cultured in normoxia are slightly reduced (not significant), while GSSG levels are slightly increased (not significant) in normoxia compared to physioxia.

Cardiac organoids cultured in 5 mM glucose showed a significantly reduced GSH/GSSG ratio compared to 30 mM glucose (Figure 14). 30 mM glucose was utilized to represent an excess of this nutrient, whereas 5 mM is based on typical physiological values of blood glucose and tissue supply. Results suggest tolerance of high concentrations and possible dependence on medium glucose. Furthermore, typical growth media glucose, as applied in the culturing for variation in oxygen availability (17 mM), can also be considered hyperglycemic.[86] As noted in Figure 14, the direct

comparison of the two experimental sets is confined by the difference in applied medium composition. With this limitation in mind, GSH/GSSG ratios and levels of GSH and GSSG match for 17 and 30 mM glucose in normoxia (Figures 15 and 16). This may further indicate glucose dependence as 30 mM glucose does not seem to represent a harmful excess, and 17 mM covers metabolic needs. The impact of glucose metabolism and metabolic flexibility on oxidative stress has been illustrated in 1.1.1 and 1.1.2. The observed metabolic phenotype is further discussed in 3.2 below. Additionally, it must be noted that while 5% oxygen represents physiological pO_2 values of the myocardium (as a percentage of oxygen in the microenvironment)[87, 88], cardiac organoids challenged with different glucose concentrations were cultured in normoxia not to introduce confounding factors for variation in medium glucose.

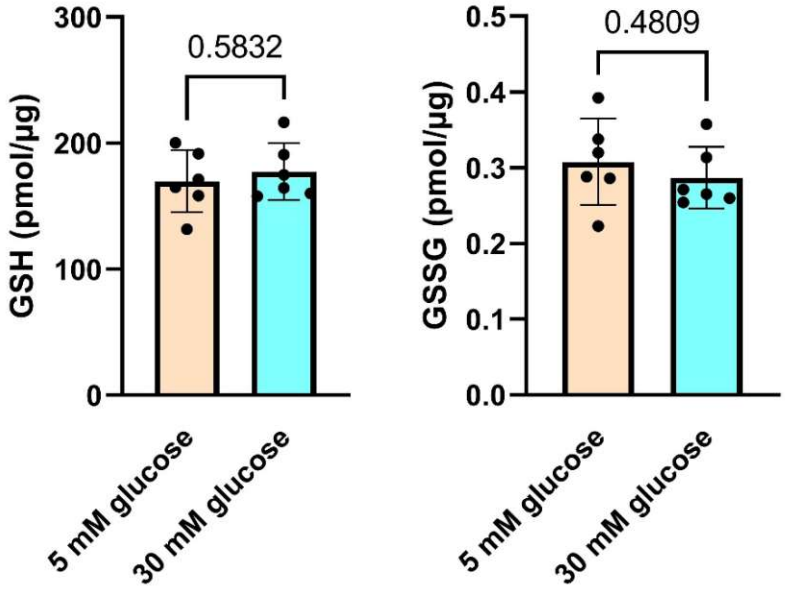

Figure 16. Absolute GSH levels of cardioids cultured in physiological glucose concentration (5 mM) are slightly reduced (not significant), while GSSG levels are slightly increased (not significant) in physiological glucose compared to high glucose (30 mM).

Overall, the reduction in GSH/GSSG ratio and the alterations in GSH and GGSG levels are less substantial than the observed values in the tissue of failing hearts. In comparison, absolute values of GSH/GSSG ratio appear to be relatively high.[45] Furthermore, distinct biological variation in all reported values was observed. The cardiac organoids seem to cope well based on the relative abundance of GSH across all conditions. In addition, no visible changes in viability were detected across all treatments before harvesting (Figure 39 in the appendix). Results indicate a different, possibly fetal, nature of cardiac organoids.

3.2 Effects of Oxygen and Nutrient Availability on the Proteome of Cardiac Organoids

As listed in detail in 2.2, the analysis of protein abundance was carried out across 24 samples (48 cardioids). This resulted in 3810 and 3858 quantified proteins across 12 samples (24 cardioids) after filtering for at least 80% valid values in at least one group for the variation of oxygen and glucose availability, respectively. A principle component analysis (PCA; Figure 17) illustrates the separation of cardioids differentially cultured in physioxia and normoxia.

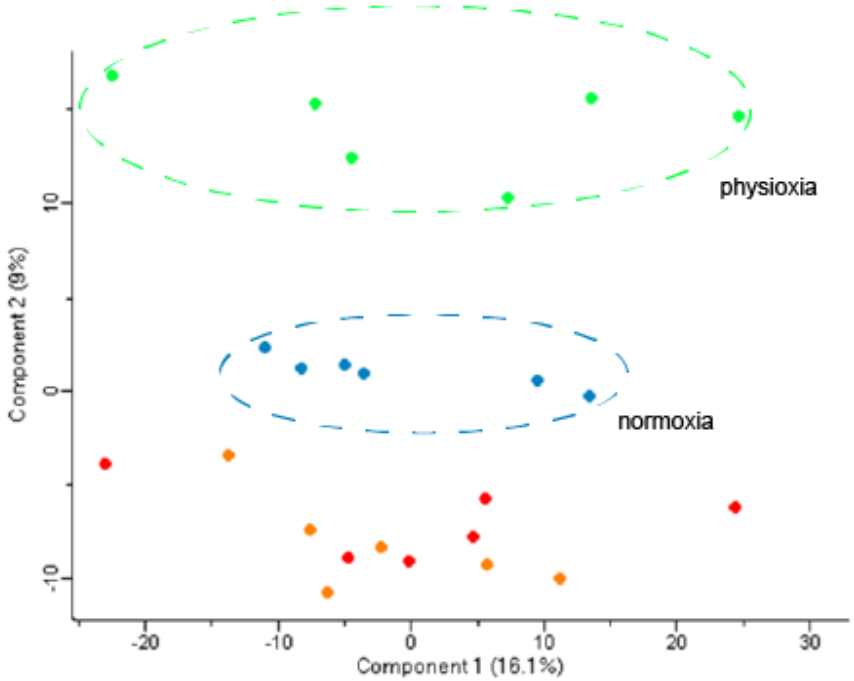

Figure 17. Principle component analysis (PCA) of analysed samples. Illustrated above are cardioids differentially cultured in 17 mM glucose for variation of atmospheric oxygen in normoxia (20% O_2; blue) and physioxia (5% O2; green). Furthermore, cultivation in normoxia included the variation in medium glucose concentration with cardioids cultured in physiological glucose (5 mM; orange) and high glucose (30 mM; red).

Due to the high variability of individual spheroids and modest response upon differential glucose availability, it was decided only to observe and include those samples for further analysis that demonstrated response according to PCA. Furthermore, the correlation between samples was inspected in a multi-scatter plot (Figures 40 and 41 in the appendix). This led to the exclusion of one biological replicate (2 spheroids out of 12) per condition (physiological/high glucose) and improved separation (Figure 18). It must be noted that these results cannot be interpreted with the same level of confidence, and these limitations must be kept in mind.

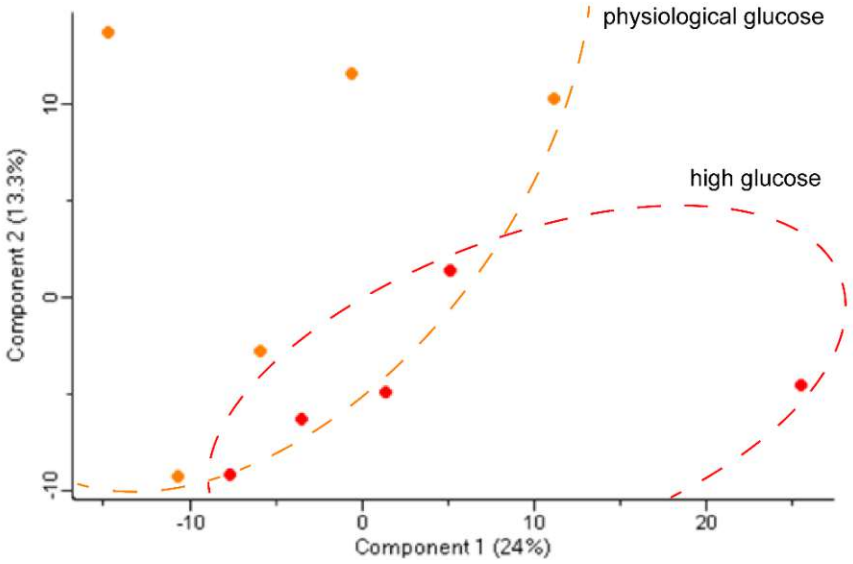

Figure 18. Principle component analysis (PCA) of the proteomic signatures of cardioids differentially cultured in normoxia for variation in medium glucose in normoxia with physiological glucose (5 mM; orange) and high glucose (30 mM; red). As discussed above, one biological replicate each was removed from further analysis based on the high variability of the samples. Response to alteration in glucose availability appears modest compared to variation in atmospheric oxygen.

3.2.1 Oxygen Levels Significantly Impact Proteomic Remodelling

Proteins significantly more abundant in normoxia match the results of cellular glutathione status analysis. A lower GSH/GGSG ratio correlates with increased expression of antioxidative enzymes (Figure 19; marked in pink) under higher oxygen. Elevated levels of the mitochondrial-specific superoxide dismutase isoform SOD2 and the abundance of mitochondrial proteins suggest disturbed redox homeostasis by upregulated mitochondrial activity, which is to be expected when oxygen is readily available. Correspondingly, cardioids cultured under higher oxygen demonstrated markedly higher expression of mitochondrial proteins (Figure 19; marked in orange).

Gene ontology analysis of biological processes (GOBP) of corresponding proteins significantly more expressed in normoxia resulted in the enrichment of multiple processes, as shown in Figure 20. Next to the expected enrichment of global mitochondrial processes such as mitochondrial translation and morphogenesis, it is noteworthy to mention elevation in the expression of fatty acid β-oxidation enzymes and respiratory electron transport chain in normoxia compared to physioxia. The increased production of ATP and mitochondrial biogenesis is further associated with higher expression levels of dehydrogenase E1 and transketolase domain-containing 1 (DHTKD1). DHTKD1 is further reported to be crucial in maintaining mitochondrial redox homeostasis.[89]

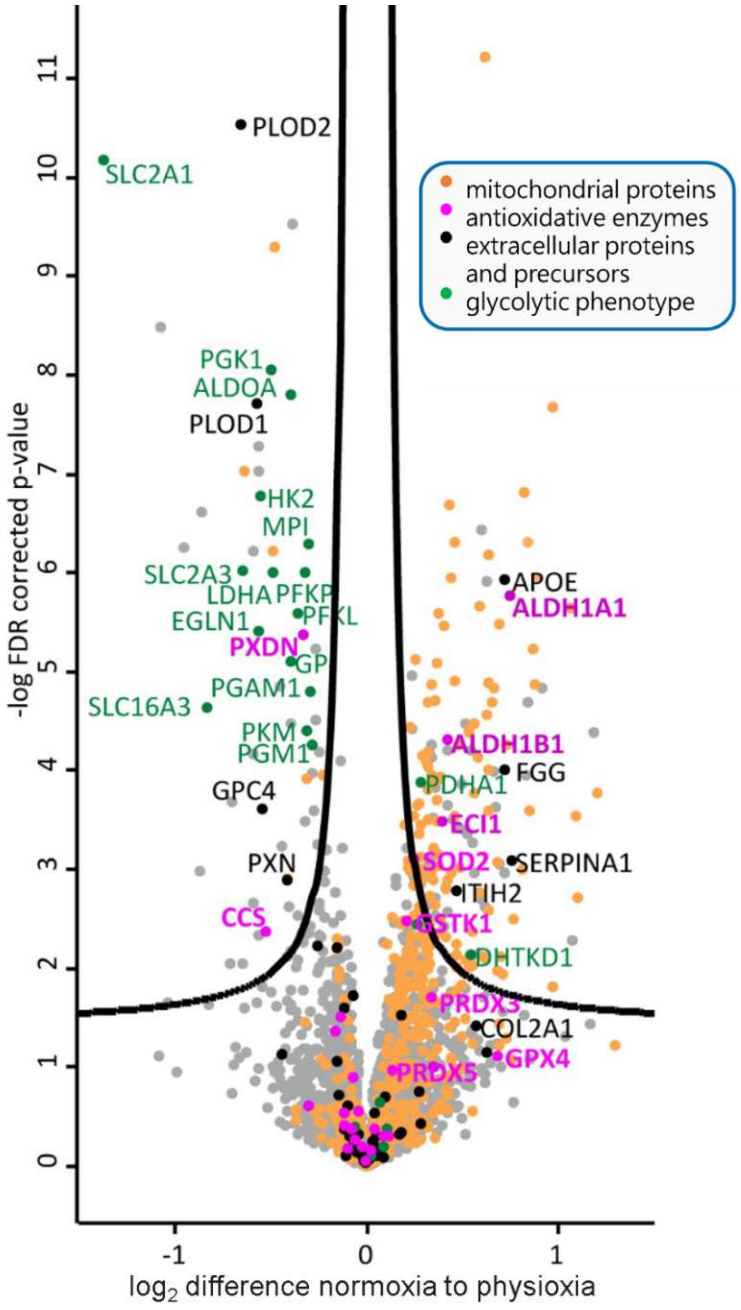

Figure 19. Volcano plot illustrating changes in the proteome for cardioids cultured in different atmospheric oxygen conditions for 48 h. Student *t*-testing revealed 113 significant differentially expressed proteins. Proteins more abundant in normoxia (20% O_2) are illustrated on the right side of the plot, whereas proteins more abundant in physioxia (5% O_2) are displayed on the left side. SERPINA1 and ITIH2 (right) constitute protease inhibitors. FGG (right) is associated with fibrinogen- and fibrin-associated cell adhesion and spreading.

As illustrated in Figure 19, the reduction in atmospheric oxygen leads to increased carbohydrate metabolism and glycolysis dependence for ATP synthesis, manifested by higher expression of core glycolytic proteins, including the key enzymes of glycolysis (e.g., ALDOA, PGK and PFK) and glucose transporters (e.g., SLC2A1 and SLC2A3). Additional mobilization of substrates for glycolysis is illustrated with enzymes such as mannose-6 phosphate isomerase (MPI), which facilitates the conversion of

mannose 6-phosphate to fructose 6-phosphate (F6P).[90] Dependence on glycolysis is further corroborated by GOBP analysis with significantly more expressed proteins in 5% oxygen as input (Figure 21).

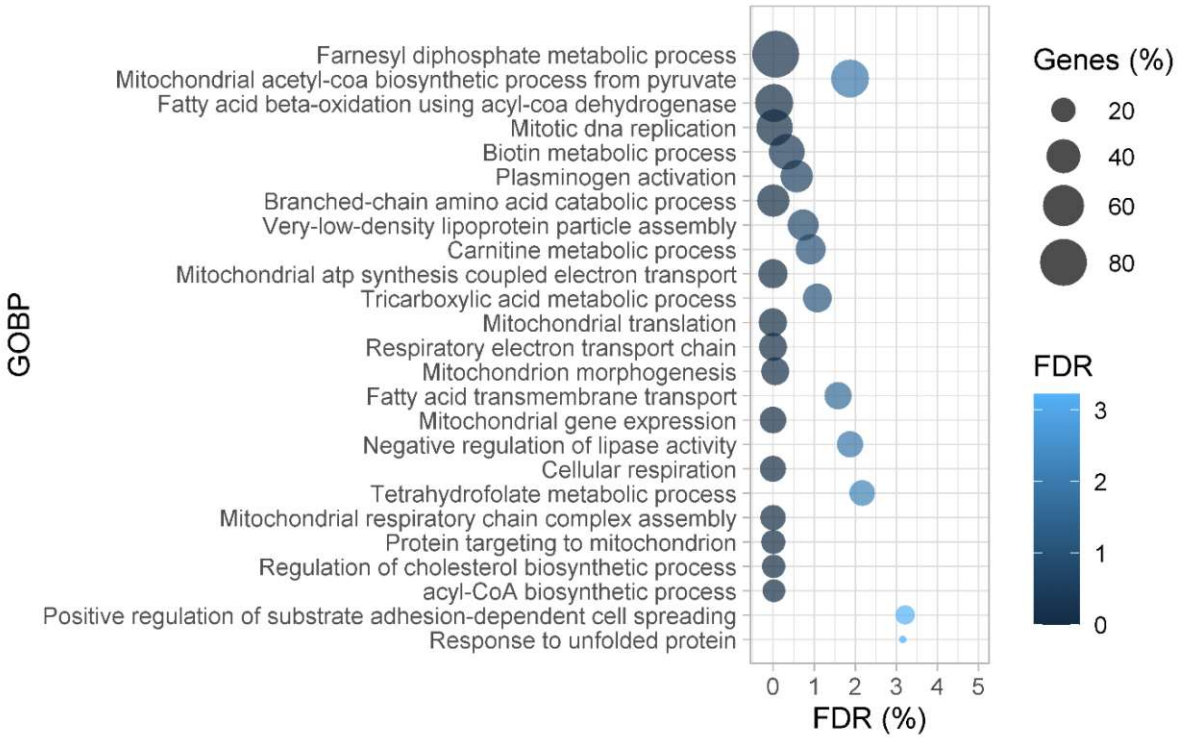

Figure 20. Gene ontology-enrichment analysis of biological processes (GOBP) of significantly more abundant proteins in normoxia compared to physioxia. The list of terms was manually reduced for redundancy. So far unmentioned proteomic signatures include increased fatty acid transport (e.g., carnitine metabolic process), response to unfolded proteins (correlating with increases in oxidative stress or mitochondrial translation) and possibly lipid storage (regulation of cholesterol biosynthetic process; negative regulation of lipase activity).

Of note, other proteins involved in carbohydrate metabolism are also more abundant in physioxia. PKM catalyses the dephosphorylation of phosphoenolpyruvate (PEP) and yields the net ATP production of glycolysis. Energy regeneration is thereby independent of oxygen supply and mitochondrial respiration. PKM1 activity is thus crucial for the accommodation of glycolytic flux and PDH activity to maintain metabolic flexibility and homeostasis.[91, 92] Increased lactate dehydrogenase A (LDHA) levels suggest that the cellular energy demand is not matched in oxygen supply. Conversion of pyruvate to lactate is crucial for the regeneration of NAD^+. Limited TCA activity (as seen in Figure 20) correlates with the observed lower expression of the key regulator PDH (PDHA1).[90] Furthermore, monocarboxylate transporter 4 (MCT4; encoded by the SLC16A3 gene) is reported to play a predominant role in the transport of lactate efflux from highly glycolytic cells. Upregulation of MCT4 may be facilitated by AMPK and hypoxia-inducible factor 1-alpha (HIF-1α).[93]

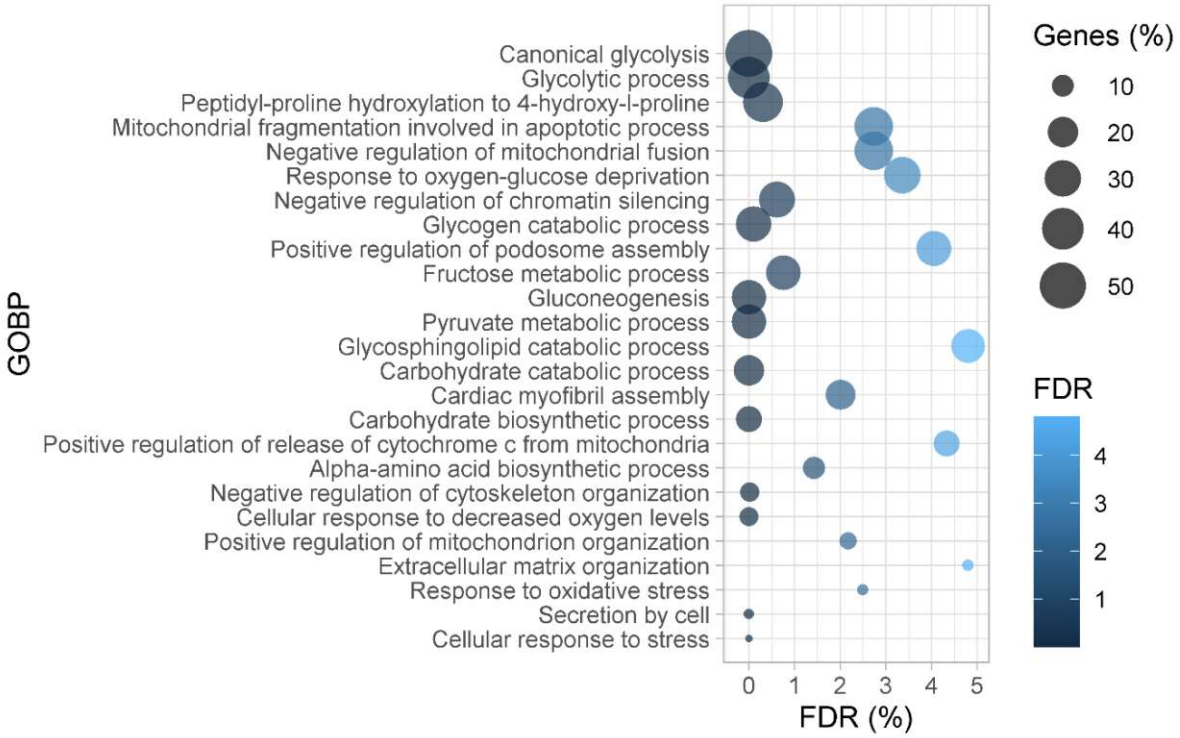

Figure 21. Gene ontology-enrichment analysis of biological processes (GOBP) of significantly more abundant proteins in physioxia compared to normoxia. The list of terms was manually reduced for redundancy.

So far, results indicate carbohydrate metabolism induction in response to oxygen deprivation, also reported for cardiac ischemia and heart failure.[19] Indeed, HK2, the principal regulated hexokinase isoform found in muscle and the heart, can also be induced by hypoxia. HK2 is localised to the outer mitochondrial membrane (OMM) and therefore has direct access to ATP for glucose phosphorylation.[94] Gene ontology analysis (Figure 21) illustrates that cardioids cultured in 5% O_2 experience cellular stress and oxygen-glucose deprivation. Mitochondrial autophagy and apoptosis seem to occur as well. Additionally, antioxidants such as the copper chaperone for SOD1 (CCS) and peroxidasin homolog (PXDN) are upregulated in physioxia. PXDN, a heme-containing peroxidase augmenting oxidative stress and regulation of autophagy, is reportedly involved in cardiovascular diseases.[95]

In conjunction, the results indicate hypoxic conditions at 5% oxygen. Multiple proteins significantly more expressed in physioxia are involved in the cellular response to stress and hypoxia, especially in peptidyl and protein hydroxylation. The hypoxia-inducible factor prolyl hydroxylase 2 (HIF-PH2; encoded by the EGLN1 gene) is thought to be the most critical sensor of cellular oxygen levels. Under normoxia, the oxygenase activity of the enzyme hydroxylates proline-402 and proline-564 of HIF-1α and therefore marks it for ubiquitin-proteasomal degradation. In the beginning absence of

oxygen, this mechanism is limited and leads to the regulatory activity of HIF-1α and cellular efforts to increase the abundance of the oxygen sensor, as illustrated in Figure 22. HIF-1α has been reported to play a critical role in the pathogenesis and progression of various diseases, including cardiac hypertrophy and heart failure.[96, 97]

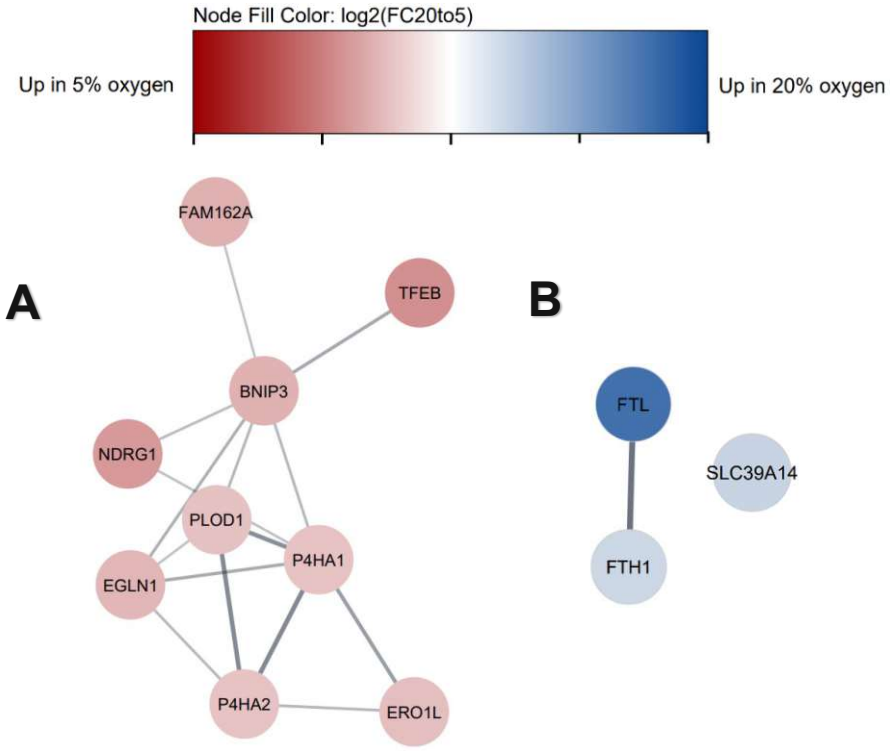

Figure 22. STRING protein-interaction analyses of proteins significantly more expressed in physioxia or hypoxia show distinct clustering (excerpt). (A) Illustrated above are proteins significantly upregulated in 5% oxygen, constituting the cellular response to stress and hypoxia. Those include enzymes further involved in collagen synthesis and modification. (B) Proteomic results of cardiac organoids cultured in 5% oxygen indicate a reduced abundance of iron transporters (FTL, FTH1, SLC39A14). Hydroxylation of HIF-1α is reduced under low cellular iron concentrations, hypoxia, or increased mitochondrial ROS production. This further illustrates the complex interplay of multiple factors in redox homeostasis being affected by both 5% and 20% oxygen.[98] HIF-1α plays a crucial role in repressing cell stress pathways. Multiple associated downstream effects, such as increased glucose transport and glycolysis, mitophagy, ECM stiffness and mitigation of ROS production, can be observed in 5% O_2.[97]

Additionally, proteins involved in the synthesis and assembly of collagen (P4HA1, P4HA2, PLOD1, PLOD2) are upregulated in 5% oxygen (Figures 19 and 22A). The induction of these enzymes by HIF-1α is associated with extracellular matrix remodelling (ECM) under hypoxic conditions. Proteomic analysis of failing hearts has illustrated a relative abundance of proteins responsible for the modification of the ECM as well as the reduction in several ion transporters (Figure 22B).[45, 98, 99]

While 5% oxygen was considered physiological in the experimental design, cardioids appear hypoxic. (Homogenous) oxygen diffusion and uptake may be limited due to the

three-dimensional organization of spheroid structure and cavity formation. Actual oxygen availability has to be accounted for in follow-up experiments.

3.2.2 The Cardioid Model Exhibits an Embryonic Metabolic Phenotype

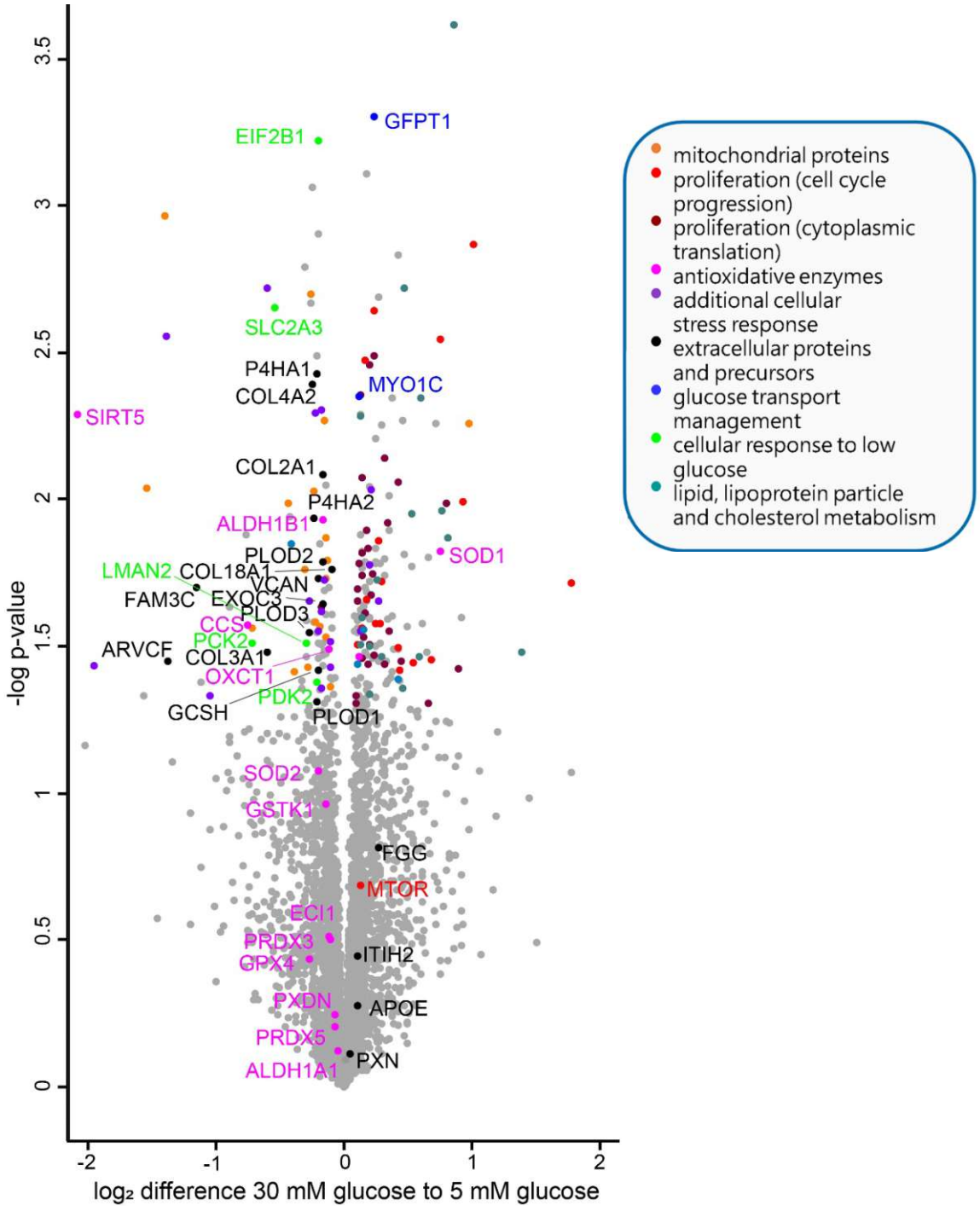

Figure 23. Scatter plot illustrating changes in the proteome after 48 of differential treatment. Proteins more abundant in high glucose (30 mM) are illustrated on the right side of the plot, whereas proteins more abundant in physiological glucose (5 mM) are displayed on the left side. Student *t*-testing revealed 245 significantly differentially expressed proteins. Due to the high variability of individual spheroids and modest response in alteration of glucose availability, the Student *t*-test *p*-value was not corrected for permutation-based FDR. The resulting limitations were considered in further interpretation.

As mentioned before, changes in the proteome of cardioids cultured in different medium glucose concentrations are not as significant as those due to variations in oxygen availability. While considering the apparent limitations, proteomic signatures can still be observed in the differentially treated cardiac organoids (as illustrated in Figure 23).

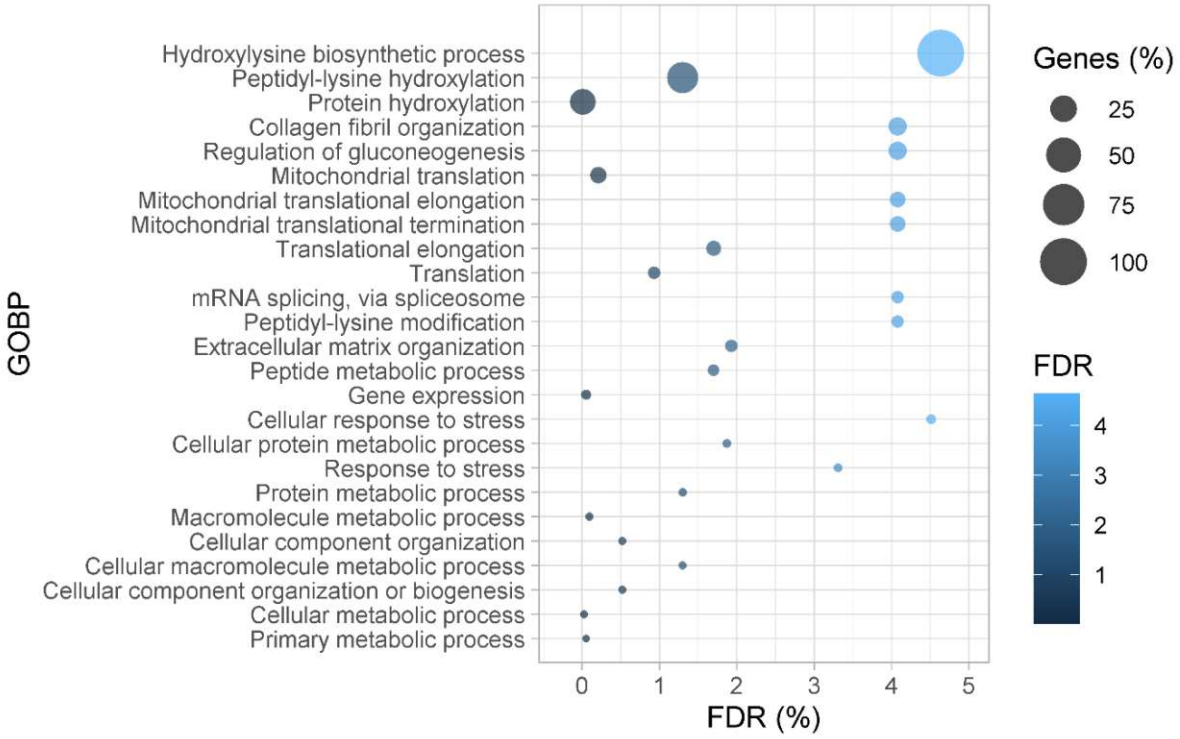

Figure 24. Gene ontology-enrichment analysis of biological processes (GOBP) of significantly more abundant proteins in cardiac organoids cultured in physiological (5 mM) compared to high glucose concentration (30 mM). The list of terms was manually reduced for redundancy. The modest response to alteration in medium glucose concentration compared to variation in oxygen availability can be observed in the generality of the listed enriched GOBP terms.

Proteins significantly more abundant in cardioids cultured in 5 mM glucose are predominantly involved in the remodelling of the ECM and the synthesis and modification of collagen fibrils, as indicated by gene ontology-enrichment analysis (Figure 24). Respective proteins include various forms of collagens (COL18A1, COL2A1, COL3A1, COL4A2), procollagen lysine 5- dioxygenases (PLOD1, PLOD2, PLOD3) and prolyl 4-hydroxylase (P4HA1, P4HA2). In contrast to the variation in oxygen availability discussed above, no associated HIF-1α activity (based on increased HIF-PH2 abundance) can be observed. Reported enzymes and collagens cluster into a distinct network in STRING protein-interaction analysis (Figure 25A), matching the preliminary findings in the tissue of failing hearts and AC16 cells exposed to increased atmospheric oxygen.[45]

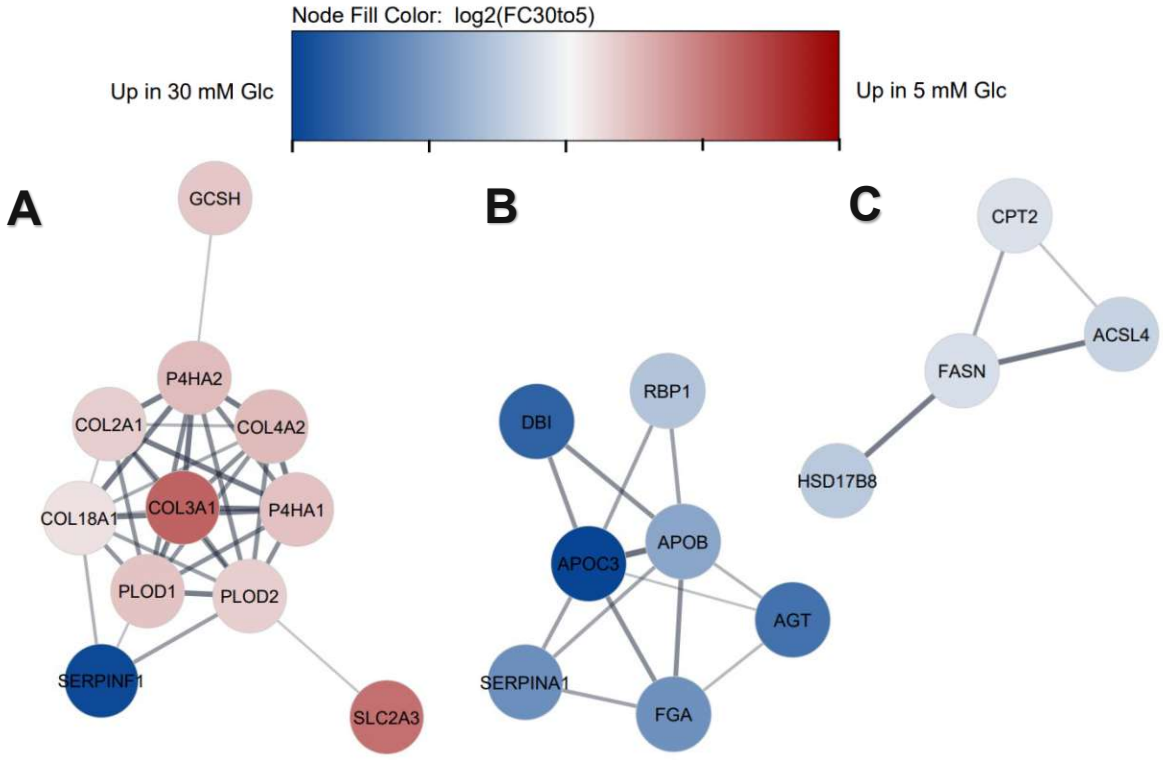

Figure 25. STRING protein-interaction analyses of proteins significantly more expressed in 5 mM or 30 mM glucose (Glc) show distinct clustering (excerpt). (A) Proteins involved in ECM remodelling are significantly more abundant in 5 mM glucose. COL3A1 has been suggested to induce the development and progression of ischemic HF. Furthermore, an increased abundance of GLUT3 (SLC2A3) indicates cellular efforts for glucose import. In contrast to preliminary findings in the tissue of failing hearts, levels of pigment-epithelium-derived factor (PEDF; encoded by the SERPINF1 gene; no reported serine protease inhibitory activity) do not correlate with differentially expressed collagens and is significantly less abundant in 5 mM.[45] PEDF is proposed as a regulator of ECM remodelling and proliferation, and reduced levels have been reported in the presence of increased oxidative stress and ROS.[100] (B) Proteins involved in the metabolism and transport of cholesterol and other lipids are shown to be more abundant in 30 mM glucose. (C) Relative abundance in fatty acid synthase (encoded by the FASN gene), long-chain-fatty acid-CoA ligase 4 (encoded by the ACSL4 gene), and carnitine O-palmitoyltransferase (mitochondrial; encoded by the CPT2 gene) represents increased fatty acid synthesis, lipid synthesis and β-oxidation, respectively. Results indicate certain metabolic flexibility and could imply abundant nutrients, cellular building blocks, and increased proliferation.[90]

In contrast to cardioids differentially cultured in varying oxygen environments, SOD1 was significantly more abundant in 30 mM. As the isoform is primarily located in the cytoplasm, this may be allocated to increased glycolytic flux. SOD2 can again be associated with an increased mitochondrial activity.[101, 102] However, the enzyme was not significantly abundant in 5 mM glucose. Increased levels of CCS may still hint at oxidative stress associated SOD2 activity. ECM remodelling, as listed above, can be facilitated in oxidative stress as superoxides are reported to induce collagen secretion and the activity of several lysyl and prolyl hydroxylases.[103, 104]

Gene ontology-enrichment analysis indicates nutrient deprivation and increased cellular stress at 5 mM glucose (Figures 23 and 24). While proteins involved in

response to low glucose and glucose transport (GLUT1, GLUT3) are significantly more abundant in 5 mM, no upregulation in glycolytic enzymes can be observed. Findings further include increased translation of mitochondrial proteins and organization of mitochondrial matrix, possibly indicating early mitochondrial maturation and adaption to the altered nutrient environment.[105, 106] Inversely, high glucose has been reported to inhibit the maturation of cardiac cells.[107] However, metabolic acclimatization might not be advanced as no change in the overall activity of glycolysis, OXPHOS or β-oxidation can be identified based on relative protein abundance. Still, a significant abundance of PDK2 in low glucose conditions can be observed (Figure 23). PDK2 can assert regulation of glucose and fatty acid metabolism by directly impacting PDH activity and therefore controlling influx to TCA and OXPHOS.[90] The relative abundance (not significant; Table 1) of identified PDH subunits may further illustrate mitochondrial maturation. An immature or insufficient mitochondrial function may lead to additional cellular redox stress in a low-glucose environment.[108] SIRT5 is significantly more abundant in 5 mM glucose. It has been proposed to play a vital role in the regulation of cardiac (mitochondrial) metabolism and redox homeostasis.[109]

Table 1. Reported protein abundance of PDH subunits in cardiac organoids cultured in 5 mM glucose (Glc) compared to 30 mM glucose. Results imply facilitated control over pyruvate turnover for TCA influx and increased mitochondrial activity.

Gene	Protein	Student *t*-test *p*-value	Difference (30 mM Glc to 5 mM Glc)
PDHA1	Pyruvate dehydrogenase E1 component subunit alpha, somatic form, mitochondrial	0.1449	0.9362
PDHB	Pyruvate dehydrogenase E1 component subunit beta, mitochondrial	0.1511	0.7996
PDHX	Pyruvate dehydrogenase protein X component, mitochondrial	0.1877	0.9264

As mentioned in 3.1, cardioids cultured in high glucose (30 mM) do not appear to experience additional cellular stress. A significant metabolic burden imposed on cardiac organoids, resulting in disturbed homeostasis, can neither be observed in proteomic analysis (Figures 23 and 26). Results indicate the utilization of abundant nutrients (compared to cardioids cultured in 5 mM) and management of metabolic flux towards translation (ribosomal biogenesis), lipid biosynthesis and proliferation.

GFPT1 (which is significantly more abundant in 30 mM glucose) is the rate-limiting enzyme controlling glucose's flux into the hexosamine biosynthetic pathway (HBP). The subsequently obtained uridine diphosphate N-acetylglucosamine (UDP-GlcNAc) is used for the posttranslational modification of various intracellular proteins, including

proteins that participate not only in nutrient sensing but also in stress response. While the results do not indicate severely disturbed homeostasis, protein O-GlcNacylation levels are reported to associate with cardiac hypertrophy, heart failure and diabetic cardiomyopathy. Acute increases are thought to be cardioprotective in I/R injury. Further research in this area is needed to illuminate the role of HBP in cardiac pathogenesis and HF.[110]

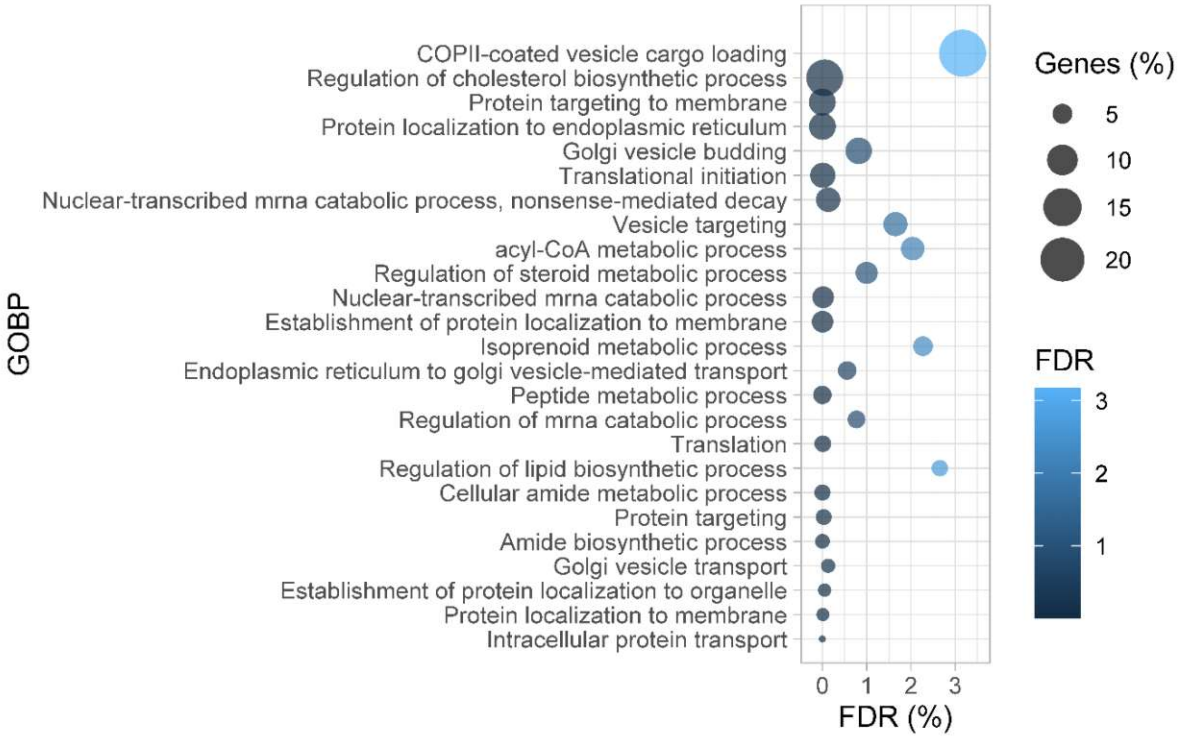

Figure 26. Gene ontology-enrichment analysis of biological processes (GOBP) of significantly more abundant proteins in cardiac organoids cultured in high (30 mM) compared to physiological glucose concentration (5 mM).

Further findings specific to high media glucose concentration are elaborated in Figure 25 and Table 2. Higher expression of lactoylglutathione lyase (GLO1), a protein tightly associated with excess glucose, indicates increased hemithioacetal adducts formed by the reaction of aldehydes, such as methylglyoxal and glutathionyl groups. While methylglyoxal is formed as a byproduct of several metabolic pathways, it mainly arises from glyceraldehyde phosphate and dihydroxyacetone phosphate inside glycolysis. GLO1 participates in the glutathione-dependent detoxification from methylglyoxal. Otherwise, elevated levels of methylglyoxal would drive the formation of advanced glycation endproducts (AGEs). The associated damage to biomolecules (e.g., histones, lipoproteins) is reported to drive inflammation, atherosclerosis and cancerogenesis unto others. Based on glutathione status and the proteome, cellular efforts keep glycolytic and oxidative stress in homeostatic ranges.[111]

Table 2. Incubation of cardiac organoids in high glucose (30 mM) significantly alters the abundance of the proteins listed below. Lower levels of voltage-dependent anion-selective channel protein 3 (VDAC3) have been reported in the tissue of failing hearts and AC16 cells cultured in normoxia.[45] Furthermore, elevated levels of angiotensinogen (AGT; significantly more abundant in 30 mM) have been associated with heart failure and the progression of heart disease in the literature. Angiotensinogen can give rise to all angiotensin peptide variants through sequential enzymatic cleavage. In physiological conditions, the renin-angiotensin system is critical for maintaining cardiac performance. In disease, AGT has been observed to be abundant in the progression of ischemia and cardiac hypertrophic remodelling. The implication of the abundance of lactoylglutathione lyase (GLO1) is discussed above.

Gene	Protein	Student *t*-test *p*-value	Difference (30 mM Glc to 5 mM Glc)
VDAC3	Voltage-dependent anion-selective channel protein 3	0.0263	0.8598
AGT	Angiotensinogen	0.0110	1.7045
GLO1	Lactoylglutathione lyase	0.0324	1.3394

Distinct cellular metabolic adaptations and protein signatures characteristic to pathological aspects of heart disease could be identified, with shared changes in collagen synthesis and modification, ECM remodelling, response to oxidative stress, secretion of extracellular proteins, mitochondrial activity and lipid metabolism occurring across all treatments. Multiple findings in our preliminary proteomic data of failing hearts and differentially cultured AC16 cells can also be observed in hSC-derived cardiac organoids exposed to alterations in nutrient and oxygen environment.[45] However, results also indicate that the metabolic phenotype does not fully match expected alterations in cardiac pathology.

The impact of glucose deprivation or excess may accumulate over time, with further significant changes in the cellular proteome occurring beyond the observed treatment duration. As for 48 h of treatment, results in glutathione status and proteomic signatures suggest both a high tolerance of and increased metabolic dependence on glucose. In combination with the detected tolerance against hypoxic conditions, cardiac organoids (cardioids) appear to exhibit a (leftover) embryonic phenotype.[112, 113] Observations further indicate deficiencies in mitochondrial activity and fatty acid utilization. Distinct unresponsiveness to changes in energy substrate availability can illustrate limitations in translational ability compared to patient-derived cardiomyocytes.

3.3 Design and Evaluation of a Differentiation Protocol for AC16 Human Proliferating Cardiomyocytes in 2D Culture

As results in 3.2 indicate that the cardiac organoid model exhibits an embryonic metabolic phenotype, with glycolysis appearing to be the preferred catabolic pathway compared to fatty acid oxidation and high glucose levels being very well tolerated, further *in vitro* models for investigating nutrient-driven redox signalling were explored. However, preliminary data and recent literature have shown apparent limitations in the mature cardiomyocyte phenotype of AC16 cells. Namely, according to proteomic analysis of AC16 cells cultured in AC16 FBS proliferation medium in normoxia, few cardiac-specific proteins are expressed compared to cardioids (Table 3).[114, 115] Therefore, as mentioned in 2.3, media composition for further differentiation of AC16 cells was explored and subsequently evaluated.

Table 3. Illustrated below is a list of (abundant) cardiomyocyte-specific proteins. Whereas a majority of markers of cardiac identity can be identified in our proteomic analysis of hSC-derived cardiac organoids (cardioids), we identified only a few of the respective proteins in AC16 cells. Cardiac markers are derived from tissue-specific proteomic mapping.[114, 115]

Gene	Protein	Cardioids	AC16
ACTC1	actin alpha cardiac muscle 1	YES	YES
ACTN2	alpha-actinin 2	YES	NO
BMP10	bone morphogenetic protein 10	NO	NO
LRRC10	leucine-rich repeat containing 10	NO	NO
MYBPC3	myosin binding protein C3	YES	NO
MYBPHL	myosin binding protein H like	NO	NO
MYH6	myosin heavy chain 6 (alpha; fast)	YES	NO
MYH7	myosin heavy chain 7 (beta; slow)	YES	NO
MYH7B	myosin heavy chain 7B (beta isoform; slow)	NO	YES
MYL4	myosin light chain 4	YES	NO
MYL7	myosin light chain 7	YES	NO
NPPA	natriuretic peptide A	NO	NO
NPPB	natriuretic peptide B	NO	NO
PLN	cardiac phospholamban	YES	NO
TNNI3	troponin I type 3 (cardiac muscle)	YES	NO
TNNT2	troponin T type 2 (cardiac muscle)	YES	NO

3.3.1 Evaluation of Media Composition

AC16 cardiomyocytes were cultured in various differentiation medium compositions, reflective of commonly applied maturation protocols reported in the literature. The proposed mechanisms for differentiation include the reduction or replacement of sera

(i.e., mitogens.), induction of gene expression by ATRA, and anti-replicative effect of nucleoside derivatives, respective of medium composition.

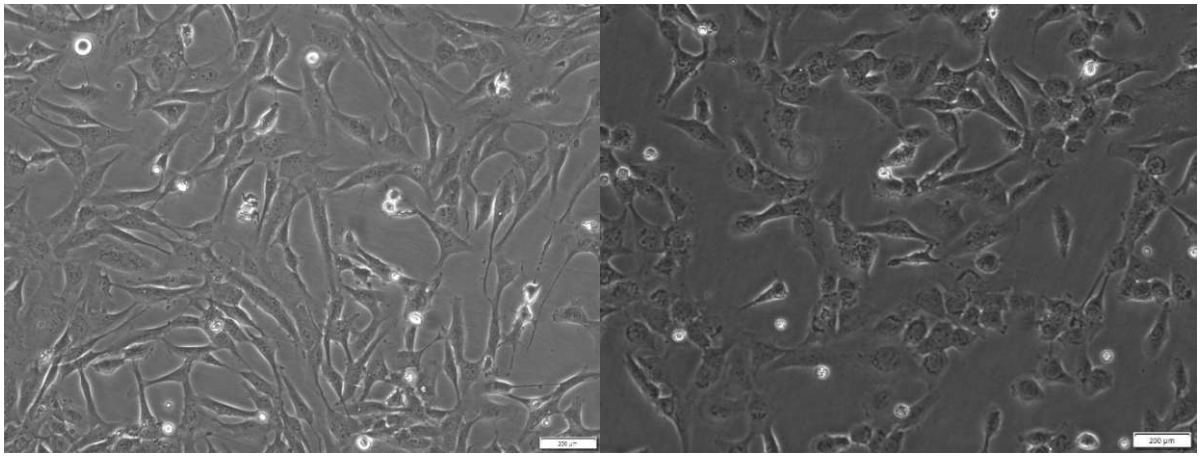

Figure 27. Microscopic image of AC16 cells after 24 h incubation in AC16 FBS proliferation medium (left) and AC16 nucleoside derivatives differentiation medium (right). The addition of nucleoside derivatives appears to induce cellular stress based on morphology and reduces cell-to-cell contact and proliferation. White bars at the lower right corner of the images indicate scale and represent 200 µm.

Cells showed no visible relative changes in morphology across treatments over 8 days of incubation, except AC16 cultured in the presence of 5-azacytidine and cytosine arabinoside (Figure 27).

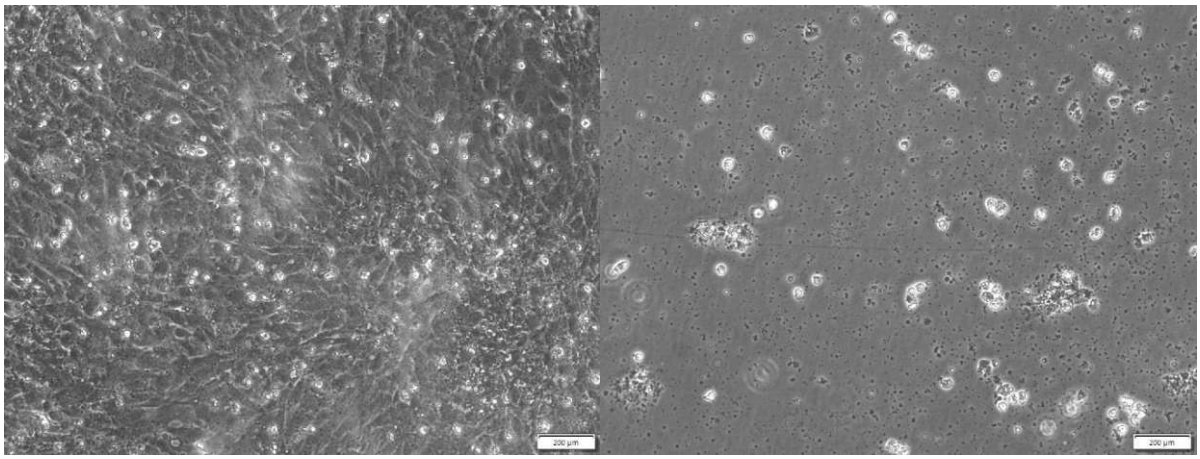

Figure 28. Microscopic image of AC16 cells after 8 days of incubation in AC16 BSA differentiation medium (left) and AC16 nucleoside derivatives differentiation medium (right). While full confluency and cellular formation observed in AC16 BSA differentiation medium are representative of the other medium compositions, treatment with 5-azacytidine and cytosine arabinoside led to complete cell death. The formation of small bodies might hint at apoptotic processes.[116] White bars at the lower right corner of the images indicate scale and represent 200 µm.

The addition of nucleoside derivatives at reported concentrations resulted in reduced cell viability and, ultimately, cell death (Figure 28). While variations in initial proliferation were observed for approximately the first 92 h, all conditions showed comparable confluency at the point of harvesting for subsequent analysis. As to be expected,

reduction in serum content, with or without ATRA treatment, does not halt cell cycle progression.

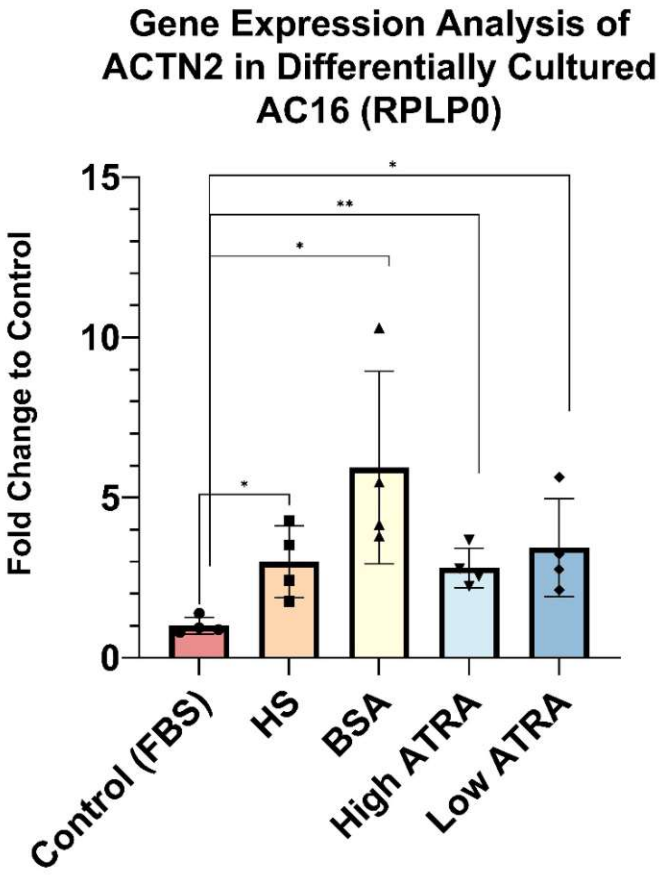

Figure 29. Results for relative gene expression analysis of alpha-actinin-2 (ACTN2) by RT-qPCR of AC16 cells differentially cultured in AC16 differentiation media candidates for 8 days compared to AC16 cells cultured in AC16 FBS proliferation medium. Cells cultured in the presence of 5-azacitidine and cytosine arabinoside (AC16 nucleoside derivatives differentiation medium) were not viable at the point of harvesting and subsequently not analysed. Transcript levels were normalized on the expression of RPLP0 (housekeeping gene; encoding for ribosomal protein lateral stalk subunit P0). AC16 BSA differentiation and AC16 high ATRA differentiation media exhibit the most promising changes in the expression of ACTN2. Individual values and standard error of the mean (SEM) are shown together with the mean value for the respective condition in all box plots. Additionally, Student *t*-test *p*-values are indicated. * indicates $p < 0.05$. ** indicates $p < 0.01$.

Gene expression analysis by reverse transcription of isolated mRNA and subsequent RT-qPCR was chosen for the evaluation of changes in differentially cultured AC16 cells. As listed in 2.3.2.4, the muscle-specific structural protein alpha-actinin-2 (encoded by the ACTN2 gene) is a commonly applied marker for the adult cardiac phenotype. The function of alpha-actinin-2 is primarily the cross-linking of actin filaments and sarcomeric titans at Z-discs.[59, 80] Results illustrate the increased expression of ACTN2 among all treatments compared to control (Figure 29). AC16 BSA differentiation medium was chosen to further investigate a potentially improved mature cardiomyocyte phenotype of AC16 cells. Not only do cells cultured in the

defined BSA/lipid concentrate medium express significantly higher levels of ACTN2 compared to the control, but this maturation approach also represents certain unique advantages. Complete reduction in serum content leads to a significant reduction in mitogens and eliminates eventual problems with lot-to-lot variability and ethical concerns.[117] Furthermore, the incorporation of additional lipids was thought to support adaption for fatty acid utilisation and mitochondrial maturation. Similar approaches with chemically defined media have recently been reported in the literature.[73, 77, 118] No follow-up studies were pursued for medium compositions containing ATRA or nucleoside derivatives. The application of media containing additional acting compounds is limited as they could ultimately introduce confounding factors in the experimental application of differentiated AC16 cells.

3.3.2 Further Inspection of the Most Promising Candidate

As the preliminary results were promising, AC16 cells cultured in AC16 BSA differentiation medium were chosen for more elaborate RT-qPCR analysis with additional markers. Additionally, the experiment was repeated with reduced treatment duration to allow for the identification of early changes in gene expression.

Troponin C, along with troponin I and troponin T, forms the protein complex of the thin filaments essential for skeletal and cardiac muscle contraction. The individual subunits provide specific functions and associate Ca^{2+}-dependently with tropomyosins, actins and myosins. Historically, the measurement of cardiac-specific isoforms (troponins I and T) has provided a significant advantage in diagnostics and prognostics for the treatment of MI. As troponin C does not have a cardiac-specific isoform, cardiac troponin I (encoded by TNNI3) and cardiac troponin T (TNNT2) were chosen to be included in subsequent analyses. Additionally, the slow-twitch skeletal muscle isoform of troponin I (encoded by TNNI1), while not exclusive to cardiac muscle but commonly utilized for phenotyping in cardiac maturation, was inspected.[59, 81]

The concrete implication of the dynamic ratio of myosin heavy chain α- and β-isoform (encoded by MYH6 and MYH7, respectively) in cardiac development and disease is yet to be fully illuminated. Both isoforms constitute the thick filament in cardiac muscle and represent the molecular motor fueling contraction by conversion of energy derived from ATP hydrolysis into mechanical force. They are, therefore, a typical marker used in cardiomyocyte identification.[15, 61, 119]

The results for relative gene expression analysis of multiple cardiac markers of AC16 cells cultured in AC16 BSA differentiation medium for 8 days are illustrated in Figure 30 below. Individual results and statistics for the respective genes are listed in Figure 42 in the appendix.

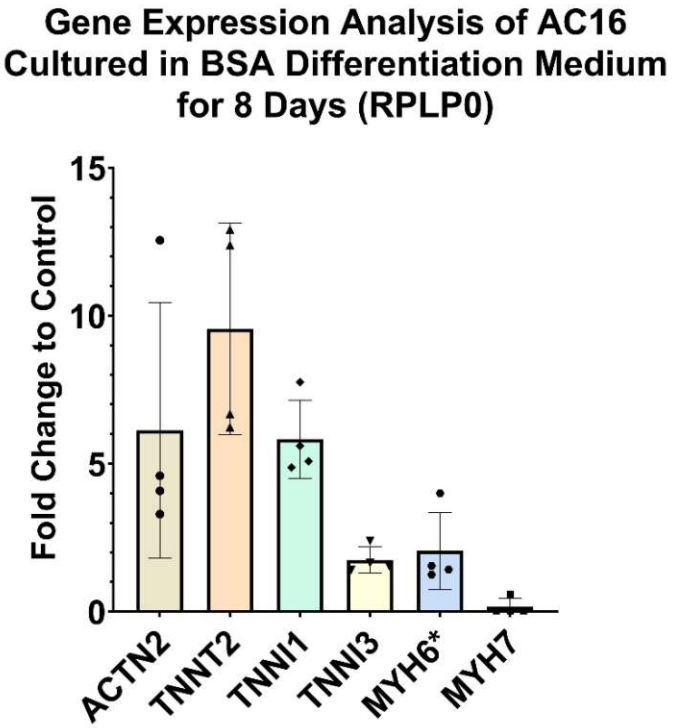

Figure 30. Results for relative gene expression analysis by RT-qPCR of AC16 cells cultured in AC16 BSA differentiation medium for 8 days compared to AC16 cells cultured in AC16 FBS proliferation medium. Transcript levels were normalized on the expression of RPLP0 (housekeeping gene). * indicates that observed changes in cardiomyocyte phenotype according to the respective transcript cannot be interpreted with complete confidence based on high variability of biological replicates and detection with Ct values close to or above 30.

AC16 cells cultured in serum-free, defined BSA/lipid concentrate medium show significantly higher expression of cardiac-specific markers ACTN2, TNNT2 and TNNI3. MYH6 appears to be upregulated (not significant), but reported Ct values for controls and treated samples were above 30. Results can, therefore, not be regarded with the same level of confidence. Transcripts of MYH7 were observed to be less abundant than in FBS proliferation medium (not significant; Student *t*-test *p*-value = 0.0886).

Overall, changes in gene expression match published reports of AC16 differentiation.[15] The relative abundance of ACTN2 and TNNT2 is furthermore often observed in cardiac development and in hiPSC-derived spheroid models, where those two proteins constitute a significant portion of the core construction.[118] Moreover, transcriptomic and proteomic mapping of structural and contractile proteins has indicated the tissue-

specific abundance of MYH6 and MYH7. Myosin heavy chain α is primarily expressed in the developing ventricle and adult atrium, whereas myosin heavy chain β is predominantly localised to the left ventricle in the adult human. Furthermore, expression of MYH7 is reported to be upregulated under stress (i.e., possibly due to a reduction in serum and mitogens). While this, in combination with the results illustrated in Figure 31, might indicate early differentiation, no definite conclusion can be made. Additionally, no information on the local origin of primary cells used for the creation of the AC16 cell line is available beyond the stated utilization of adult ventricular tissue.[61, 115, 120, 121]

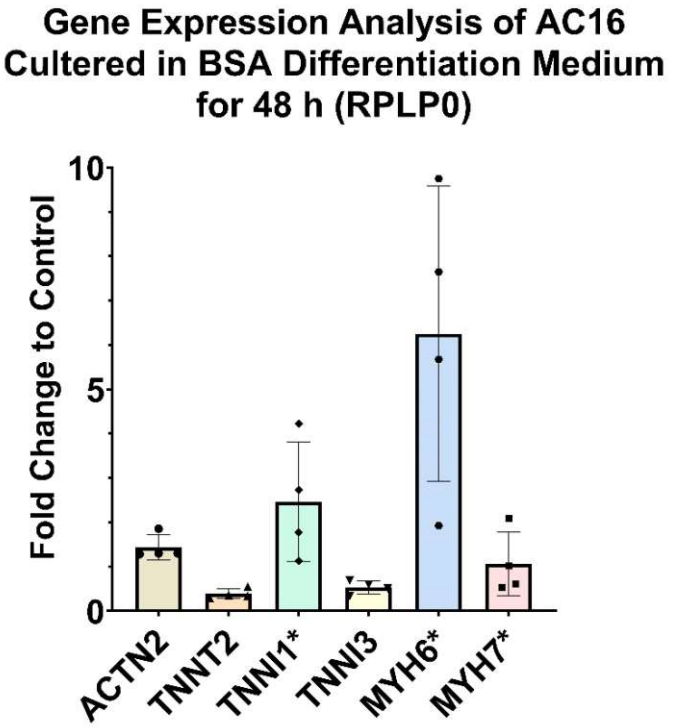

Figure 31. Results for relative gene expression analysis by RT-qPCR of AC16 cells cultured in AC16 BSA differentiation medium for 48 h compared to AC16 cells cultured in AC16 FBS proliferation medium. Transcript levels were normalized on the expression of RPLP0 (housekeeping gene). * indicates that observed changes in cardiomyocyte phenotype according to the respective transcript cannot be interpreted with complete confidence based on high variability of biological replicates (TNNI1) or detection with Ct values close to or above 30 (MYH6, MYH7).

AC16 cells cultured in AC16 BSA differentiation medium for 48 h exhibit observable changes in gene expression. Figure 31 shows that while early adaptations to medium alteration are detectible, differences in transcript levels of cardiac marker genes are less pronounced than with additional incubation days (see Figure 43 in the appendix).

Although specific to striated muscle and not exclusively to cardiomyocytes, TNNI1 can be observed to be progressively more expressed in AC16 BSA differentiation medium

compared to AC16 FBS proliferation medium after 48 h (not significant; Student *t*-test *p*-value = 0.0886) and 8 days (significant). TNNI1 is reported to participate heavily in early cardiac differentiation, and while it is the predominant form found in fetal cardiomyocytes, isoform switching to TNNI3 in mature cardiomyocytes is not complete.[81, 118] ACTN2 is also reported to be an early marker of differentiation and commonly listed in association with TNNI1.[118, 122]

Overall, high stability and low variance of reported Ct values of the housekeeping gene (Rplp0) across all samples and controls suggest analytical validity of observed changes in gene expression.[123] However, reported Ct values close to or above 30 implicate low transcriptional abundance of MYH6 across all differentially treated AC16 samples. Identified increases in MYH6 expression must therefore be regarded with precaution. Still, MYH6 is reported to be one of the more transient changes in gene expression upon cardiac differentiation. Across all cardiomyocyte *in vitro* models discussed in the literature, applied differentiation and maturation are described as slow processes.[54, 122] Commercial options for cardiomyocytes often involve elaborate maturation protocols with up to multiple months in culture. Even then, not all cells are then shown to express a complete set of cardiac markers.[80] With cardiomyocyte *in vitro* models, as discussed in 1.3.2, one has to accept the apparent limitations in translational ability and associated difficulties in laboratory reality.[54]

Of note, additional aspects of the experimental design must also be discussed. The control condition for evaluating differentiation medium candidates was not cultured in wells to prevent overgrowth during the relatively long incubation. Cell splitting and the absence of gelatine coating could have a confounding effect on differentiation and must be considered a limitation.[78] Controls for 48 h incubation in AC16 BSA differentiation medium were cultured in coated well plates as no risk of overgrowth was expected. Furthermore, while markers are widely applied and commonly used in characterising cardiac phenotype, additional confidence in the results could be gained by testing the applied primers for specificity in non-cardiac, non-muscle tissue.

While RT-qPCR was expected to be most sensitive and specific for the evaluation of small changes in gene expression of structural proteins with low abundant transcripts, characterisation of a potentially altered metabolic phenotype is yet to be carried out. Further valuable insights could be gained by measuring the oxygen consumption rate (OCR) and extracellular acidification rate (ECAR), respective key indicators of

mitochondrial respiration and glycolysis, of differentially cultured AC16 cardiomyocytes. Additional proteomics analysis to inspect for changes in metabolism and adaptation to altered nutrient and oxygen environments, while relevant for future experiments, was ultimately outside this thesis's scope. This also applies to potential imaging for screening of visual targets of adult cardiomyocyte identity (e.g., distinct elongated cellular shape, positioning in parallel fashion, multinucleated cells).

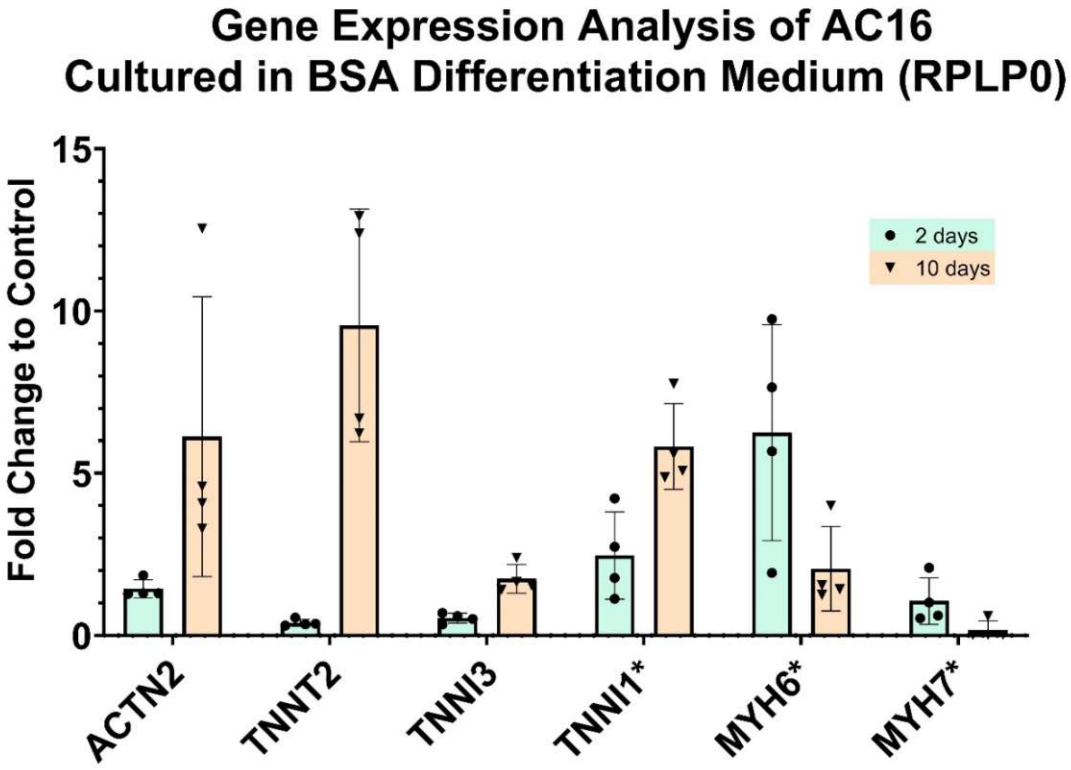

Figure 32. Combined results for relative gene expression analysis by RT-qPCR of common markers of cardiomyocyte identity after incubation of AC16 cells in serum-free, defined BSA/lipid concentrate medium for 48 h (teal; left) and 8 days (salmon; right), respectively. Transcript levels were normalized on the expression of RPLP0 (housekeeping gene). * indicates that observed changes in cardiomyocyte phenotype according to the respective transcript cannot be interpreted with complete confidence based on high variability of biological replicates (TNNI1, MYH6) or detection with Ct values close to or above 30 (MYH6, MYH7).

Combined results of the gene expression analysis of common markers of cardiomyocyte identity after incubation in serum-free, defined BSA/lipid concentrate medium for 48 h and 8 days, respectively, are illustrated in Figure 32 above. In combination, results indicate an improved cardiac phenotype on the level of transcription. Changes are observable after 48 h of treatment, illustrating the potential suitability of shorter pre-treatment maturation protocols (e.g., 72 h after seeding) prior to future experimental application of AC16 cardiomyocytes (e.g., for investigating pathomolecular mechanisms in heart disease and HF).

4 Conclusion

In order to address the crosstalk of aberrant metabolism and alterations of the myocardial redox state correlated with oxidative stress and heart failure, differentially treated hSC-derived cardiac organoids were subjected to parallel mass spectrometry-based redox metabolomic and quantitative proteomic analyses.

Low levels of medium glucose (5 mM) and atmospheric oxygen (20%) led to a notably decreased relative abundance of glutathione (GSH) to glutathione disulfide (GSSG). Overall, changes in glutathione levels were modest as the cardiac cells appeared to adapt well based on the abundance of antioxidative enzymes specific to increased glycolytic flux or mitochondrial activity. The impact of glucose and oxygen availability on the cellular redox environment, based on the observable oxidative stress, was within the homeostatic range. However, multiple proteins involved in response to cellular stress and hypoxia were significantly more abundant at 5% compared to 20% oxygen level, indicating compromised oxygen supply under physioxia (5%), most probably resulting from the distinct 3D morphology of the cardioids.

Distinct cellular metabolic adaptations and protein signatures characteristic to pathological aspects of heart disease could be identified, with analogous changes in collagen synthesis and modification, ECM remodelling, secretion of extracellular proteins, mitochondrial activity and lipid metabolism occurring across all treatments. Multiple findings in preliminary proteomic data of failing hearts and differentially cultured AC16 cells can also be observed in hSC-derived cardiac organoids exposed to alterations in nutrient and oxygen environment.

Furthermore, proteomic analysis and results in glutathione status indicate that the model exhibits an embryonic metabolic phenotype. With glycolysis appearing to be the preferred catabolic pathway compared to fatty acid oxidation and high glucose levels being very well tolerated, further *in vitro* models for investigating nutrient-driven redox signalling were explored.

In efforts to improve the translational ability of AC16 human cardiomyocytes, a collection of differentiation media was designed and subsequently assessed in composition and supposed mechanism of action. Gene expression analysis of AC16 cells cultured in a serum-free, defined bovine serum albumin/lipid concentrate medium by RT-qPCR indicates an improved cardiac phenotype according to multiple

cardiomyocyte-specific differentiation markers (ACTN2, TNNT2, TNNI3, unto others) after 8 days of treatment. Additionally, results indicate observable adaption and changes in gene expression as early as after 48 h of treatment. A maturation protocol building on these results has since been implemented and used in subsequent experiments based on AC16 cardiomyocytes. These discoveries are not only notable to accommodate the relatively scarce body of available literature but also to assess apparent limitations and to improve the translational value of a widely applied *in vitro* model for cardiopathological research.

Full elucidation of the complex interplay of molecular, cellular and whole-organism pathological changes in the various forms of heart disease, and heart failure, will require further and elaborate, multidisciplinary efforts. The utilization of cardiac *in vitro* models, appropriate to their respective translational ability, must complement investigations in patient-derived samples and *in vivo* models to drive the discovery and validation of novel options in diagnosis and treatment.

5 References

1. Tarride, J.-E., Lim, M., DesMeules, M., Luo, W., Burke, N., O'Reilly, D., Bowen, J., and Goeree, R., “A review of the cost of cardiovascular disease,” *The Canadian Journal of Cardiology*, V. 25, No. 6, 2009, e195-202.
2. Kathiresan, S., and Srivastava, D., “Genetics of human cardiovascular disease,” *Cell*, V. 148, No. 6, 2012, pp. 1242–1257.
3. Heineke, J., and Molkentin, J. D., “Regulation of cardiac hypertrophy by intracellular signalling pathways,” *Nat Rev Mol Cell Biol*, V. 7, No. 8, 2006, pp. 589–600.
4. Pepe, S., and Lakatta, E. G., “Aging hearts and vessels: masters of adaptation and survival,” *Cardiovascular research*, V. 66, No. 2, 2005, pp. 190–193.
5. National Guideline Centre (UK), “Chronic Heart Failure in Adults: Diagnosis and Management,” National Institute for Health and Care Excellence (NICE), London, 2018.
6. Roth, G. A., Mensah, G. A., Johnson, C. O., Addolorato, G., Ammirati, E., Baddour, L. M., Barengo, N. C., Beaton, A. Z., Benjamin, E. J., Benziger, C. P., Bonny, A., Brauer, M., Brodmann, M., Cahill, T. J., Carapetis, J., Catapano, A. L., Chugh, S. S., Cooper, L. T., Coresh, J., Criqui, M., DeCleene, N., Eagle, K. A., Emmons-Bell, S., Feigin, V. L., Fernández-Solà, J., Fowkes, G., Gakidou, E., Grundy, S. M., He, F. J., Howard, G., Hu, F., Inker, L., Karthikeyan, G., Kassebaum, N., Koroshetz, W., Lavie, C., Lloyd-Jones, D., Lu, H. S., Mirijello, A., Temesgen, A. M., Mokdad, A., Moran, A. E., Muntner, P., Narula, J., Neal, B., Ntsekhe, M., Moraes de Oliveira, G., Otto, C., Owolabi, M., Pratt, M., Rajagopalan, S., Reitsma, M., Ribeiro, A. L. P., Rigotti, N., Rodgers, A., Sable, C., Shakil, S., Sliwa-Hahnle, K., Stark, B., Sundström, J., Timpel, P., Tleyjeh, I. M., Valgimigli, M., Vos, T., Whelton, P. K., Yacoub, M., Zuhlke, L., Murray, C., and Fuster, V., “Global Burden of Cardiovascular Diseases and Risk Factors, 1990-2019: Update From the GBD 2019 Study,” *Journal of the American College of Cardiology*, V. 76, No. 25, 2020, pp. 2982–3021.
7. Davis, R. C., Hobbs, F. D., and Lip, G. Y., “ABC of heart failure. History and epidemiology,” *BMJ (Clinical research ed.)*, V. 320, No. 7226, 2000, pp. 39–42.
8. Braunwald, E., “Cardiovascular medicine at the turn of the millennium: triumphs, concerns, and opportunities,” *The New England journal of medicine*, V. 337, No. 19, 1997, pp. 1360–1369.

9. Li, W., Su, S.-A., Chen, J., Ma, H., and Xiang, M., “Emerging roles of fibroblasts in cardiovascular calcification,” *Journal of Cellular and Molecular Medicine*, V. 25, No. 4, 2021, pp. 1808–1816.
10. Girerd, N., Seronde, M.-F., Coiro, S., Chouihed, T., Bilbault, P., Braun, F., Kenizou, D., Maillier, B., Nazeyrollas, P., Roul, G., Fillieux, L., Abraham, W. T., Januzzi, J., Sebbag, L., Zannad, F., Mebazaa, A., and Rossignol, P., “Integrative Assessment of Congestion in Heart Failure Throughout the Patient Journey,” *JACC. Heart failure*, V. 6, No. 4, 2018, pp. 273–285.
11. Drazner, M. H., “The progression of hypertensive heart disease,” *Circulation*, V. 123, No. 3, 2011, pp. 327–334.
12. Tsao, C. W., Aday, A. W., Almarzooq, Z. I., Alonso, A., Beaton, A. Z., Bittencourt, M. S., Boehme, A. K., Buxton, A. E., Carson, A. P., Commodore-Mensah, Y., Elkind, M. S. V., Evenson, K. R., Eze-Nliam, C., Ferguson, J. F., Generoso, G., Ho, J. E., Kalani, R., Khan, S. S., Kissela, B. M., Knutson, K. L., Levine, D. A., Lewis, T. T., Liu, J., Loop, M. S., Ma, J., Mussolino, M. E., Navaneethan, S. D., Perak, A. M., Poudel, R., Rezk-Hanna, M., Roth, G. A., Schroeder, E. B., Shah, S. H., Thacker, E. L., VanWagner, L. B., Virani, S. S., Voecks, J. H., Wang, N.-Y., Yaffe, K., and Martin, S. S., “Heart Disease and Stroke Statistics-2022 Update: A Report From the American Heart Association,” *Circulation*, V. 145, No. 8, 2022, e153-e639.
13. Taubenschmid, J., and Weitzer, G., “Mechanisms of cardiogenesis in cardiovascular progenitor cells,” *International review of cell and molecular biology*, V. 293, 2012, pp. 195–267.
14. Garbern, J. C., and Lee, R. T., “Heart regeneration: 20 years of progress and renewed optimism,” *Developmental Cell*, V. 57, No. 4, 2022, pp. 424–439.
15. Zwetsloot, P. P., Végh, A. M. D., Jansen of Lorkeers, S. J., van Hout, G. P. J., Currie, G. L., Sena, E. S., Gremmels, H., Buikema, J. W., Goumans, M.-J., Macleod, M. R., Doevendans, P. A., Chamuleau, S. A. J., and Sluijter, J. P. G., “Cardiac Stem Cell Treatment in Myocardial Infarction: A Systematic Review and Meta-Analysis of Preclinical Studies,” *Circulation research*, V. 118, No. 8, 2016, pp. 1223–1232.
16. Liu, B., Duan, C.-Y., Luo, C.-F., Ou, C.-W., Sun, K., Wu, Z.-Y., Huang, H., Cheng, C.-F., Li, Y.-P., and Chen, M.-S., “Effectiveness and safety of selected bone marrow stem cells on left ventricular function in patients with acute myocardial

infarction: a meta-analysis of randomized controlled trials," *International journal of cardiology*, V. 177, No. 3, 2014, pp. 764–770.

17. Martin-Puig, S., Wang, Z., and Chien, K. R., "Lives of a heart cell: tracing the origins of cardiac progenitors," *Cell stem cell*, V. 2, No. 4, 2008, pp. 320–331.
18. Nakamura, M., and Sadoshima, J., "Mechanisms of physiological and pathological cardiac hypertrophy," *Nature reviews. Cardiology*, V. 15, No. 7, 2018, pp. 387–407.
19. Tran, D. H., and Wang, Z. V., "Glucose Metabolism in Cardiac Hypertrophy and Heart Failure," *Journal of the American Heart Association*, V. 8, No. 12, 2019, e012673.
20. Ciarambino, T., Menna, G., Sansone, G., and Giordano, M., "Cardiomyopathies: An Overview," *International Journal of Molecular Sciences*, V. 22, No. 14, 2021.
21. Towbin, J. A., "Inherited cardiomyopathies," *Circulation journal : official journal of the Japanese Circulation Society*, V. 78, No. 10, 2014, pp. 2347–2356.
22. Uriel, N., Sayer, G., Annamalai, S., Kapur, N. K., and Burkhoff, D., "Mechanical Unloading in Heart Failure," *Journal of the American College of Cardiology*, V. 72, No. 5, 2018, pp. 569–580.
23. Kolwicz, S. C., Purohit, S., and Tian, R., "Cardiac metabolism and its interactions with contraction, growth, and survival of cardiomyocytes," *Circulation research*, V. 113, No. 5, 2013, pp. 603–616.
24. Navale, A. M., and Paranjape, A. N., "Glucose transporters: physiological and pathological roles," *Biophysical Reviews*, V. 8, No. 1, 2016, pp. 5–9.
25. Lopaschuk, G. D., Karwi, Q. G., Tian, R., Wende, A. R., and Abel, E. D., "Cardiac Energy Metabolism in Heart Failure," *Circulation research*, V. 128, No. 10, 2021, pp. 1487–1513.
26. Noordali, H., Loudon, B. L., Frenneaux, M. P., and Madhani, M., "Cardiac metabolism - A promising therapeutic target for heart failure," *Pharmacology & therapeutics*, V. 182, 2018, pp. 95–114.
27. Wang, J., Xu, J., Wang, Q., Brainard, R. E., Watson, L. J., Jones, S. P., and Epstein, P. N., "Reduced cardiac fructose 2,6 bisphosphate increases hypertrophy and decreases glycolysis following aortic constriction," *PloS one*, V. 8, No. 1, 2013, e53951.
28. Wang, Q., Donthi, R. V., Wang, J., Lange, A. J., Watson, L. J., Jones, S. P., and Epstein, P. N., "Cardiac phosphatase-deficient 6-phosphofructo-2-

kinase/fructose-2,6-bisphosphatase increases glycolysis, hypertrophy, and myocyte resistance to hypoxia," *American journal of physiology. Heart and circulatory physiology*, V. 294, No. 6, 2008, H2889-97.

29. Marsin, A. S., Bertrand, L., Rider, M. H., Deprez, J., Beauloye, C., Vincent, M. F., van den Berghe, G., Carling, D., and Hue, L., "Phosphorylation and activation of heart PFK-2 by AMPK has a role in the stimulation of glycolysis during ischaemia," *Current Biology*, V. 10, No. 20, 2000, pp. 1247–1255.
30. Ritterhoff, J., and Tian, R., "Metabolism in cardiomyopathy: every substrate matters," *Cardiovasc Res*, V. 113, No. 4, 2017, pp. 411–421.
31. Zhang, L., Jaswal, J. S., Ussher, J. R., Sankaralingam, S., Wagg, C., Zaugg, M., and Lopaschuk, G. D., "Cardiac insulin-resistance and decreased mitochondrial energy production precede the development of systolic heart failure after pressure-overload hypertrophy," *Circulation. Heart failure*, V. 6, No. 5, 2013, pp. 1039–1048.
32. Makrecka-Kuka, M., Liepinsh, E., Murray, A. J., Lemieux, H., Dambrova, M., Tepp, K., Puurand, M., Käämbre, T., Han, W. H., Goede, P. de, O'Brien, K. A., Turan, B., Tuncay, E., Olgar, Y., Rolo, A. P., Palmeira, C. M., Boardman, N. T., Wüst, R. C. I., and Larsen, T. S., "Altered mitochondrial metabolism in the insulin-resistant heart," *Acta physiologica (Oxford, England)*, V. 228, No. 3, 2020, e13430.
33. Gibb, A. A., Epstein, P. N., Uchida, S., Zheng, Y., McNally, L. A., Obal, D., Katragadda, K., Trainor, P., Conklin, D. J., Brittian, K. R., Tseng, M. T., Wang, J., Jones, S. P., Bhatnagar, A., and Hill, B. G., "Exercise-Induced Changes in Glucose Metabolism Promote Physiological Cardiac Growth," *Circulation*, V. 136, No. 22, 2017, pp. 2144–2157.
34. Zhou, B., and Tian, R., "Mitochondrial dysfunction in pathophysiology of heart failure," *The Journal of clinical investigation*, V. 128, No. 9, 2018, pp. 3716–3726.
35. Jaswal, J. S., Keung, W., Wang, W., Ussher, J. R., and Lopaschuk, G. D., "Targeting fatty acid and carbohydrate oxidation--a novel therapeutic intervention in the ischemic and failing heart," *Biochimica et biophysica acta*, V. 1813, No. 7, 2011, pp. 1333–1350.
36. Lionetti, V., Stanley, W. C., and Recchia, F. A., "Modulating fatty acid oxidation in heart failure," *Cardiovasc Res*, V. 90, No. 2, 2011, pp. 202–209.

37. Kloner, R. A., and Nesto, R. W., “Glucose-insulin-potassium for acute myocardial infarction: continuing controversy over cardioprotection,” *Circulation*, V. 117, No. 19, 2008, pp. 2523–2533.
38. Wang, Z. V., Deng, Y., Gao, N., Pedrozo, Z., Li, D. L., Morales, C. R., Criollo, A., Luo, X., Tan, W., Jiang, N., Lehrman, M. A., Rothermel, B. A., Lee, A.-H., Lavandero, S., Mammen, P. P. A., Ferdous, A., Gillette, T. G., Scherer, P. E., and Hill, J. A., “Spliced X-box binding protein 1 couples the unfolded protein response to hexosamine biosynthetic pathway,” *Cell*, V. 156, No. 6, 2014, pp. 1179–1192.
39. Wambolt, R. B., Henning, S. L., English, D. R., Dyachkova, Y., Lopaschuk, G. D., and Allard, M. F., “Glucose utilization and glycogen turnover are accelerated in hypertrophied rat hearts during severe low-flow ischemia,” *Journal of molecular and cellular cardiology*, V. 31, No. 3, 1999, pp. 493–502.
40. Omar, M. A., Wang, L., and Clanachan, A. S., “Cardioprotection by GSK-3 inhibition: role of enhanced glycogen synthesis and attenuation of calcium overload,” *Cardiovasc Res*, V. 86, No. 3, 2010, pp. 478–486.
41. Giordano, F. J., “Oxygen, oxidative stress, hypoxia, and heart failure,” *The Journal of clinical investigation*, V. 115, No. 3, 2005, pp. 500–508.
42. Izzo, C., Vitillo, P., Di Pietro, P., Visco, V., Strianese, A., Virtuoso, N., Ciccarelli, M., Galasso, G., Carrizzo, A., and Vecchione, C., “The Role of Oxidative Stress in Cardiovascular Aging and Cardiovascular Diseases,” *Life*, V. 11, No. 1, 2021.
43. Tomin, T., Schittmayer, M., Honeder, S., Heininger, C., and Birner-Gruenberger, R., “Irreversible oxidative post-translational modifications in heart disease,” *Expert Review of Proteomics*, V. 16, No. 8, 2019, pp. 681–693.
44. Duarte-Jurado, A. P., Gopar-Cuevas, Y., Saucedo-Cardenas, O., Loera-Arias, M. d. J., Montes-de-Oca-Luna, R., Garcia-Garcia, A., and Rodriguez-Rocha, H., “Antioxidant Therapeutics in Parkinson's Disease: Current Challenges and Opportunities,” *Antioxidants*, V. 10, No. 3, 2021, p. 453.
45. Tomin, T., Schittmayer, M., Sedej, S., Bugger, H., Gollmer, J., Honeder, S., Darnhofer, B., Liesinger, L., Zuckermann, A., Rainer, P. P., and Birner-Gruenberger, R., “Mass Spectrometry-Based Redox and Protein Profiling of Failing Human Hearts,” *International Journal of Molecular Sciences*, V. 22, No. 4, 2021.
46. Kiyuna, L. A., Albuquerque, R. P. E., Chen, C.-H., Mochly-Rosen, D., and Ferreira, J. C. B., “Targeting mitochondrial dysfunction and oxidative stress in

heart failure: Challenges and opportunities," *Free radical biology & medicine*, V. 129, 2018, pp. 155–168.

47. Xiang, M., Lu, Y., Xin, L., Gao, J., Shang, C., Jiang, Z., Lin, H., Fang, X., Qu, Y., Wang, Y., Shen, Z., Zhao, M., and Cui, X., "Role of Oxidative Stress in Reperfusion following Myocardial Ischemia and Its Treatments," *Oxidative Medicine and Cellular Longevity*, V. 2021, 2021, p. 6614009.
48. Makrecka-Kuka, M., Liepinsh, E., Murray, A. J., Lemieux, H., Dambrova, M., Tepp, K., Puurand, M., Käämbre, T., Han, W. H., Goede, P. de, O'Brien, K. A., Turan, B., Tuncay, E., Olgar, Y., Rolo, A. P., Palmeira, C. M., Boardman, N. T., Wüst, R. C. I., and Larsen, T. S., "Altered mitochondrial metabolism in the insulin-resistant heart," *Acta Physiologica*, V. 228, No. 3, 2020, e13430.
49. Zhao, R.-Z., Jiang, S., Zhang, L., and Yu, Z.-B., "Mitochondrial electron transport chain, ROS generation and uncoupling (Review)," *International Journal of Molecular Medicine*, V. 44, No. 1, 2019, pp. 3–15.
50. Yan, L.-J., "Redox imbalance stress in diabetes mellitus: Role of the polyol pathway," *Animal models and experimental medicine*, V. 1, No. 1, 2018, pp. 7–13.
51. Jain, M., Brenner, D. A., Cui, L., Lim, C. C., Wang, B., Pimentel, D. R., Koh, S., Sawyer, D. B., Leopold, J. A., Handy, D. E., Loscalzo, J., Apstein, C. S., and Liao, R., "Glucose-6-phosphate dehydrogenase modulates cytosolic redox status and contractile phenotype in adult cardiomyocytes," *Circulation research*, V. 93, No. 2, 2003, e9-16.
52. Padrón-Barthe, L., Villalba-Orero, M., Gómez-Salinero, J. M., Acín-Pérez, R., Cogliati, S., López-Olañeta, M., Ortiz-Sánchez, P., Bonzón-Kulichenko, E., Vázquez, J., García-Pavía, P., Rosenthal, N., Enríquez, J. A., and Lara-Pezzi, E., "Activation of Serine One-Carbon Metabolism by Calcineurin Aβ1 Reduces Myocardial Hypertrophy and Improves Ventricular Function," *Journal of the American College of Cardiology*, V. 71, No. 6, 2018, pp. 654–667.
53. Teskey, G., Abrahem, R., Cao, R., Gyurjian, K., Islamoglu, H., Lucero, M., Martinez, A., Paredes, E., Salaiz, O., Robinson, B., and Venketaraman, V., "Glutathione as a Marker for Human Disease," *Advances in clinical chemistry*, V. 87, 2018, pp. 141–159.
54. van der Velden, J., Asselbergs, F. W., Bakkers, J., Batkai, S., Bertrand, L., Bezzina, C. R., Bot, I., Brundel, B., Carrier, L., Chamuleau, S., Ciccarelli, M.,

Dawson, D., Davidson, S. M., Dendorfer, A., Duncker, D. J., Eschenhagen, T., Fabritz, L., Falcão-Pires, I., Ferdinandy, P., Giacca, M., Girao, H., Gollmann-Tepeköylü, C., Gyongyosi, M., Guzik, T. J., Hamdani, N., Heymans, S., Hilfiker, A., Hilfiker-Kleiner, D., Hoekstra, A. G., Hulot, J.-S., Kuster, D. W. D., van Laake, L. W., Lecour, S., Leiner, T., Linke, W. A., Lumens, J., Lutgens, E., Madonna, R., Maegdefessel, L., Mayr, M., van der Meer, P., Passier, R., Perbellini, F., Perrino, C., Pesce, M., Priori, S., Remme, C. A., Rosenhahn, B., Schotten, U., Schulz, R., Sipido, K., Sluijter, J. P. G., van Steenbeek, F., Steffens, S., Terracciano, C. M., Tocchetti, C. G., Vlasman, P., Yeung, K. K., Zacchigna, S., Zwaagman, D., and Thum, T., "Animal models and animal-free innovations for cardiovascular research: current status and routes to be explored. Consensus document of the ESC working group on myocardial function and the ESC Working Group on Cellular Biology of the Heart," *Cardiovasc Res*, 2022.

55. Oh, J. G., and Ishikawa, K., "Experimental Models of Cardiovascular Diseases: Overview," *Methods in molecular biology (Clifton, N.J.)*, V. 1816, 2018, pp. 3–14.
56. Xin, M., Olson, E. N., and Bassel-Duby, R., "Mending broken hearts: cardiac development as a basis for adult heart regeneration and repair," *Nat Rev Mol Cell Biol*, V. 14, No. 8, 2013, pp. 529–541.
57. Buckberg, G. D., Nanda, N. C., Nguyen, C., and Kocica, M. J., "What Is the Heart? Anatomy, Function, Pathophysiology, and Misconceptions," *Journal of Cardiovascular Development and Disease*, V. 5, No. 2, 2018.
58. Harrison, T. M., "Improving neurodevelopment in infants with complex congenital heart disease," *Birth defects research*, V. 111, No. 15, 2019, pp. 1128–1140.
59. Onódi, Z., Visnovitz, T., Kiss, B., Hambalkó, S., Koncz, A., Ágg, B., Váradi, B., Tóth, V. É., Nagy, R. N., Gergely, T. G., Gergő, D., Makkos, A., Pelyhe, C., Varga, N., Reé, D., Apáti, Á., Leszek, P., Kovács, T., Nagy, N., Ferdinandy, P., Buzás, E. I., Görbe, A., Giricz, Z., and Varga, Z. V., "Systematic transcriptomic and phenotypic characterization of human and murine cardiac myocyte cell lines and primary cardiomyocytes reveals serious limitations and low resemblances to adult cardiac phenotype," *Journal of molecular and cellular cardiology*, V. 165, 2022, pp. 19–30.
60. Hofbauer, P., Jahnel, S. M., Papai, N., Giesshammer, M., Deyett, A., Schmidt, C., Penc, M., Tavernini, K., Grdseloff, N., Meledeth, C., Ginistrelli, L. C., Ctortecka,

C., Šalic, Š., Novatchkova, M., and Mendjan, S., “Cardioids reveal self-organizing principles of human cardiogenesis,” *Cell*, V. 184, No. 12, 2021, 3299-3317.e22.

61. Davidson, M. M., Nesti, C., Palenzuela, L., Walker, W. F., Hernandez, E., Protas, L., Hirano, M., and Isaac, N. D., “Novel cell lines derived from adult human ventricular cardiomyocytes,” *Journal of molecular and cellular cardiology*, V. 39, No. 1, 2005, pp. 133–147.
62. Hofbauer, P., Jahnel, S. M., and Mendjan, S., “In vitro models of the human heart,” *Development (Cambridge, England)*, V. 148, No. 16, 2021.
63. Kurreck, J., Engels, J. W., and Lottspeich, F., eds., “Bioanalytik,” 4. Auflage, Springer Spektrum, Berlin, Heidelberg, 2022, 1183 pp.
64. Duncan, M. W., Aebersold, R., and Caprioli, R. M., “The pros and cons of peptide-centric proteomics,” *Nat Biotechnol*, V. 28, No. 7, 2010, pp. 659–664.
65. Lenčo, J., Jadeja, S., Naplekov, D. K., Krokhin, O. V., Khalikova, M. A., Chocholouš, P., Urban, J., Broeckhoven, K., Nováková, L., and Švec, F., “Reversed-Phase Liquid Chromatography of Peptides for Bottom-Up Proteomics: A Tutorial,” *Journal of Proteome Research*, 2022.
66. Meier, F., Brunner, A.-D., Koch, S., Koch, H., Lubeck, M., Krause, M., Goedecke, N., Decker, J., Kosinski, T., Park, M. A., Bache, N., Hoerning, O., Cox, J., Räther, O., and Mann, M., “Online Parallel Accumulation-Serial Fragmentation (PASEF) with a Novel Trapped Ion Mobility Mass Spectrometer,” *Molecular & cellular proteomics : MCP*, V. 17, No. 12, 2018, pp. 2534–2545.
67. Cox, J., Hein, M. Y., Luber, C. A., Paron, I., Nagaraj, N., and Mann, M., “Accurate proteome-wide label-free quantification by delayed normalization and maximal peptide ratio extraction, termed MaxLFQ,” *Molecular & cellular proteomics : MCP*, V. 13, No. 9, 2014, pp. 2513–2526.
68. Meier, F., Beck, S., Grassl, N., Lubeck, M., Park, M. A., Raether, O., and Mann, M., “Parallel Accumulation-Serial Fragmentation (PASEF): Multiplying Sequencing Speed and Sensitivity by Synchronized Scans in a Trapped Ion Mobility Device,” *Journal of Proteome Research*, V. 14, No. 12, 2015, pp. 5378–5387.
69. Tomin, T., Schittmayer, M., and Birner-Gruenberger, R., “Addressing Glutathione Redox Status in Clinical Samples by Two-Step Alkylation with N-ethylmaleimide Isotopologues,” *Metabolites*, V. 10, No. 2, 2020.

70. Kitteringham, N. R., Jenkins, R. E., Lane, C. S., Elliott, V. L., and Park, B. K., “Multiple reaction monitoring for quantitative biomarker analysis in proteomics and metabolomics,” *Journal of chromatography. B, Analytical technologies in the biomedical and life sciences*, V. 877, No. 13, 2009, pp. 1229–1239.
71. Peterson, A. C., Russell, J. D., Bailey, D. J., Westphall, M. S., and Coon, J. J., “Parallel reaction monitoring for high resolution and high mass accuracy quantitative, targeted proteomics,” *Molecular & cellular proteomics : MCP*, V. 11, No. 11, 2012, pp. 1475–1488.
72. Cooks, R.G., “Aston Labs: MRM-Profiling for Lipidomics and Metabolomics,” Department of Chemistry, Purdue University, 2022, https://aston.chem.purdue.edu/research/mrm.html.
73. Feyen, D. A. M., McKeithan, W. L., Bruyneel, A. A. N., Spiering, S., Hörmann, L., Ulmer, B., Zhang, H., Briganti, F., Schweizer, M., Hegyi, B., Liao, Z., Pölönen, R.-P., Ginsburg, K. S., Lam, C. K., Serrano, R., Wahlquist, C., Kreymerman, A., Vu, M., Amatya, P. L., Behrens, C. S., Ranjbarvaziri, S., Maas, R. G. C., Greenhaw, M., Bernstein, D., Wu, J. C., Bers, D. M., Eschenhagen, T., Metallo, C. M., and Mercola, M., “Metabolic Maturation Media Improve Physiological Function of Human iPSC-Derived Cardiomyocytes,” *Cell reports*, V. 32, No. 3, 2020, p. 107925.
74. Deng, H., Yu, B., Yu, Y., Tian, G., and Yang, L., “NO66 overexpression rescues ethanol-induced cell apoptosis in human AC16 cardiomyocytes by suppressing PTEN and activating the PI3K/Akt signaling,” *Acta biochimica et biophysica Sinica*, V. 52, No. 10, 2020, pp. 1093–1101.
75. Fukushima, A., Zhang, L., Huqi, A., Lam, V. H., Rawat, S., Altamimi, T., Wagg, C. S., Dhaliwal, K. K., Hornberger, L. K., Kantor, P. F., Rebeyka, I. M., and Lopaschuk, G. D., “Acetylation contributes to hypertrophy-caused maturational delay of cardiac energy metabolism,” *JCI Insight*, V. 3, No. 10, 2018.
76. Branco, A. F., Pereira, S. P., Gonzalez, S., Gusev, O., Rizvanov, A. A., and Oliveira, P. J., “Gene Expression Profiling of H9c2 Myoblast Differentiation towards a Cardiac-Like Phenotype,” *PloS one*, V. 10, No. 6, 2015, e0129303.
77. Lee, S. T., Oh, S. W., Kim, D. Y., Han, J. Y., Moon, S. Y., and Lim, J. M., “Serum replacement with a growth factor-free synthetic substance in culture medium contributes to effective establishment of mouse embryonic stem cells of various origins,” *Fertility and sterility*, V. 86, 4 Suppl, 2006, pp. 1137–1145.

78. Freshney, R. I., “Culture of Animal Cells - A Manual of Basic Technique and Specialized Applications: A Manual of Basic Technique and Specialized Applications,” 7th ed., John Wiley & Sons Incorporated, Hoboken, 2016, 758 pp.
79. Guo, Y., and Pu, W. T., “Cardiomyocyte Maturation: New Phase in Development,” *Circulation research*, V. 126, No. 8, 2020, pp. 1086–1106.
80. PromoCell GmbH, “Technical Library Human Cardiac Myocytes,” 12 pp.
81. Sheng, J.-J., and Jin, J.-P., “TNNI1, TNNI2 and TNNI3: Evolution, regulation, and protein structure-function relationships,” *Gene*, V. 576, 1 Pt 3, 2016, pp. 385–394.
82. Červenák, Z., Červenák, F., Adamičková, A., Šalingová, B., Gažová, A., and Kyselovič, J., “Normalization strategy for selection of reference genes for RT-qPCR analysis in left ventricles of failing human hearts,” *BMC Cardiovasc Disord*, V. 22, No. 1, 2022, p. 180.
83. Ieda, M., Fu, J.-D., Delgado-Olguin, P., Vedantham, V., Hayashi, Y., Bruneau, B. G., and Srivastava, D., “Direct reprogramming of fibroblasts into functional cardiomyocytes by defined factors,” *Cell*, V. 142, No. 3, 2010, pp. 375–386.
84. Al-Salam, S., and Hashmi, S., “Myocardial Ischemia Reperfusion Injury: Apoptotic, Inflammatory and Oxidative Stress Role of Galectin-3,” *CPB*, V. 50, No. 3, 2018, pp. 1123–1139.
85. Dhalla, N. S., Elmoselhi, A. B., Hata, T., and Makino, N., “Status of myocardial antioxidants in ischemia-reperfusion injury,” *Cardiovasc Res*, V. 47, No. 3, 2000, pp. 446–456.
86. Chlup, R., Krejci, J., O'Connell, M., Sebestova, B., Plicka, R., Jezova, L., Brozova, T., Doubravova, B., Zalesakova, H., Durajkova, E., Vojtek, J., and Bartek, J., “Glucose concentrations in blood and tissue - a pilot study on variable time lag,” *Biomedical papers of the Medical Faculty of the University Palacky, Olomouc, Czechoslovakia*, V. 159, No. 4, 2015, pp. 527–534.
87. Carreau, A., El Hafny-Rahbi, B., Matejuk, A., Grillon, C., and Kieda, C., “Why is the partial oxygen pressure of human tissues a crucial parameter? Small molecules and hypoxia,” *Journal of Cellular and Molecular Medicine*, V. 15, No. 6, 2011, pp. 1239–1253.
88. Winegrad, S., Henrion, D., Rappaport, L., and Samuel, J. L., “Self-protection by cardiac myocytes against hypoxia and hyperoxia,” *Circulation research*, V. 85, No. 8, 1999, pp. 690–698.

89. Xu, W., Zhu, H., Gu, M., Luo, Q., Ding, J., Yao, Y., Chen, F., and Wang, Z., “DHTKD1 is essential for mitochondrial biogenesis and function maintenance,” *FEBS letters*, V. 587, No. 21, 2013, pp. 3587–3592.
90. Berg, J. M., Tymoczko, J. L., Gatto jr., G. J., and Stryer, L., “Stryer Biochemie,” 8. Aufl. 2018, Springer Spektrum, Berlin, Heidelberg, 2018, 1401 pp.
91. Li, Q., Li, C., Elnwasany, A., Sharma, G., An, Y. A., Zhang, G., Elhelaly, W. M., Lin, J., Gong, Y., Chen, G., Wang, M., Zhao, S., Dai, C., Smart, C. D., Liu, J., Luo, X., Deng, Y., Tan, L., Lv, S.-J., Davidson, S. M., Locasale, J. W., Lorenzi, P. L., Malloy, C. R., Gillette, T. G., Vander Heiden, M. G., Scherer, P. E., Szweda, L. I., Fu, G., and Wang, Z. V., “PKM1 Exerts Critical Roles in Cardiac Remodeling Under Pressure Overload in the Heart,” *Circulation*, V. 144, No. 9, 2021, pp. 712–727.
92. Li, Q., Li, C., Elnwasany, A., Sharma, G., An, Y. A., Zhang, G., Elhelaly, W. M., Lin, J., Gong, Y., Chen, G., Wang, M., Zhao, S., Dai, C., Smart, C. D., Liu, J., Luo, X., Deng, Y., Tan, L., Lv, S.-J., Davidson, S. M., Locasale, J. W., Lorenzi, P. L., Malloy, C. R., Gillette, T. G., Vander Heiden, M. G., Scherer, P. E., Szweda, L. I., Fu, G., and Wang, Z. V., “PKM1 Exerts Critical Roles in Cardiac Remodeling Under Pressure Overload in the Heart,” *Circulation*, V. 144, No. 9, 2021, pp. 712–727.
93. Felmlee, M. A., Jones, R. S., Rodriguez-Cruz, V., Follman, K. E., and Morris, M. E., “Monocarboxylate Transporters (SLC16): Function, Regulation, and Role in Health and Disease,” *Pharmacological reviews*, V. 72, No. 2, 2020, pp. 466–485.
94. Printz, R. L., Osawa, H., Ardehali, H., Koch, S., and Granner, D. K., “Hexokinase II gene: structure, regulation and promoter organization,” *Biochemical Society transactions*, V. 25, No. 1, 1997, pp. 107–112.
95. Li, C., Liu, Z., Xu, Q., Peng, H., Cao, J., Zhou, H., Zhang, G., Cheng, G., and Shi, R., “PXDN reduces autophagic flux in insulin-resistant cardiomyocytes via modulating FoxO1,” *Cell Death Dis*, V. 12, No. 5, 2021, p. 418.
96. Movafagh, S., Crook, S., and Vo, K., “Regulation of hypoxia-inducible factor-1a by reactive oxygen species: new developments in an old debate,” *Journal of cellular biochemistry*, V. 116, No. 5, 2015, pp. 696–703.
97. Guimarães-Camboa, N., Stowe, J., Aneas, I., Sakabe, N., Cattaneo, P., Henderson, L., Kilberg, M. S., Johnson, R. S., Chen, J., McCulloch, A. D., Nobrega, M. A., Evans, S. M., and Zambon, A. C., “HIF1α Represses Cell Stress

Pathways to Allow Proliferation of Hypoxic Fetal Cardiomyocytes," *Developmental Cell*, V. 33, No. 5, 2015, pp. 507–521.

98. Shah, Y. M., and Xie, L., "Hypoxia-inducible factors link iron homeostasis and erythropoiesis," *Gastroenterology*, V. 146, No. 3, 2014, pp. 630–642.
99. Gilkes, D. M., Bajpai, S., Chaturvedi, P., Wirtz, D., and Semenza, G. L., "Hypoxia-inducible factor 1 (HIF-1) promotes extracellular matrix remodeling under hypoxic conditions by inducing P4HA1, P4HA2, and PLOD2 expression in fibroblasts," *The Journal of Biological Chemistry*, V. 288, No. 15, 2013, pp. 10819–10829.
100. Harju, N., "Regulation of oxidative stress and inflammatory responses in human retinal pigment epithelial cells," *Acta ophthalmologica*, 100 Suppl 273, 2022, pp. 3–59.
101. Islam, M. N., Rauf, A., Fahad, F. I., Emran, T. B., Mitra, S., Olatunde, A., Shariati, M. A., Rebezov, M., Rengasamy, K. R. R., and Mubarak, M. S., "Superoxide dismutase: an updated review on its health benefits and industrial applications," *Critical Reviews in Food Science and Nutrition*, V. 62, No. 26, 2022, pp. 7282–7300.
102. Zelko, I. N., Mariani, T. J., and Folz, R. J., "Superoxide dismutase multigene family: a comparison of the CuZn-SOD (SOD1), Mn-SOD (SOD2), and EC-SOD (SOD3) gene structures, evolution, and expression," *Free Radical Biology and Medicine*, V. 33, No. 3, 2002, pp. 337–349.
103. Lijnen, P., Petrov, V., van Pelt, J., and Fagard, R., "Inhibition of superoxide dismutase induces collagen production in cardiac fibroblasts," *Am J Hypertens*, V. 21, No. 10, 2008, pp. 1129–1136.
104. Wang, P., Zhou, S., Xu, L., Lu, Y., Yuan, X., Zhang, H., Li, R., Fang, J., and Liu, P., "Hydrogen peroxide-mediated oxidative stress and collagen synthesis in cardiac fibroblasts: blockade by tanshinone IIA," *Journal of Ethnopharmacology*, V. 145, No. 1, 2013, pp. 152–161.
105. Wang, F., Zhang, D., Zhang, D., Li, P., and Gao, Y., "Mitochondrial Protein Translation: Emerging Roles and Clinical Significance in Disease," *Frontiers in Cell and Developmental Biology*, V. 9, 2021, p. 675465.
106. D'Souza, A. R., and Minczuk, M., "Mitochondrial transcription and translation: overview," *Essays in Biochemistry*, V. 62, No. 3, 2018, pp. 309–320.
107. Nakano, H., Minami, I., Braas, D., Pappoe, H., Wu, X., Sagadevan, A., Vergnes, L., Fu, K., Morselli, M., Dunham, C., Ding, X., Stieg, A. Z., Gimzewski,

J. K., Pellegrini, M., Clark, P. M., Reue, K., Lusis, A. J., Ribalet, B., Kurdistani, S. K., Christofk, H., Nakatsuji, N., and Nakano, A., “Glucose inhibits cardiac muscle maturation through nucleotide biosynthesis,” *eLife*, V. 6, 2017.

108. Dai, D.-F., Danoviz, M. E., Wiczer, B., Laflamme, M. A., and Tian, R., “Mitochondrial Maturation in Human Pluripotent Stem Cell Derived Cardiomyocytes,” *Stem cells international*, V. 2017, 2017, p. 5153625.

109. Kumar, S., and Lombard, D. B., “Functions of the sirtuin deacylase SIRT5 in normal physiology and pathobiology,” *Critical reviews in biochemistry and molecular biology*, V. 53, No. 3, 2018, pp. 311–334.

110. Olson, A. K., Bouchard, B., Zhu, W. Z., Chatham, J. C., and Des Rosiers, C., “First characterization of glucose flux through the hexosamine biosynthesis pathway (HBP) in ex vivo mouse heart,” *Journal of Biological Chemistry*, V. 295, No. 7, 2020, pp. 2018–2033.

111. Chakraborty, S., Gogoi, M., and Chakravortty, D., “Lactoylglutathione lyase, a critical enzyme in methylglyoxal detoxification, contributes to survival of Salmonella in the nutrient rich environment,” *Virulence*, V. 6, No. 1, 2015, pp. 50–65.

112. Dionigi, B., Ahmed, A., Pennington, E. C., Zurakowski, D., and Fauza, D. O., “A comparative analysis of human mesenchymal stem cell response to hypoxia in vitro: Implications to translational strategies,” *Journal of Pediatric Surgery*, V. 49, No. 6, 2014, pp. 915–918.

113. Reis, R., “Encyclopedia of Tissue Engineering and Regenerative Medicine,” Elsevier Science & Technology, San Diego, 2019, 1436 pp.

114. Uhlén, M., Fagerberg, L., Hallström, B. M., Lindskog, C., Oksvold, P., Mardinoglu, A., Sivertsson, Å., Kampf, C., Sjöstedt, E., Asplund, A., Olsson, I., Edlund, K., Lundberg, E., Navani, S., Szigyarto, C. A.-K., Odeberg, J., Djureinovic, D., Takanen, J. O., Hober, S., Alm, T., Edqvist, P.-H., Berling, H., Tegel, H., Mulder, J., Rockberg, J., Nilsson, P., Schwenk, J. M., Hamsten, M., Feilitzen, K. von, Forsberg, M., Persson, L., Johansson, F., Zwahlen, M., Heijne, G. von, Nielsen, J., and Pontén, F., “Proteomics. Tissue-based map of the human proteome,” *Science (New York, N.Y.)*, V. 347, No. 6220, 2015, p. 1260419.

115. Doll, S., Dreßen, M., Geyer, P. E., Itzhak, D. N., Braun, C., Doppler, S. A., Meier, F., Deutsch, M.-A., Lahm, H., Lange, R., Krane, M., and Mann, M.,

"Region and cell-type resolved quantitative proteomic map of the human heart," *Nature Communications*, V. 8, No. 1, 2017, p. 1469.

116. Chen, Q., Kang, J., and Fu, C., "The independence of and associations among apoptosis, autophagy, and necrosis," *Sig Transduct Target Ther*, V. 3, No. 1, 2018, p. 18.

117. Subbiahanadar Chelladurai, K., Selvan Christyraj, J. D., Rajagopalan, K., Yesudhason, B. V., Venkatachalam, S., Mohan, M., Chellathurai Vasantha, N., and Selvan Christyraj, Johnson Retnaraj Samuel, "Alternative to FBS in animal cell culture - An overview and future perspective," *Heliyon*, V. 7, No. 8, 2021, e07686.

118. Ergir, E., La Cruz, J. O.-D., Fernandes, S., Cassani, M., Niro, F., Sousa, D., Vrbský, J., Vinarský, V., Perestrelo, A. R., Debellis, D., Cavalieri, F., Pagliari, S., Redl, H., Ertl, P., and Forte, G., "Generation and Maturation of Human iPSC-derived Cardiac Organoids in Long Term Culture," *bioRxiv*, 2022, 2022.03.07.483273.

119. Barrick, S. K., and Greenberg, M. J., "Cardiac myosin contraction and mechanotransduction in health and disease," *Journal of Biological Chemistry*, V. 297, No. 5, 2021, p. 101297.

120. Vigil-Garcia, M., Demkes, C. J., Eding, J. E. C., Versteeg, D., Ruiter, H. de, Perini, I., Kooijman, L., Gladka, M. M., Asselbergs, F. W., Vink, A., Harakalova, M., Bossu, A., van Veen, T. A. B., Boogerd, C. J., and van Rooij, E., "Gene expression profiling of hypertrophic cardiomyocytes identifies new players in pathological remodelling," *Cardiovasc Res*, V. 117, No. 6, 2021, pp. 1532–1545.

121. Gacita, A. M., Fullenkamp, D. E., Ohiri, J., Pottinger, T., Puckelwartz, M. J., Nobrega, M. A., and McNally, E. M., "Genetic Variation in Enhancers Modifies Cardiomyopathy Gene Expression and Progression," *Circulation*, V. 143, No. 13, 2021, pp. 1302–1316.

122. Grancharova, T., Gerbin, K. A., Rosenberg, A. B., Roco, C. M., Arakaki, J. E., DeLizo, C. M., Dinh, S. Q., Donovan-Maiye, R. M., Hirano, M., Nelson, A. M., Tang, J., Theriot, J. A., Yan, C., Menon, V., Palecek, S. P., Seelig, G., and Gunawardane, R. N., "A comprehensive analysis of gene expression changes in a high replicate and open-source dataset of differentiating hiPSC-derived cardiomyocytes," *Sci Rep*, V. 11, No. 1, 2021, p. 15845.

123. Udvardi, M. K., Czechowski, T., and Scheible, W.-R., “Eleven golden rules of quantitative RT-PCR,” *The Plant Cell*, V. 20, No. 7, 2008, pp. 1736–1737.

124. Betts, J.G., Young, K.a., Wise, J.A., Johnson, E., Poe, B., Kruse, D.H, Korol, O., Johnson, J.E., Womble, M., DeSaix, P., “Anatomy and Physiology,” OpenStax, Houston, Texas, 2013.

6 Appendix

6.1 Mitochondrial Metabolism and the Electron Transport Chain

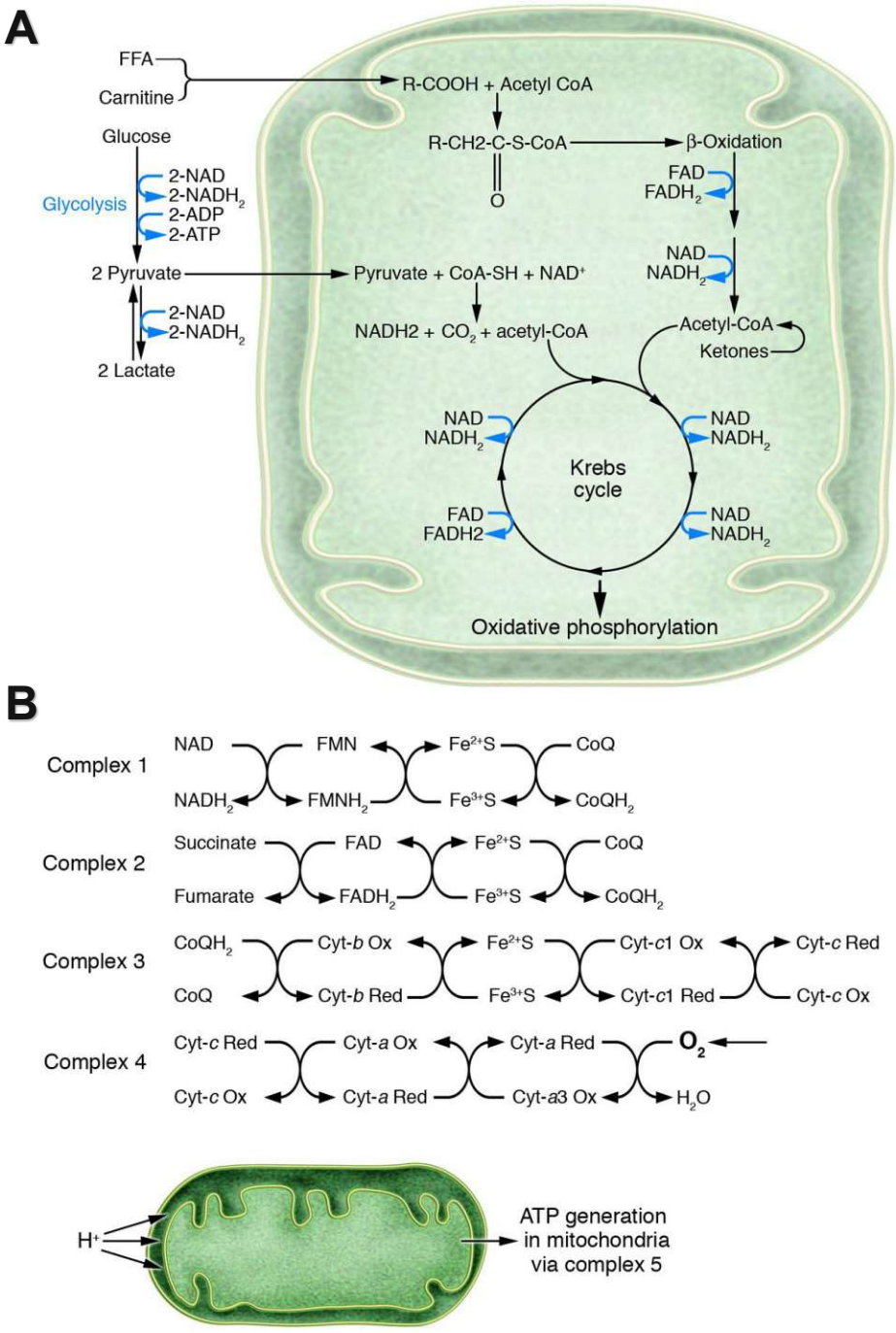

Figure 33. (A) The overview of cardiomyocyte fuel utilization includes various substrates to generate reduced redox equivalents ($FADH_2$ and $NADH_2$). (B) The process of oxidative phosphorylation includes specific electron transfer steps among redox equivalents, reduced and oxidised iron-sulfur (FeS), coenzyme Q (CoQ) and cytochromes a-c1 (Cyt) in complexes 1-4. The resulting accumulation of protons between the outer and inner mitochondrial membrane provides the gradient driving ATP production in complex 5 (ATP synthase). FAD and $FADH_2$ indicate flavin adenine dinucleotide in the fully oxidised and reduced form. FFA indicates free fatty acids. FMN and $FMNH_2$ indicate oxidised and reduced forms of flavin mononucleotide. $NADH_2$ indicates NADH + H^+.Illustration by Giordano, F.J. et al. with permission by the American Society for Clinical Investigation.[41]

6.2 Anatomy of the Human Heart

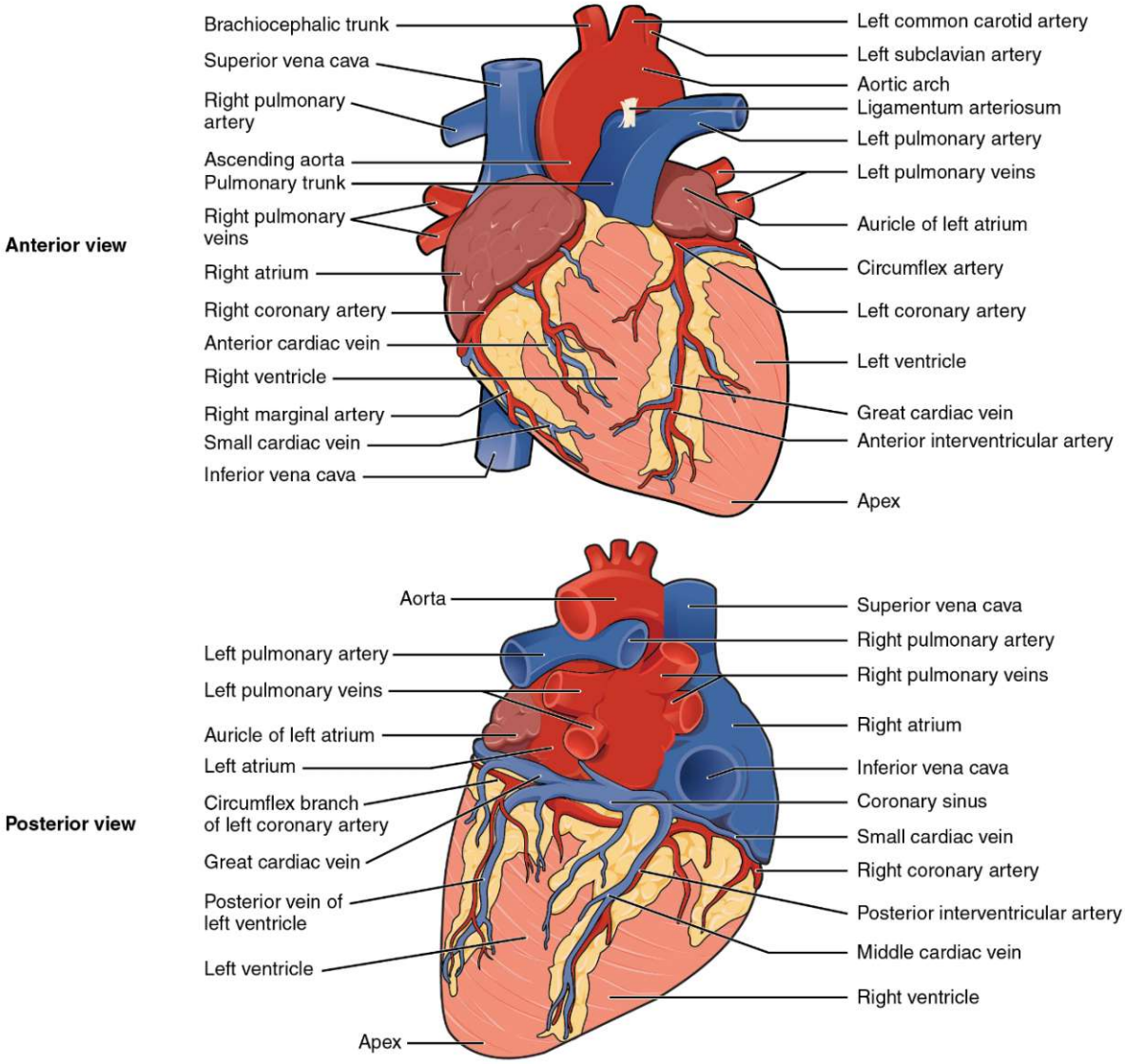

Figure 34. The anterior and posterior view of the anatomy of the human heart. Illustration by Betts, J.G. et al. with permission by OpenStax. Access for free at https://openstax.org/books/anatomy-and-physiology/pages/1-introduction.[124]

6.3 Parameters for MRM Analysis of Glutathione Status

Table 4. MRM transitions and method parameters per analyte ([m/z]) for LC-MS/MS analysis of glutathione status. CE indicates collision energy. Q indicates quadrupole. IS indicates internal standard ($^{13}C_2$,^{15}N-GSH-d5-NEM). CE and Bias are listed as [V].

	Parent	Product	Dwell Time	Q1 Pre Bias	CE	Q3 Pre Bias
GSH	308	179	65	-11	-19	-23
GSSG	613	355	65.6	-14	-20	-25
GSH-NEM	433	304	65.6	-10	-17	-21
	433	201	65.6	-16	-21	-21
GSH-d5-NEM	438	309	65.6	-10	-17	-21
	438	206	65.6	-16	-21	-21
IS	441	312	100	-10	-17	-21
	441	206	100	-16	-21	-21

6.4 GSH-NEM Calibration Curve for Glutathione Status Analysis

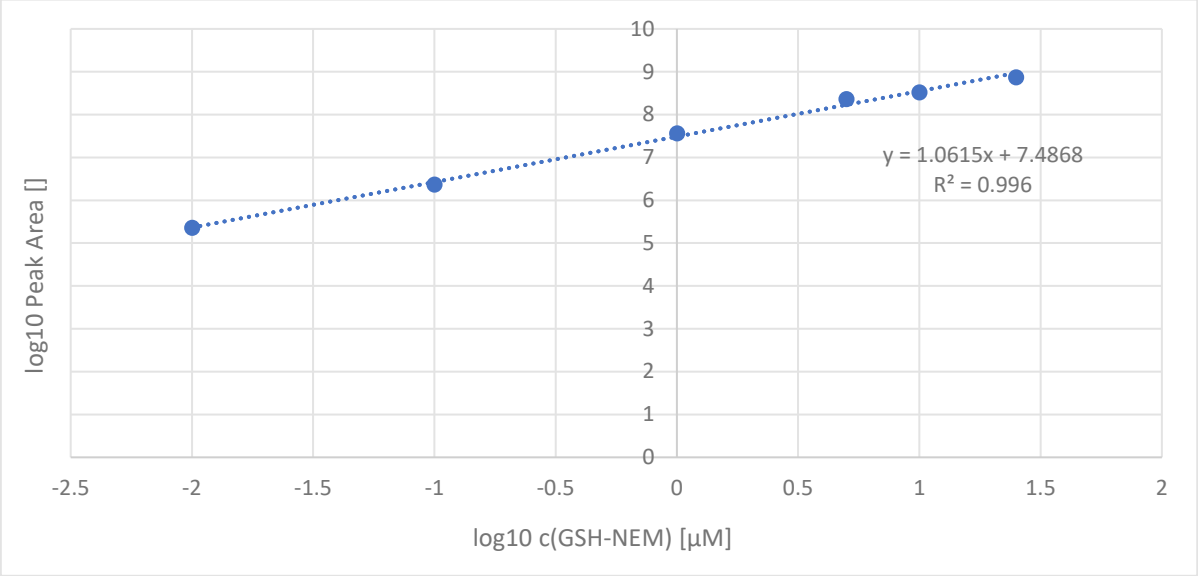

Figure 35. GSH-NEM calibration curve for redox metabolomic analysis of glutathione status.

6.5 BCA Assay for Protein Estimation in Cardioid Samples

In short, the BCA assay for protein quantification is a colourimetric measurement combining the reduction of Cu^{2+} to Cu^{+} by proteins in an alkaline solution with the selective and sensitive detection of Cu^{+} by chelation. The purple-coloured complex is measured at 580 nm, allowing protein estimation over a broad linear range.

Dilution Scheme for Standard Test Tube Protocol and Microplate Procedure (Working Range = 20–2,000 µg/mL)			
Vial	**Volume of Diluent (µL)**	**Volume and Source of BSA (µL)**	**Final BSA Concentration (µg/mL)**
A	0	300 of Stock	2000
B	125	375 of Stock	1500
C	325	325 of Stock	1000
D	175	175 of vial B dilution	750
E	325	325 of vial C dilution	500
F	325	325 of vial E dilution	250
G	325	325 of vial F dilution	125
H	400	100 of vial G dilution	25
I	400	0	0 = Blank

Figure 36. Dilution scheme for the preparation of diluted albumin (BSA) standards as to the manufacturer's (Thermo Fisher Scientific - Waltham, MA, USA) instruction.

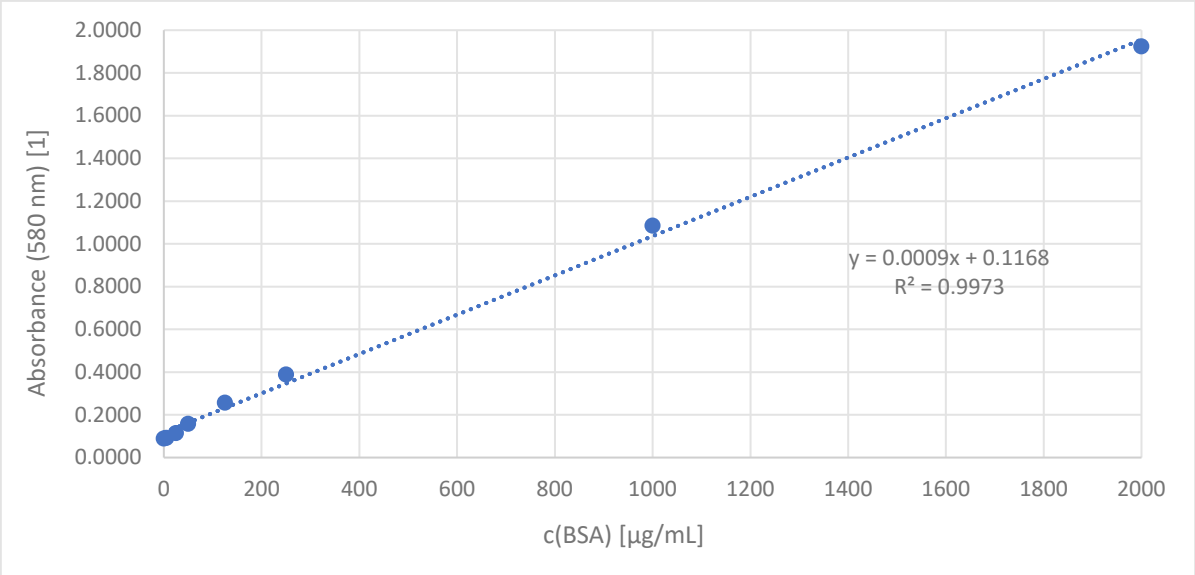

Figure 37. Resulting calibration curve for the BCA assay for protein content estimation in cardioid samples.

6.6 Acting Substances in Differentiation Media

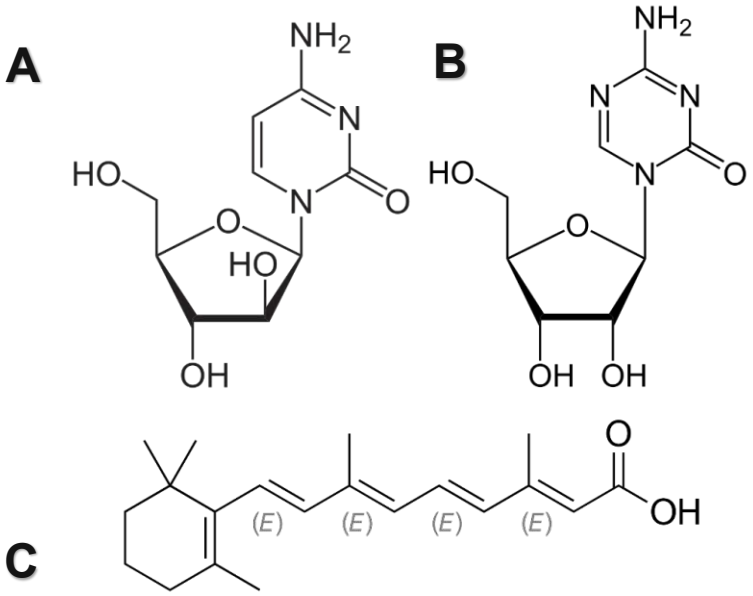

Figure 38. Chemical structures of the acting substances used in the evaluation of different approaches in media composition for the maturation of AC16 cells: (A) Cytosine arabinoside. (B) Azacytidine. (C) All-trans retinoic acid.

6.7 Primer Sequences for qPCR Analysis of Differentiation Markers

Table 5. List of primers used for RT-qPCR analysis. Tm indicates melting temperature. GC indicates guanine-cytosine content.

Gene	Protein	Primer	Sequence (5'-3')	Tm [°C]	GC [%]
ACTN2	alpha-actinin 2	forward	GAAGCACAAGCCACCCAAGG	69.1	60.0
		reverse	CACCAGCAATATCCGACACCA	68.0	52.3
MYH6	myosin heavy chain 6 (alpha; fast)	forward	GCTGGTCACCAACAATCCCTA	66.0	52.3
		reverse	CGTCAAAGGCACTATCGGTGG	68.6	57.1
MYH7	myosin heavy chain 7 (beta; slow)	forward	ACTGCCGAGACCGAGTATG	62.9	57.8
		reverse	GCGATCCTTGAGGTTGTAGAGC	66.1	54.5
RPLP0	ribosomal protein lateral stalk subunit P0	forward	GCGTCCTCGTGGAAGTGACA	68.9	60.0
		reverse	GCATCTGCTTGGAGCCCACA	71.0	60.0
TNNI1	troponin I type 1 (skeletal muscle; slow)	forward	CCGGAAGTCGAGAGAAAACCC	68.0	57.1
		reverse	TCAATGTCGTATCGCTCCTCA	65.6	47.6
TNNI3	troponin I type 3 (cardiac muscle)	forward	TTTGACCTTCGAGGCAAGTTT	64.7	42.8
		reverse	CCCGGTTTTCCTTCTCGGTG	69.7	60.0
TNNT2	troponin T type 2 (cardiac muscle)	forward	ACAGAGCGGAAAAGTGGGAAG	66.5	52.3
		reverse	TCGTTGATCCTGTTTCGGAGA	66.9	47.6

6.8 Microscopic image of cardiac organoids

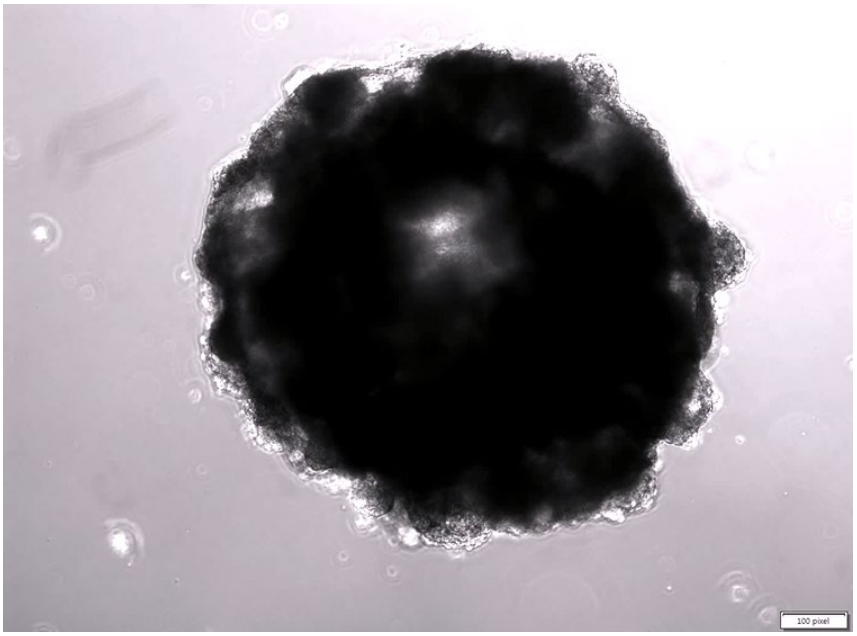

Figure 39. Illustrated above is a cardiac organoid after 48 h in 5 mM glucose. Form and shape are representative of cardioids across all conditions. The characteristic spheroid formation and central cavity can easily be identified.

6.9 Multi-scatter plots for analysis of correlation between samples

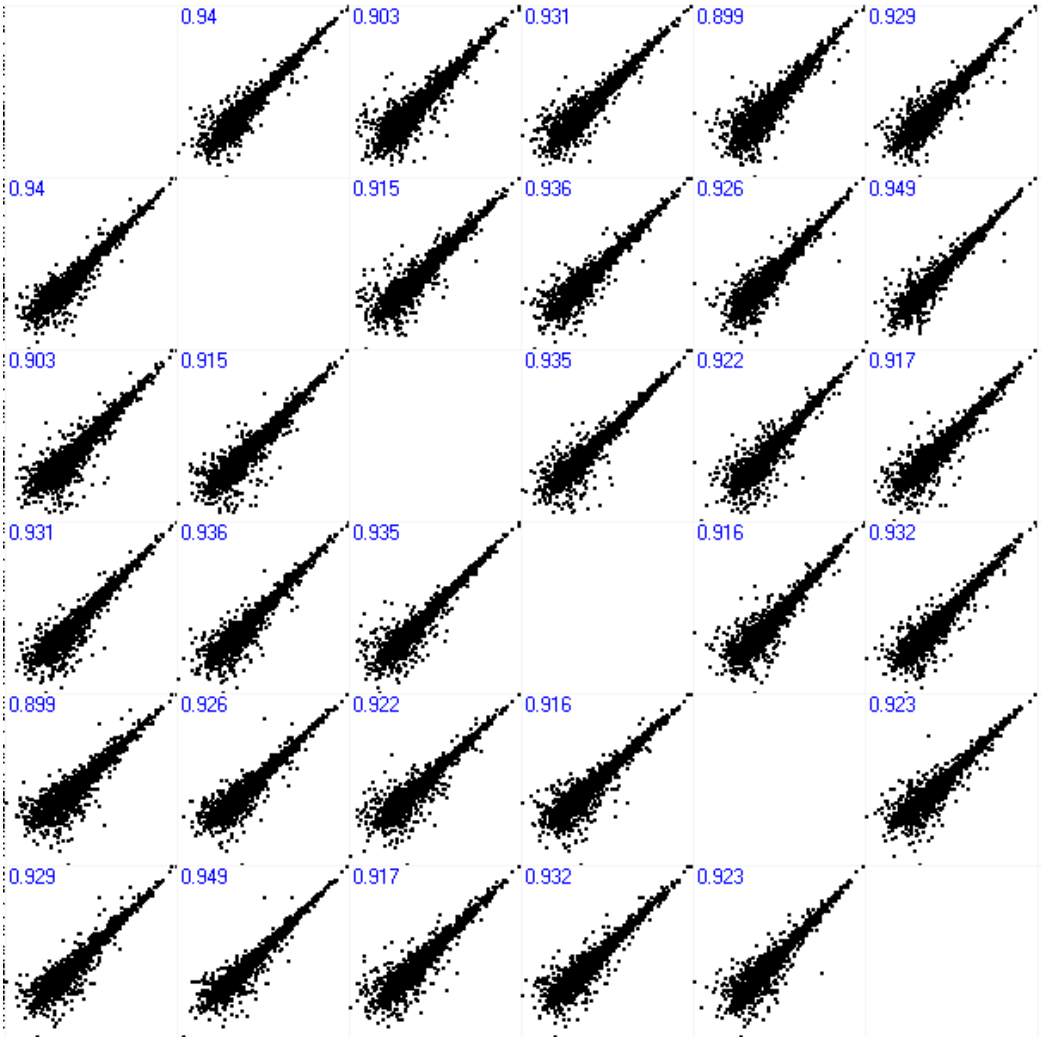

Figure 40. Multi-scatter plot for the analysis of the similarity of proteomic signatures of cardiac organoids cultured in 5 mM glucose. Listed are the correlations (including R^2) of samples 13 to 18 from left to right and top to bottom, respectively. Variation in sample 17, together with PCA, was the basis for exclusion in subsequent analysis.

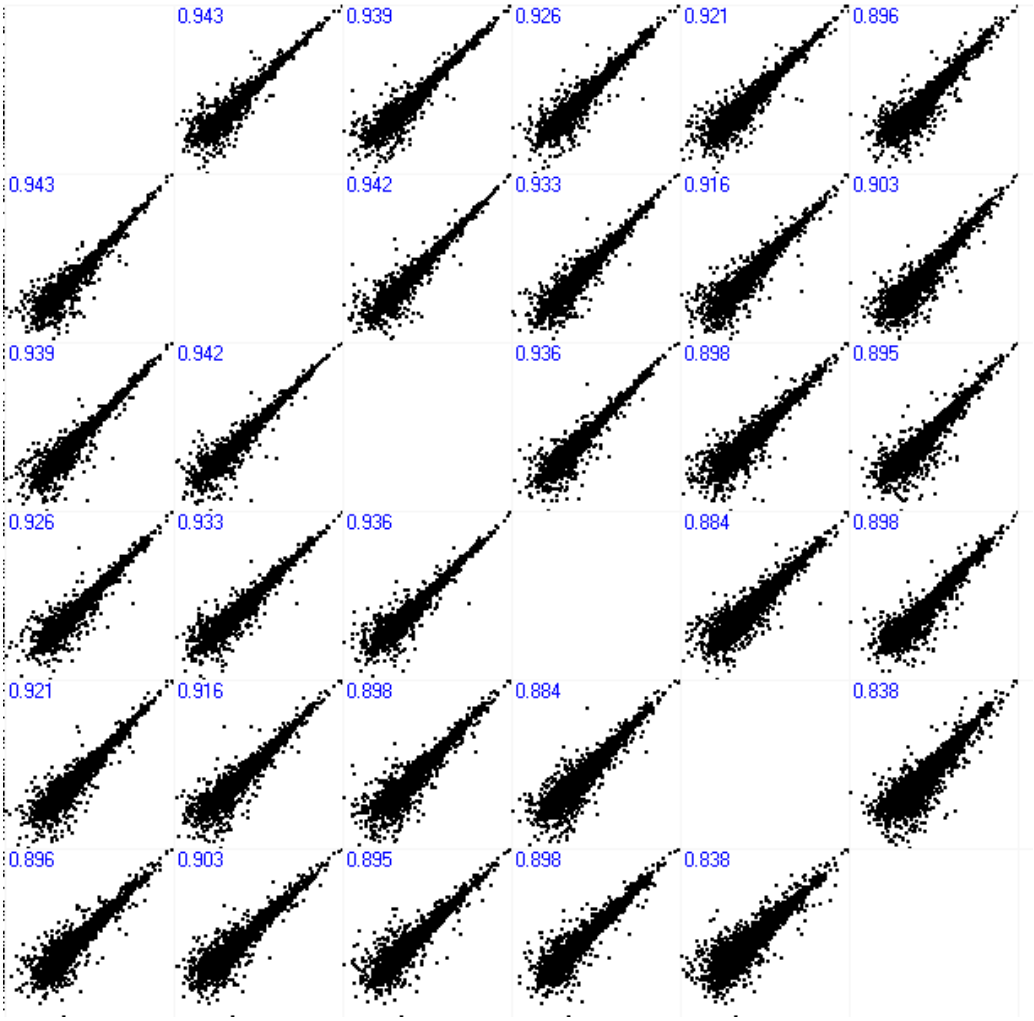

Figure 41. Multi-scatter plot for the analysis of the similarity of proteomic signatures of cardiac organoids cultured in 30 mM glucose. Listed are the correlations (including R^2) of samples 19 to 24 from left to right and top to bottom, respectively. Variation in sample 24, together with PCA, was the basis for exclusion in subsequent analysis.

6.10 Gene Expression Analysis of AC16 Cells Cultured in BSA Differentiation Medium for 8 days

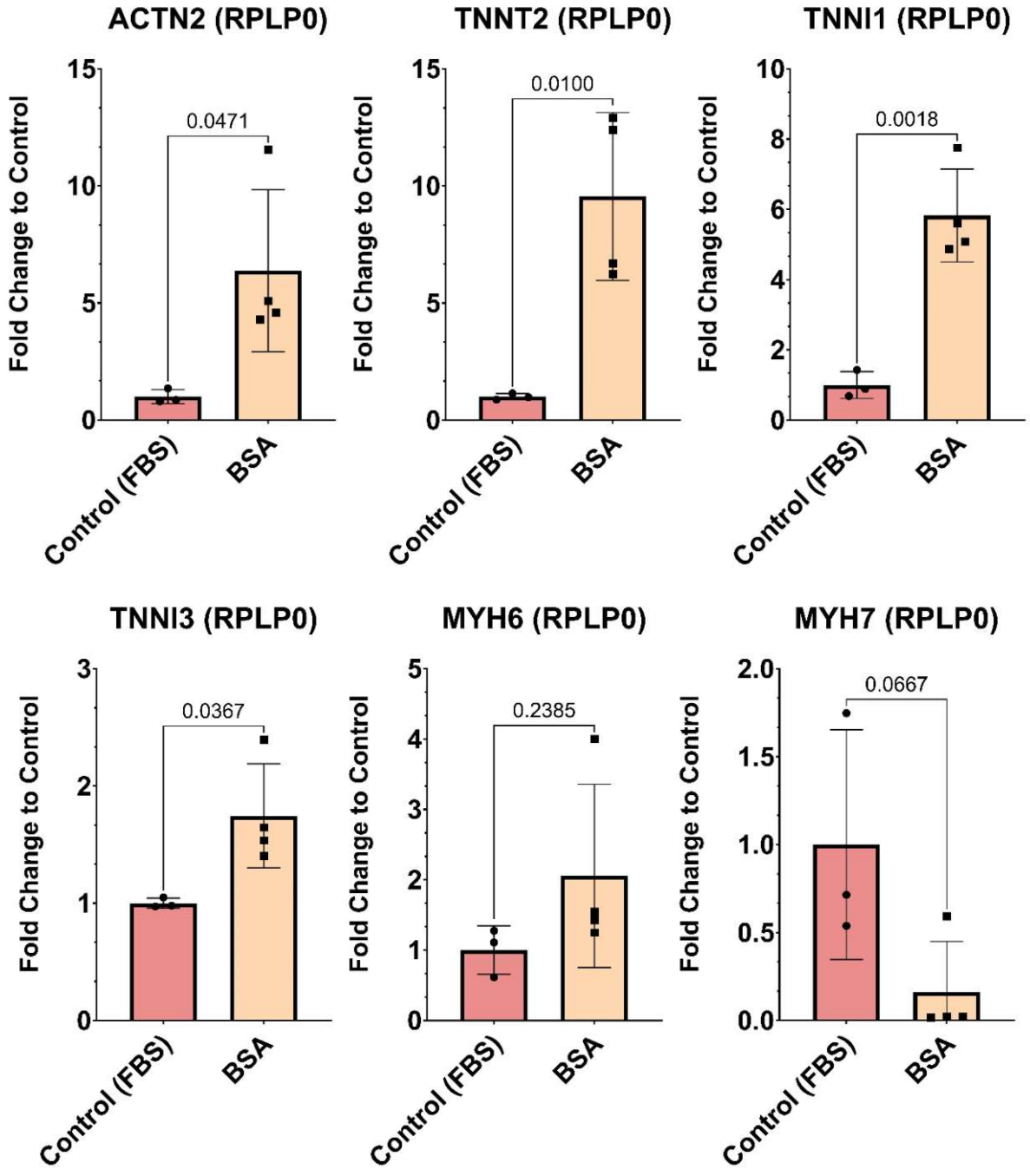

Figure 42. Illustrated above are the individual results for relative gene expression analysis by RT-qPCR of AC16 cells cultured in AC16 BSA differentiation medium for 8 days compared to AC16 FBS proliferation medium. Transcript levels were normalized on the expression of ribosomal protein lateral stalk subunit P0 (RPLP0; housekeeping gene). Individual values and standard error of the mean (SEM) are listed together with the mean value for the respective condition in all box plots. Additionally, Student *t*-test *p*-values are listed. Remeasurement of stored (-20 °C) samples was only carried out for three replicates of the control as sample volume was limited due to prior analysis.

6.11 Gene Expression Analysis of AC16 Cells Cultured in BSA Differentiation Medium for 48 h

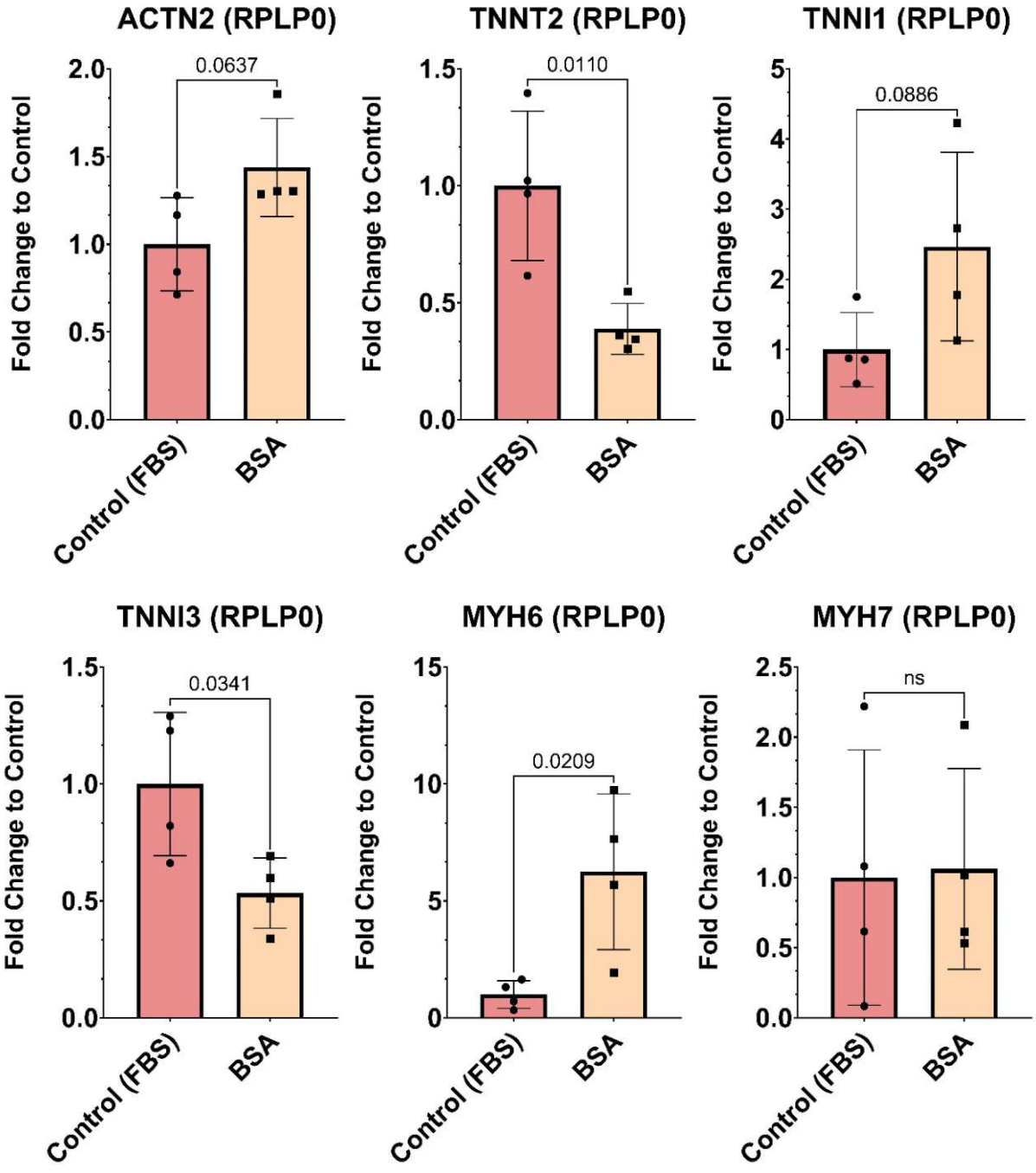

Figure 43. Illustrated above are the individual results for relative gene expression analysis by RT-qPCR of AC16 cells cultured in AC16 BSA differentiation medium for 48 h compared to AC16 FBS proliferation medium. Transcript levels were normalized on the expression of ribosomal protein lateral stalk subunit P0 (RPLP0; housekeeping gene). Individual values and standard error of the mean (SEM) are listed together with the mean value for the respective condition in all box plots. Additionally, Student *t*-test *p*-values are listed.